3-8-2004

Time dependent mechanical behavior of welded Tuff

Jaak J.K. Daemen
University of Nevada, Reno, daemen@mines.unr.edu

George Danko
University of Nevada, Reno, danko@unr.edu

Amy J. Smiecinski
University of Nevada, Las Vegas, smiecins@unlv.nevada.edu

Final Technical Report – Part 2

Time Dependent Mechanical Behavior of Welded Tuff

Long – Term Drift Stability
Task 18 YM Project
Document ID: TR-03-018
Revision: 0

Prepared for U.S. DOE/UCCSN
Cooperative Agreement DE-FC28-98NV12081

Lumin Ma and Jaak Daemen
Department of Mining Engineering/Mail Stop 173
University of Nevada, Reno 89557

Originator:

[redacted]
Jaak Daemen — 3-8-04 Date

Approvals:

[redacted]
Technical Reviewer, George Danko — 3-8-04 Approval Date

[redacted]
Principal Investigator, Jaak Daemen — 3-8-04 Approval Date

[redacted]
QA Manager, Amy Smiecinski — 6-1-04 Approval Date

TABLE OF CONTENTS

LIST OF FIGURES

LIST OF TABLES

LIST OF SYMBOLS

D	Diameter
E_S	Secant elastic modulus
K_I	Stress intensity factor
K_{IC}	Critical stress intensity factor or fracture toughness
L	Thickness
P	Load
s	Second
S	Sensitivity
t	Time
α, β	Constants in primary creep equation
ε	Strain
ε_e	Elastic strain component
ε_{in}	Inelastic strain component
ε_{long}	Ultimate strain of specimens for long term tests
ε_{loss}	Maximum reduction of ultimate strain for slow tests
ε_{max}	Ultimate strain (axial strain at maximum stress)
ε_{pr}	Strain generated during primary creep
ε_s	Strain generated in secondary creep
ε_{short}	Ultimate strain of specimens for short term tests
ε_{time}	Strain component resulted from time effect
ε_{total}	Total axial strain
ε_0	Initial axial strain
$\dot{\varepsilon}$	Axial strain rate
$\dot{\varepsilon}_{pr}$	Strain rate during primary creep
$\dot{\varepsilon}_s$	Strain rate during secondary creep
σ	Stress
σ_{loss}	Strength reduction
σ_{max}	Ultimate strength

CHAPTER 1 INTRODUCTION

1.1 Introduction

This part of the Technical Report includes four types of experimental studies: strain rate dependence, uniaxial creep, Brazilian (Indirect splitting) tensile strength and uniaxial compressive strength. These are presented in four chapters. One hundred twenty one specimens have been tested in uniaxial compression. Ninety three of these are included in the strain rate dependence study, presented in Chapter 2. Uniaxial compression strain rates range from about 10^{-8} to 10^{-2} s^{-1}. Results of twenty eight tests are presented in Chapter 5, which describes uniaxial compression testing of specimens containing major lithophysal cavities. Fourteen specimens have been tested in uniaxial creep, presented in Chapter 3. Brazilian testing has been performed on 158 specimens. Results are presented in Chapter 4. The chapter on Brazilian testing includes a study of strain rate dependency of the splitting tensile strength, conducted by performing Brazilian tests at strain rates from about 10^{-6} to about 10^{-2} s^{-1}.

The test results in the form of electronic data can be accessed at the website: http://hrcweb.nevada.edu/data/tda/tda.htm#18. The UCCSN Data ID numbers are Uniaxial (including the tests for strain rate dependence study): 018LM.001; Creep: 018LM.003; and Brazilian: 018LM.002.

1.2 Specimen preparation

All the specimens are prepared from rock cores. The rock cores are received from the Sample Management Facility (SMF), Yucca Mountain Site Characterization Project. They belong to the Topopah Spring Tuff. The nominal diameters of the cores are 2.4 inch (60.96 mm) and 1.78 inch (45.21 mm). Most cores contain various flaws such as lithophysae, vapor-phase altered zones, cracks, etc. Lithophysae are gas-formed voids created soon after emplacement of the ash-flow tuff. Vapor-phase altered zones are regions of tuff matrix altered by gases in the early stages of tuff emplacement (Martin, III et al, 1993). Some lithophysae and vapor-phase altered zones are visible on the surface of the cores. Others are not, and can only be recognized after the core breaks. When preparing a specimen, lithophysal cavities and large vapor-phase altered zones are avoided, except for the testing described in Chapter 5, which was designed intentionally to look at the influence of lithophysae on the mechanical response of the rock. Small vapor-phase altered zones appear so frequently that often they are difficult to avoid.

All the specimens are prepared in the sequence: cut to length → grind top and bottom → measure dimensions and weight → measure moisture content (moisture content for a small number of specimens is measured immediately after testing, for a few is not measured) → install strain gages → take photos → test → take photos. This process follows ASTM D 4543-85. Photos are included in the electronic database referenced in Section 1.1.

1.3 Numbering of specimens and tests

Every rock core is received with a barcode. It has an eight-digit number. All the test specimens are numbered to inherit the barcodes of rock cores from which the specimens are prepared. In addition to the barcode, two more pieces of information are incorporated to number or identify a specimen: serial number of the specimen in the rock core and type of test. Fig. 1.1 gives a description of the rule of specimen numbering.

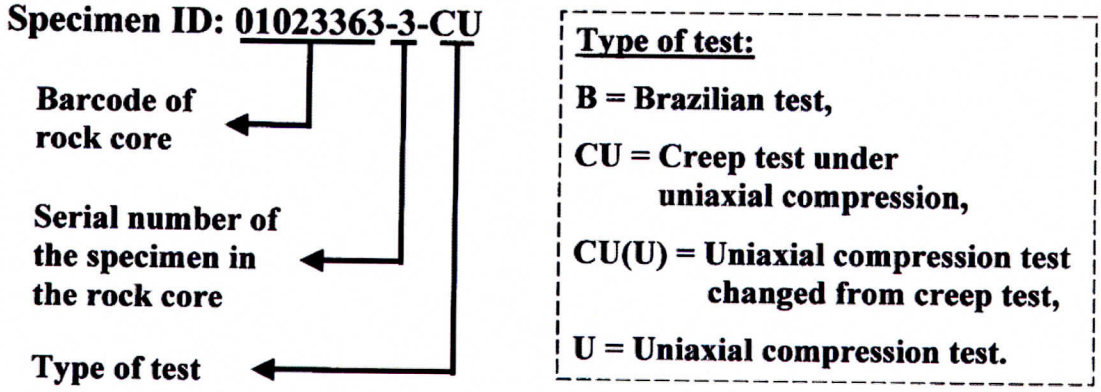

Figure 1.1 Rule of specimen numbering

Each test is performed with one specimen. A test is identified with the ID of the specimen that is tested. Serial number refers to the number this particular specimen is assigned when a section of core is long enough to allow preparation of more than one test specimens.

1.4 Experimental setup

All tests are done in an MTS (Material Testing System) testing machine. Load is measured using a load cell. Displacement is measured using an LVDT (Linear Variable Differential Transducer) in the machine. Strain for most of the specimens is measured using 120-ohm electric resistance strain gages. Strain for a small number of specimens is measured using 350-ohm strain gages and/or extensometers. Six strain gages are installed on most specimens. Four measure axial strain. Two measure lateral strain. All strain gages are cemented at about midheight of the specimen. Strain in each direction is calculated by taking the average of all measurements in that direction. When using extensometers, two are used, for measuring axial strain only. The average of the two measurements is calculated as the axial strain. All the tests are conducted at room temperature and humidity.

1.5 Moisture contents

Moisture contents of the rock samples received are low (typically $< 0.8\%$). The rock samples have been stored in cardboard core boxes over extended periods of time, typically years. We have stored all specimens in a rock mechanics laboratory, at room

temperature and humidity (in a very dry climate). When we received the specimens they were packaged in plastic bags, and we left them in the bags until they were prepared for testing.

1.6 Testing standards and implementing procedures

The following standards and implementing procedures are followed in the studies in this part:

ASTM D 2938-95, "Standard Test Method for Unconfined Compressive Strength of Intact Rock Core Specimens."

ASTM D3967-95a, "Standard Test Method for Splitting Tensile Strength of Intact Rock Core Specimens."

ASTM D 4543-85 (Reapproved 1991), "Standard Practice for Preparing Rock Core Specimens and Determining Dimensional and Shape Tolerances."

IPR-010 - Splitting (Brazilian) Tensile Strength Test of Rock - Revision 0

IPR-011- Determining Uniaxial Compressive Strength of Rock - Revision 0

IPR-012 - Preparation of Rock Core Specimens for the Determination of Mechanical Properties of Rock - Revision 0

For tests aimed at studying time dependence, tests were conducted at slower and at faster rates than required by the standards.

CHAPTER 2 STRAIN RATE DEPENDENCE STUDY

2.1 Experimental description

Strain rate dependence is one aspect of the time dependent behavior of rock. For extremely brittle rocks as in this study, one important characteristic is that their mechanical properties depend on the rate at which deformation is applied. The strain rate dependence of brittle rocks is attributed to crack initiation and growth. Crack growth and development depend on multiple factors. Of the factors applied load and time are most important. The purpose of this study is to investigate the strain rate dependence of welded Topopah Spring tuff. Ninety three specimens have been tested. All these specimens are collected from Alcove #5 which is located in the middle nonlithophysal unit. Sixty five of these do not contain obvious flaws, and are tested at different strain rates. Another group of specimens is tested to study failure patterns and explore how the ultimate strengths are influenced by gross defects at a given strain rate. Most of the specimens in this second group are tested at the strain rate of 10^{-5} s^{-1} that falls in the time duration in ASTM D 2938-95 for standard uniaxial compression tests.

Specimens for conducting a study of strain rate dependence ideally should have relatively uniform mechanical properties. Although one might prefer to study a perfectly homogeneous uniform rock to investigate the fundamental time dependency of a brittle material, there is considerable merit in investigating the time dependent behavior of an intrinsically highly variable and heterogeneous rock such as welded tuff, e.g. in part in order to determine whether or not it is feasible to identify the time dependent behavior, i.e. to isolate from among the highly variable properties those variations which can be ascribed to time dependency. We selected those specimens according to the rules: 1) they are collected from a localized area. 2) they contain no major obvious flaws. The majority of the specimens contain some small vapor-phase altered zones or spots, either on the surface or in the body. Photographs of all specimens tested are included in the database on the website referenced in Section 1.1 of this part of the report. The selected specimens are randomly divided into six groups to test at six strain rates. The strain rates range from 10^{-8} to $10^{-2}\,s^{-1}$. The number of specimens in each group is not the same.

At the time of testing all specimens had a low moisture content. Among the 65 specimens used for the strain rate dependence testing, the moisture contents have been measured for 62. Forty five of these moisture contents have been measured before testing. The mean moisture content is 0.70%. Standard deviation is 0.1%. The moisture content of 17 specimens has been measured after testing. The mean is 0.75%. The standard deviation is 0.07%.

2.2 Experimental results

Tables 2.1 and 2.2 (at the end of this chapter) show source information for all specimens and a summary of test results, respectively. Fig. 2.1 gives three representative stress–strain curves. All the specimens exhibit very small inelastic deformation. Fig. 2.2 shows a test performed with two loading-unloading cycles before loading to failure. The

unloading is started at 76% of its ultimate strength. Its permanent strain is almost ignorable ($<< 4\times10^{-5}$). This test specimen was collected from the location close to where the specimens for strain rate dependence study were collected. They have indistinguishable appearance and mechanical properties.

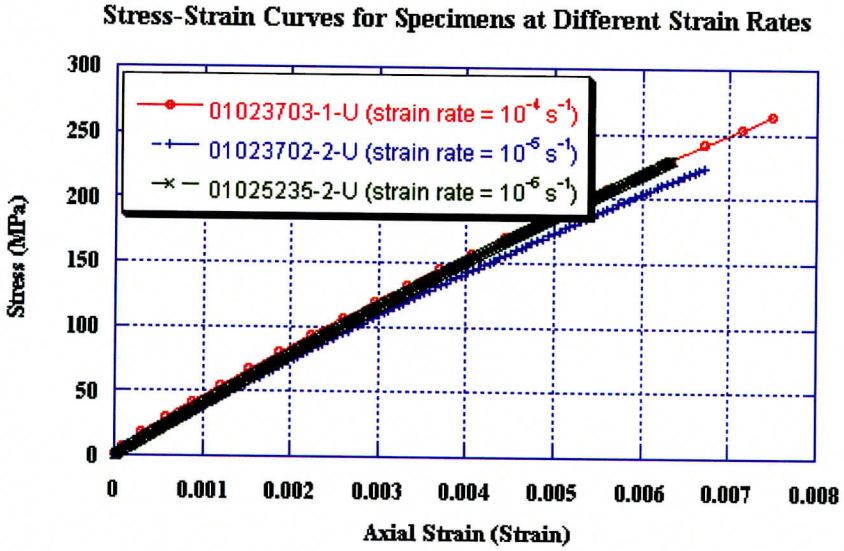

Figure 2.1 Axial stress–strain curves for three specimens loaded in uniaxial compression, at strain rates of 10^{-4}, 10^{-5} and 10^{-6} s^{-1}.

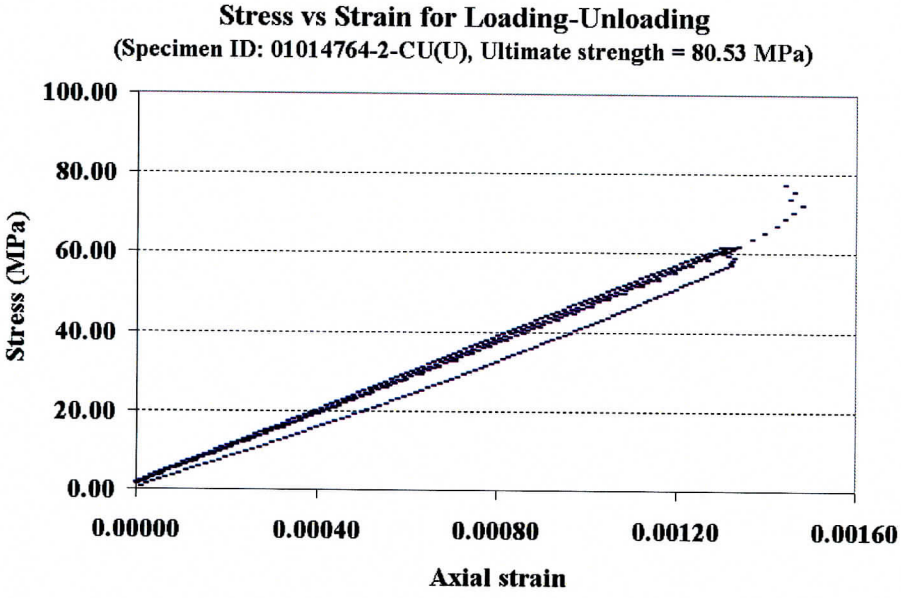

Figure 2.2 Two loading-unloading loops of stress-strain curve showing permanent deformation of the specimen (Specimen ID: 01014764-2-CU(U), Ultimate strength = 80.53 MPa)

For each strain rate, the ultimate strengths (σ_{max}) fluctuate significantly. The corresponding (ultimate) axial strains (ε_{max}) also vary dramatically. Relatively, the secant moduli (E_S) at ultimate strength are less variable. Table 2.3 gives the statistics of these three parameters for 18 specimens tested at the strain rate of 10^{-5} s^{-1}.

Table 2.3 Statistics of three parameters for 18 specimens tested at strain rate of 10^{-5} s^{-1} (Non-Q, for information only)

	ε_{max}	σ_{max}, MPa	E_S, GPa
Minimum	0.00331	122.28	31.02
Maximum	0.00822	291.64	40.64
Mean	0.00607	214.28	35.49
Median	0.00626	224.62	35.78
Std Deviation	0.00142 (23.4%)*	49.19 (23%)*	2.57 (7.2%)*

* % of mean

Fig. 2.3 shows a broken specimen. It illustrates the typical pattern of how these specimens fail. The specimen fails nearly parallel to its axis, or the loading direction, by predominantly longitudinal splitting. Some shearing can be observed on some of the angled fractures, which is typical for most tests. There is a large vapor-phase altered spot (in white color) inside the specimen. Such inclusions usually affect the strength significantly. They are difficult, often impossible, to detect before testing.

Figure 2.3 Specimen after failure: typical longitudinal tensile splitting. Note vapor-phase altered spot (inside circle). Tested at $1.1\times10^{-8}s^{-1}$.

All the tests in the strain rate dependence study are performed using displacement control. The displacement rate is held constant for each test. Displacement is measured by the machine LVDT. This measurement includes the deformation of steel platens and spacers, includes the machine frame deformation (although the frame is extremely stiff), and includes the deformation of each contact pair of specimen, platens, spacers and load cell. As a result, the strain rate calculated from the strain measured by strain gages on the specimen is not constant, especially at the beginning of loading (Fig. 2.4). The strain–time relation is not a perfectly straight line, as shown in Fig. 2.4. For the strain rate dependence study, we assume that it is accurate enough if we treat this relation as linear. Doing so simplifies the problem without loss of significance. The strain rate is calculated by taking the slope of the dashed line in Fig. 2.4, i.e. the strain is averaged over the full duration of the test.

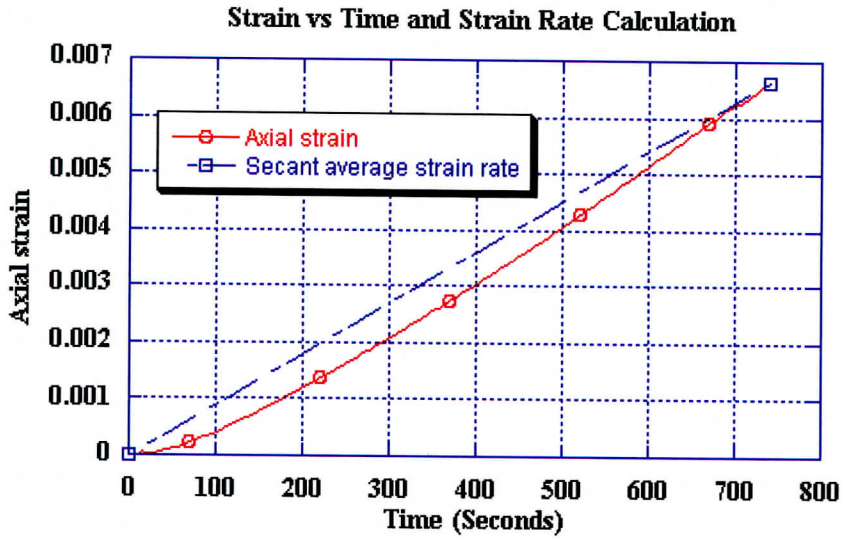

Figure 2.4 Typical axial strain versus time for a displacement rate controlled test. Secant average strain rate calculation.

2.3 Experimental observations

For specimens that do not contain obvious flaws (we call them flawless hereafter), usual failure is axial splitting. After testing, undulating smooth fracture surface(s) are observed. Sometimes a crack propagation path is clearly visible. When breaking, flawless specimens generate large noise, shock and much dust. This indicates that much strain energy is released. When performing a high strain rate test, a specimen usually breaks into a large number of small approximately equal-sized pieces. This is especially true for high strength specimens.

For flawed specimens failure occurs in various ways. Generally failure initiates at flaws. When a specimen contains a lithophysal cavity or a large vapor-phase altered zone, failure most likely starts from or around the flaw. If a specimen contains more than one

lithophysal cavity, the largest one usually plays the decisive role in the failure. Frequently one or more pre-existing fracture surfaces can be seen after a specimen breaks.

Fig. 2.5 gives the strengths of specimens with and without obvious lithophysal cavities, at the strain rate of $10^{-5}s^{-1}$. Each specimen classified as "with flaws" contains at least one or two visible cavities. The cavities are contained at about midheight of each specimen, and are oriented approximately along the axial direction. Their lengths range from 0.6 to 1.2 inch. Their widths are small compared to their lengths (Fig. 2.6).

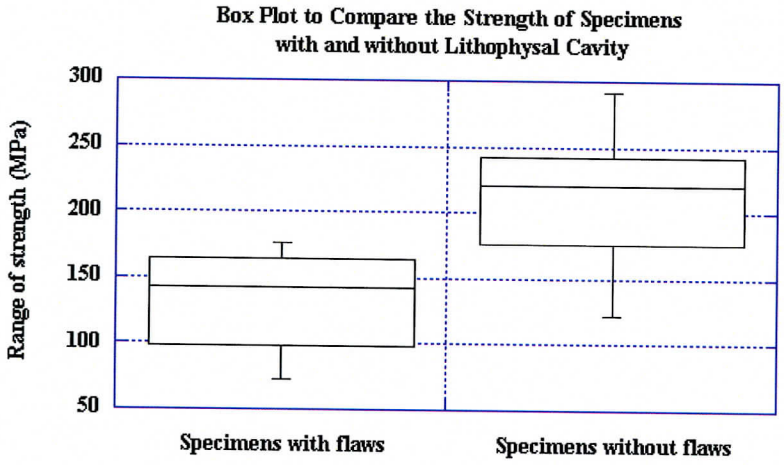

Figure 2.5 Strength of specimens with and without flaws, the former defined here as containing obvious lithophysal cavities with at least one dimension of at least about 0.6 inch. The box plots give a five-number summary for each case: lowest, lower fourth, median, upper fourth and highest strength.

Figure 2.6 Specimens with flaws (cavities)

Specimen length affects strength. Fig. 2.7 shows a plot of strength versus ratio of length to diameter. The strength decreases with an increase in length. As already mentioned the specimens of various lengths are randomly grouped for strain rate dependence studies. It is assumed that the length effect from group to group is cancelled out.

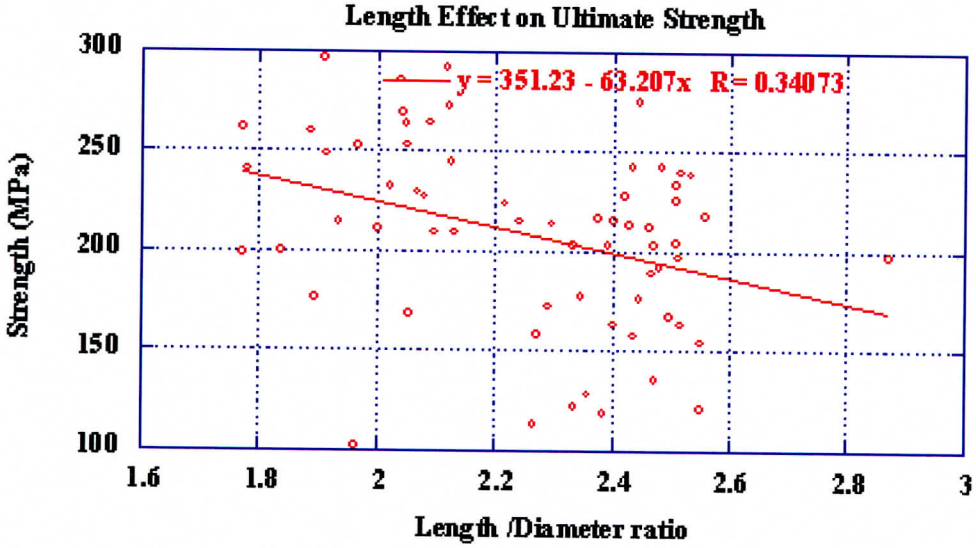

Figure 2.7 Effect of specimen length on strength

The ultimate strength is highly correlated to its corresponding ultimate axial strain. The correlation coefficient from specimens tested at a strain rate of $10^{-5}s^{-1}$ is as high as 0.95. As a result, the elastic moduli of the specimens evaluated at ultimate strength are much more constant than the strengths (Table 2.3). The ultimate strength of a specimen is mainly governed by ultimate axial strain. The ultimate axial strain is the value of the strain at the point of failure. The ultimate axial strain is in turn influenced by the flaws in the specimen. Even for the specimens that do not contain obvious flaws, small or hidden ones affect their strength. With an increase of the length of the specimen, the probability of containing hidden flaws in the specimen increases. This partially explains why the strength has a length effect (Hudson, 1993).

A relative increase of lateral strain compared to axial strain is found in the second half of the loading path for many tests. This is especially true shortly before the specimen fails. Fig. 2.8 gives stress-volumetric strain curves for three tests. A rapid decrease of volumetric strain rate exhibiting a weak dilatancy can be seen near the peak of each curve.

A slight strain rate dependent volumetric strain decrease with a decrease of logarithm of strain rate is illustrated in Fig. 2.9. This may indicate a time dependent dilatancy. Fifty three specimens with reliable lateral strain measurements have been used to construct this plot.

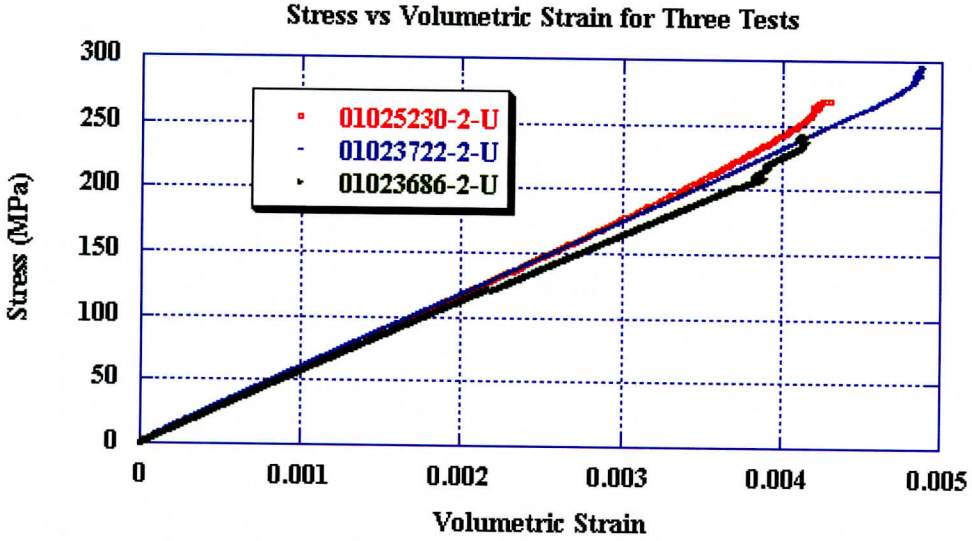

Figure 2.8 Axial stress versus volumetric strain curves for three tests showing dilatancy (Specimen IDs: 01025230-2-U, 01023722-2-U, 01023686-2-U)

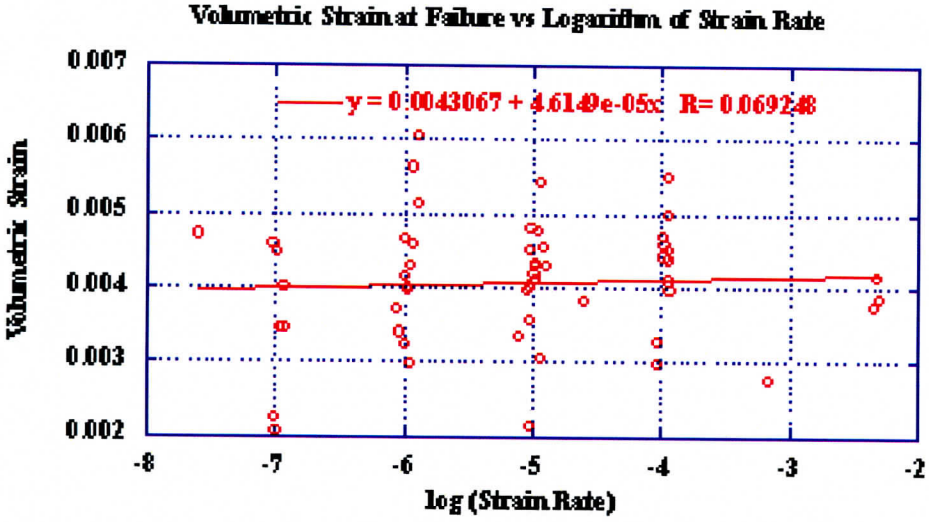

Figure 2.9 Volumetric strain at failure versus logarithm of strain rate

2.4 Analysis

Figs. 2.10, 2.11 and 2.12 give ultimate strength versus $\log \dot{\varepsilon}$ ($\dot{\varepsilon}$ is strain rate), ultimate axial strain versus $\log \dot{\varepsilon}$ and secant modulus at ultimate strength versus $\log \dot{\varepsilon}$. All three parameters decrease with decrease of $\log \dot{\varepsilon}$. A sensitivity analysis indicates that ultimate

strength is more sensitive to $\log\dot{\varepsilon}$ than the other two parameters. The sensitivity of ultimate strength to $\log\dot{\varepsilon}$ can be expressed as

$$S(\sigma_{\max}, \log\dot{\varepsilon}) = \frac{d\sigma_{\max}}{d\log\dot{\varepsilon}} \times \frac{\log\dot{\varepsilon}}{\sigma_{\max}} \tag{2.1}$$

The sensitivity of the ultimate axial strain to $\log\dot{\varepsilon}$, $S(\varepsilon_{max}, \log\dot{\varepsilon})$ and the sensitivity of the secant modulus to $\log\dot{\varepsilon}$, $S(E_S, \log\dot{\varepsilon})$ can be calculated similarly. It can be derived as shown in Eq. (2.2). Eq. (2.2) originates from the relation in Eq. (2.3). Eqs. (2.4) and (2.5) give the derivation.

$$S(\sigma_{\max}, \log\dot{\varepsilon}) = S(\varepsilon_{\max}, \log\dot{\varepsilon}) + S(E_S, \log\dot{\varepsilon}) \tag{2.2}$$

$$\sigma_{\max} = E_S \times \varepsilon_{\max} \tag{2.3}$$

Take derivatives on both sides in Eq. (2.3) with respect to $\log\dot{\varepsilon}$

$$\frac{d\sigma_{\max}}{d\log\dot{\varepsilon}} = \varepsilon_{\max} \times \frac{dE_S}{d\log\dot{\varepsilon}} + E_S \times \frac{d\varepsilon_{\max}}{d\log\dot{\varepsilon}} \tag{2.4}$$

Multiply $\frac{\log\dot{\varepsilon}}{\sigma_{\max}}$ on both sides of Eq. (2.4) and apply the relation in Eq. (2.3)

$$\frac{d\sigma_{\max}}{d\log\dot{\varepsilon}} \times \frac{\log\dot{\varepsilon}}{\sigma_{\max}} = \frac{dE_S}{d\log\dot{\varepsilon}} \times \frac{\log\dot{\varepsilon}}{E_S} + \frac{d\varepsilon_{\max}}{d\log\dot{\varepsilon}} \times \frac{\log\dot{\varepsilon}}{\varepsilon_{\max}} \tag{2.5}$$

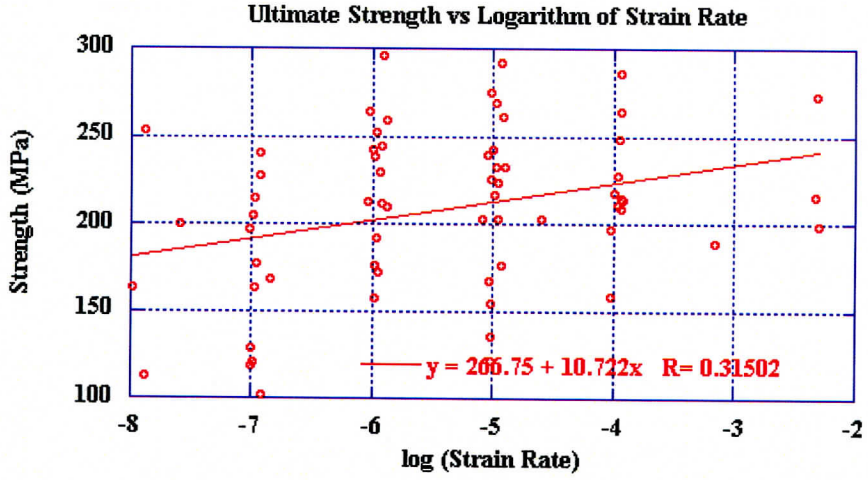

Figure 2.10 Ultimate strength versus $\log\dot{\varepsilon}$

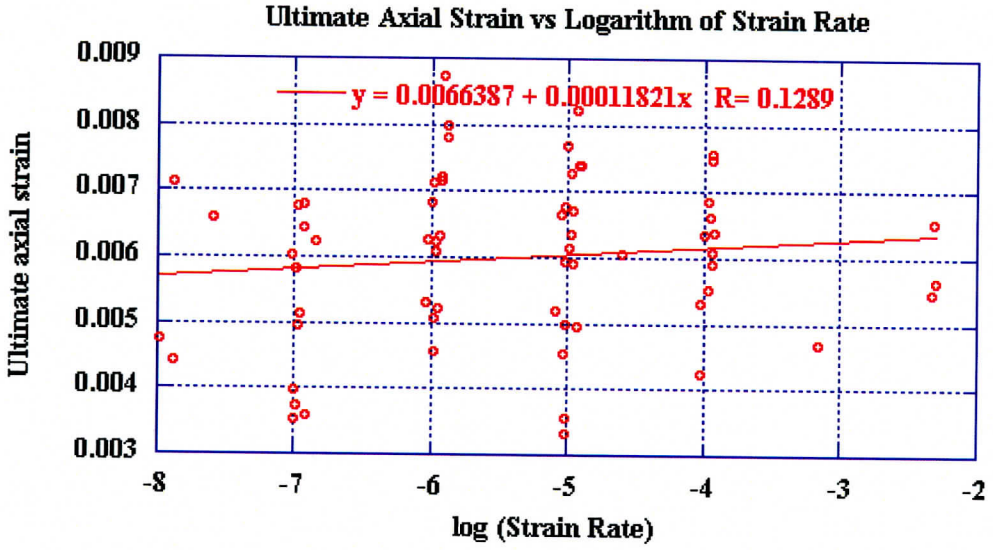

Figure 2.11 Ultimate strain versus $\log \dot{\varepsilon}$

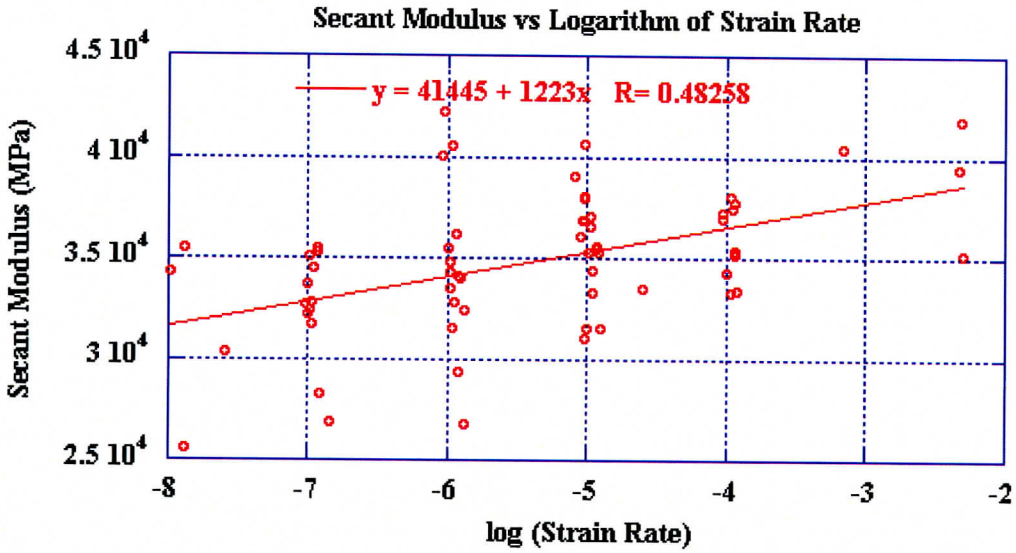

Figure 2.12 Secant modulus versus $\log \dot{\varepsilon}$

We propose a diagram that decomposes a strain component caused by strain rate effect from total strain (Fig. 2.13). With the aid of Fig. 2.13, it can be easily understood how the estimated equations in the Figs. 2.10, 2.11 and 2.12 interact. Assume a specimen has experienced a short-term test (high strain rate). Its σ-ε curve is shown as *O-A* in Fig. 2.13. If it experienced a long-term test (low strain rate), the σ-ε curve would be *O-B*. Compared with the short-term test, it would suffer a reduction in maximum stress, σ_{loss}, a reduction in maximum strain, ε_{loss}, and a secant modulus reduction. The secant modulus

reduction is the difference in slopes between dashed lines *O-A* and *O-B*. From Fig. 2.13, it can be seen that σ_{loss} is not caused by ε_{loss} alone, but is caused by a strain component between *B* and *C* as well. Since it is a time related strain component, we denote it by ε_{time}. This component is reflected in the secant modulus reduction indicated in Fig. 2.12. We are dealing with an extremely brittle rock. The time effect component results mainly from crack growth. For both short-term and long-term tests, the ultimate axial strain can be decomposed as

$$\varepsilon_{short} = \varepsilon_e + \varepsilon_{in} \tag{2.6}$$

$$\varepsilon_{long} = \varepsilon_e + \varepsilon_{in} + \varepsilon_{time} \tag{2.7}$$

where ε_e is an elastic strain component and ε_{in} an inelastic strain component.

In this study, $\varepsilon_{long} < \varepsilon_{short}$. The time effect strain component ε_{time} for each strain rate can be determined based on σ_{loss}, ε_{loss} and E_S (E_S must be evaluated at point *A*). The latter three parameters can be determined from the equations in Figs. 2.10, 2.11 and 2.12. The highest strain rate is used as a baseline. The three parameters σ_{max}, ε_{max} and E_S evaluated at the baseline are considered the limits as $t \rightarrow 0$.

$$\varepsilon_{time} = \frac{\sigma_{loss}}{E_S} - \varepsilon_{loss} \tag{2.8}$$

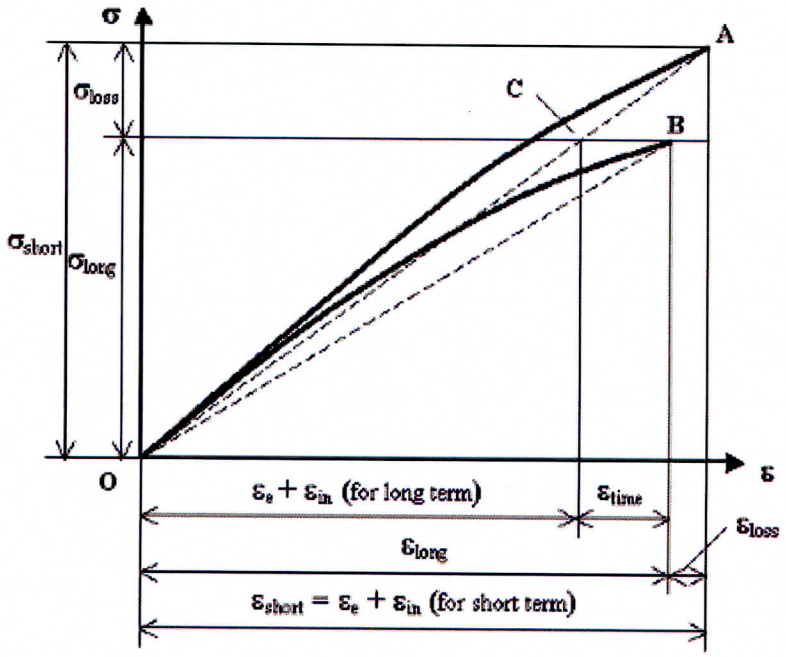

Figure 2.13 Diagram for strain rate dependent strain analysis. It helps calculate time effected strain component ε_{time}.

Applying the equations in Figs. 2.10, 2.11 and 2.12 as well as Eq. (2.8), a plot of the $\varepsilon_{time}/\varepsilon_{total}$ versus $\log \dot{\varepsilon}$ is obtained in Fig. 2.14, where ε_{total} is the total axial strain either for a short-term or a long-term case. This plot is a slightly convex upward curve. The time effect strain component increases with decreasing strain rate at a slightly increasing rate. This explains why the strength decreases with a decrease of the strain rate at a faster rate than the axial strain. When the strain rate decreases from 10^{-4} to $10^{-8} s^{-1}$, the time effect strain increases from 5.1% to 16.5% of the total axial strain.

The plot in Fig. 2.14 could be obtained in a different way: regress ultimate strength, ultimate axial strain and secant modulus on logarithm of time to obtain three equations, then use the three estimated equations and Eq. (2.8) to determine ε_{time}. Doing so a very close result would be obtained. This latter approach is somewhat more accurate since it eliminates two small errors. The first error comes from the strain rate approximation in Fig. 2.4, and the second from weak collinearities when regressing ultimate axial strain on $\log \dot{\varepsilon}$ and secant modulus on $\log \dot{\varepsilon}$.

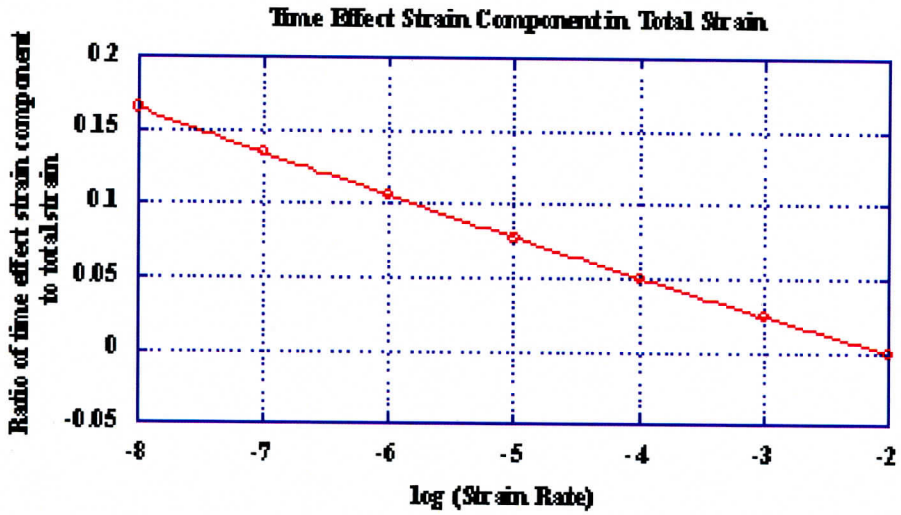

Figure 2.14 Ratio of time effect strain component to total axial strain versus $\log \dot{\varepsilon}$ (Non-Q, for information only).

2.5 Conclusions

Ninety three cylindrical rock specimens have been tested in uniaxial compression. Sixty five are selected for strain rate dependence study. We studied strain rate dependence of ultimate strength, ultimate axial strain and secant modulus evaluated at ultimate strength. We studied the correlation between ultimate strengths and ultimate axial strains, flaw effect of specimens, size effect of specimens, and strain rate dependence of volumetric strain change showing possible dilatancy. The following can be concluded:

1) Ultimate strength, ultimate axial strain and secant modulus are strain rate dependent. Strain rate dependent ultimate strength reduction is accounted for by ultimate axial strain reduction and secant modulus reduction. Secant modulus reduction reflects a strain component due to strain rate effect. The strain component caused by the strain rate effect is statistically and mathematically determinable. It can be approximately determined using the new method suggested in this study. For the tested welded tuff the strain rate effect strain component increases from 5.1% to 16.5% of the total axial strain when the strain rate decreases from 10^{-4} to 10^{-8} s^{-1}.

2) Ultimate strength is governed by ultimate axial strain. Ultimate axial strain is in turn dominated by the flaws contained in the specimen. A failure process is caused by fracture development initiated at flaws such as lithophysal cavities, vapor-phase altered spots, cracks, etc.

2.6 Recommendations

- Perform strain rate dependence at different moisture contents, at different temperatures, and under range of confining pressures.

- Make a more detailed investigation of the failure mode dependency on strain rate. Observations during testing clearly show that at lower strain rates specimens tend to break into a relatively small number of relatively large pieces (e.g. Fig. 2.3), while testing at very fast rates tends to break the specimens into a much larger number of much smaller fragments.

- Also most noticeable over the course of very fast testing is such tests generate a very large number of extremely small particles, i.e. a dust cloud.

- Fractography of the fragment surfaces might assist in clarifying the mechanics leading to failure (e.g. Ameen, 1995).

- The relation between strain rate and particle size distribution may deserve further investigation: it may provide deeper insight into the mechanics of in situ fragment size distribution (joint density or frequency) as a function of the velocity at which joints were formed (e.g. static versus dynamic (earthquakes)).

Table 2.1 Source information of all specimens for strain rate dependence study

(Note: all specimens were collected from middle nonlithophysal unit of Topopah Spring Tuff. This note is Non-Q, for information only.)

Serial #	Specimen ID	Borehole	Range in Borehole (ft)
1	01023358-U	ESF-MD-NICHE 4788#1	6.6-7.1
2	01023362-U	ESF-MD-NICHE 3107#7	11.6-12.1
3	01023367-1-U	ESF-MD-NICHE 3107#7	8.1-9.6
4	01023367-2-U	ESF-MD-NICHE 3107#7	8.1-9.6
5	01023370-1-U	ESF-MD-NICHE 3107#7	20.9-21.5
6	01023568-1-CU(U)	ESF-HD-WH-3	8.1-9.0
7	01023570-1-U	ESF-HD-WH-3	24.2-25.7
8	01023570-U	ESF-HD-WH-3	24.2-25.7
9	01023575-1-U	ESF-HD-WH-4	26.1-27.3
10	01023575-2-U	ESF-HD-WH-4	26.1-27.3
11	01023576-2-U	ESF-HD-WH-4	33.0-34.1
12	01023576-3-U	ESF-HD-WH-4	33.0-34.1
13	01023579-1-U	ESF-HD-WH-5	12.4-13.0
14	01023580-U	ESF-HD-WH-5	24.4-25.0
15	01023581-2-U	ESF-HD-WH-5	27.7-28.4
16	01023582-1-U	ESF-HD-WH-5	33.0-34.2
17	01023586-3-U	ESF-HD-WH-3	31.0-31.6
18	01023657-1-U	ESF-HD-WH-36	15.9-18.3
19	01023657-3-U	ESF-HD-WH-36	15.9-18.3
20	01023657-4-U	ESF-HD-WH-36	15.9-18.3
21	01023660-1-U	ESF-HD-WH-36	26.9-27.6
22	01023662-1-U	ESF-HD-WH-36	28.2-29.7
23	01023662-2-U	ESF-HD-WH-36	28.2-29.7
24	01023662-3-U	ESF-HD-WH-36	28.2-29.7
25	01023663-1-U	ESF-HD-WH-36	30.5-31.8
26	01023663-2-U	ESF-HD-WH-36	30.5-31.8
27	01023664-U	ESF-HD-WH-36	33.6-34.1
28	01023667-1-U	ESF-HD-WH-37	0.6-1.9
29	01023667-2-U	ESF-HD-WH-37	0.6-1.9
30	01023668-3-U	ESF-HD-WH-37	2.2-4.4
31	01023682-2-U	ESF-HD-WH-5	33.0-34.2
32	01023682-3-U	ESF-HD-WH-37	4.5-6.1
33	01023686-1-U	ESF-HD-WH-37	11.3-13.1
34	01023686-2-U	ESF-HD-WH-37	11.3-13.1
35	01023687-1-U	ESF-HD-WH-37	14.9-17.4
36	01023687-2-U	ESF-HD-WH-37	14.9-17.4
37	01023687-3-U	ESF-HD-WH-37	14.9-17.4

Table 2.1 (Continued)

38	01023689-2-U	ESF-HD-WH-37	19.6-21.1
39	01023690-1-U	ESF-HD-WH-37	22.7-23.7
40	01023691-1-U	ESF-HD-WH-37	26.7-27.5
41	01023691-2-U	ESF-HD-WH-37	26.7-27.5
42	01023692-U	ESF-HD-WH-37	21.7-22.2
43	01023694-1-U	ESF-HD-WH-37	31.3-32.5
44	01023694-2-U	ESF-HD-WH-37	31.3-32.5
45	01023695-1-U	ESF-HD-WH-37	34.9-35.8
46	01023695-2-U	ESF-HD-WH-37	34.9-35.8
47	01023697-1-U	ESF-HD-WH-50	4.8-6.0
48	01023697-4-U	ESF-HD-WH-50	4.8-6.0
49	01023701-1-U	ESF-HD-WH-50	11.9-13
50	01023702-2-U	ESF-HD-WH-50	15.1-16.2
51	01023702-3-U	ESF-HD-WH-50	15.1-16.2
52	01023703-1-U	ESF-HD-WH-50	16.5-17.3
53	01023703-2-U	ESF-HD-WH-50	16.5-17.3
54	01023706-1-U	ESF-HD-WH-50	19.7-20.5
55	01023707-1-U	ESF-HD-WH-50	11.9-13.0
56	01023707-2-U	ESF-HD-WH-50	22.7-24.0
57	01023707-3-U	ESF-HD-WH-50	22.7-24.0
58	01023722-2-U	ESF-HD-WH-50	35.9-36.9
59	01023732-U	ESF-HD-WH-26	10.9-11.3
60	01023740-1-U	ESF-HD-WH-26	20.9-22.2
61	01023740-2-U	ESF-HD-WH-26	20.9-22.2
62	01023743-1-U	ESF-HD-WH-26	23.2-24.0
63	01023745-1-U	ESF-HD-WH-26	24.5-25.1
64	01023747-1-U	ESF-HD-WH-26	25.7-26.8
65	01023747-3-U	ESF-HD-WH-26	25.7-26.8
66	01023749-2-U	ESF-HD-WH-26	30.0-30.9
67	01023750-U	ESF-HD-WH-26	31.4-31.8
68	01023751-1-U	ESF-HD-WH-26	33.0-33.7
69	01023754-2-U	ESF-HD-WH-32	4.7-5.7
70	01023760-1-U	ESF-HD-WH-37	22.7-23.7
71	01023760-2-U	ESF-HD-WH-37	22.7-23.7
72	01025224-1-U	ESF-HD-WH-32	27.2-28.8
73	01025224-3-U	ESF-HD-WH-32	27.2-28.8
74	01025225-1-U	ESF-HD-WH-32	28.9-29.9
75	01025225-2-U	ESF-HD-WH-32	28.9-29.9
76	01025226-1-U	ESF-HD-WH-32	32-33.1
77	01025227-1-U	ESF-HD-WH-32	33.8-35.6

Table 2.1 (Continued)

78	01025227-2-U	ESF-HD-WH-32	33.8-35.6
79	01025230-1-U	ESF-HD-WH-33	4.4-6.3
80	01025230-2-U	ESF-HD-WH-33	4.4-6.3
81	01025231-1-U	ESF-HD-WH-33	8.9-10.0
82	01025231-2-U	ESF-HD-WH-33	8.9-10.0
83	01025232-1-U	ESF-HD-WH-33	10.2-10.9
84	01025233-1-U	ESF-HD-WH-33	13.9-14.5
85	01025234-1-U	ESF-HD-WH-33	18.0-19.1
86	01025235-1-U	ESF-HD-WH-33	19.8-20.6
87	01025235-2-U	ESF-HD-WH-33	19.8-20.6
88	01025259-1-U	ESF-HD-WH-33	21.3-21.9
89	01025260-1-U	ESF-HD-WH-33	24.0-24.7
90	01025261-1-U	ESF-HD-WH-33	25.8-26.5
91	01025262-U	ESF-HD-WH-33	28.5-29.0
92	01025263-U	ESF-HD-WH-33	31.8-32.4
93	01025264-U	ESF-HD-WH-33	37.2-37.7

Note: the DTN for the specimen source information in this table is 018LM.001.

Table 2.2 Summary of all test results for all specimens in strain rate dependence study

Serial #	Specimen ID	Nominal diameter (in)	Length of Specimen (in)	Strain Rate (/s)	Strength (MPa)	Young's Modulus (GPa)	Poisson's Ratio	Moisture content (%)
1	01023358-U	1.78	4.17	1.38E-05	238.93	32.82	0.19	0.294
2	01023362-U	1.78	4.48	1.20E-05	108.79	35.48	0.2	0.390
3	01023367-1-U	1.78	4.30	9.85E-06	167.59	34.98	0.12	0.407
4	01023367-2-U	1.78	4.22	1.05E-05	110.36	34.41	0.14	0.444
5	01023370-1-U	1.78	4.15	1.29E-05	228.16	37.05	0.22	0.388
6	01023568-1-CU(U)	2.4	5.40	6.07E-06	140.85	46.46	0.21	0.534*
7	01023570-1-U	2.4	4.74	1.45E-05	142.12	22.77	N/A	0.742*
8	01023570-U	2.4	4.78	1.41E-05	98.35	28.32	0.25	0.653
9	01023575-1-U	2.4	4.23	1.33E-07	223.10	34.61	N/A	0.772*
10	01023575-2-U	2.4	4.71	1.35E-07	101.80	28.34	N/A	0.733*
11	01023576-2-U	2.4	5.66	1.08E-07	128.59	33.38	N/A	0.769*
12	01023576-3-U	2.4	6.04	1.10E-08	163.28	35.71	N/A	0.702*
13	01023579-1-U	2.4	5.93	1.11E-05	135.97	37.63	0.19	N/A
14	01023580-U	2.4	5.50	1.24E-06	172.00	34.10	0.19	0.706*
15	01023581-2-U	2.4	5.38	1.15E-07	183.54	35.25	N/A	0.648*
16	01023582-1-U	2.4	5.60	1.24E-05	202.98	33.66	0.19	0.744*
17	01023586-3-U	2.4	4.92	1.34E-08	253.29	36.47	N/A	0.721*
18	01023657-1-U	2.4	6.02	1.13E-05	233.16	37.14	0.17	0.727*
19	01023657-3-U	2.4	5.70	1.18E-05	216.95	35.58	0.16	0.796*
20	01023657-4-U	2.4	4.26	1.33E-05	261.63	36.18	0.18	0.620
21	01023660-1-U	2.4	4.93	1.32E-07	168.10	33.08	N/A	0.663*
22	01023662-1-U	2.4	6.02	1.15E-07	204.55	35.04	0.12	0.672
23	01023662-2-U	2.4	5.93	9.89E-06	203.36	37.64	0.16	0.783*

Table 2.2 (Continued)

24	01023662-3-U	2.4	5.67	1.44E-05	163.95	41.73	N/A	0.877
25	01023663-1-U	2.4	5.40	1.21E-05	275.96	34.94	0.18	0.701*
26	01023663-2-U	2.4	5.80	1.11E-08	173.21	36.55	N/A	0.811*
27	01023664-U	2.4	6.04	1.08E-05	239.62	36.39	0.18	0.788*
28	01023667-1-U	2.4	5.87	1.19E-06	176.63	38.96	0.15	0.616
29	01023667-2-U	2.4	5.21	1.39E-07	215.07	32.83	N/A	0.450*
30	01023668-3-U	2.4	5.44	1.36E-08	113.21	28.15	N/A	0.886*
31	01023682-2-U	2.4	6.12	1.16E-07	121.15	35.09	0.23	0.645
32	01023682-3-U	2.4	5.25	1.09E-05	142.7	34.15	0.16	N/A
33	01023686-1-U	2.4	4.72	1.28E-06	252.54	37.12	0.18	0.535
34	01023686-2-U	2.4	5.96	1.16E-06	242.43	36.16	0.16	0.494
35	01023687-1-U	2.4	5.87	1.05E-05	275.22	41.43	0.16	0.509
36	01023687-2-U	2.4	5.83	1.04E-06	213.02	40.36	0.16	0.636
37	01023687-3-U	2.4	4.27	1.31E-07	241.02	35.58	0.19	0.702
38	01023689-2-U	2.4	5.81	1.13E-04	228.02	35.45	0.16	0.825*
39	01023690-1-U	2.4	4.59	1.35E-04	248.61	36.44	0.15	0.561
40	01023691-1-U	2.4	4.53	1.43E-06	259.94	34.35	0.16	0.633
41	01023691-2-U	2.4	4.35	1.47E-05	172.71	31.14	0.19	0.812
42	01023692-U	2.4	5.51	1.18E-04	213.68	34.40	0.15	0.776*
43	01023694-1-U	2.4	4.69	1.12E-05	155.73	39.72	0.15	0.652
44	01023694-2-U	2.4	5.10	1.35E-06	244.80	34.44	0.18	0.640
45	01023695-1-U	2.4	5.30	1.11E-04	107.78	36.72	0.16	0.634
46	01023695-2-U	2.4	5.74	1.20E-05	203.02	36.00	0.13	0.680
47	01023697-1-U	2.4	5.38	1.37E-07	215.19	31.85	N/A	0.654*
48	01023697-4-U	2.4	5.76	1.26E-07	163.16	29.95	N/A	0.644*
49	01023701-1-U	2.4	5.84	1.16E-05	242.89	32.36	0.17	0.861*

Table 2.2 (Continued)

50	01023702-2-U	2.4	5.32	1.17E-05	223.90	34.48	0.15	0.769
51	01023702-3-U	2.4	5.94	1.25E-05	253.72	31.09	0.21	0.745
52	01023703-1-U	2.4	5.01	1.25E-04	264.53	35.07	0.15	0.753
53	01023703-2-U	2.4	4.64	1.31E-04	214.41	35.39	0.15	0.696
54	01023706-1-U	2.4	4.41	2.78E-08	199.89	31.12	0.12	0.877
55	01023707-1-U	2.4	5.95	1.17E-06	192.01	34.07	0.15	0.792
56	01023707-2-U	2.4	4.70	1.42E-07	143.24	29.14	0.16	0.757
57	01023707-3-U	2.4	4.85	1.33E-05	232.55	30.56	0.18	0.722
58	01023722-2-U	2.4	4.58	1.38E-06	296.47	35.75	0.19	0.645
59	01023732-U	2.4	5.60	9.80E-06	122.28	40.26	0.12	0.479
60	01023740-1-U	2.4	6.02	1.09E-05	225.33	38.02	0.15	0.654
61	01023740-2-U	2.4	5.92	1.00E-05	121.69	35.94	0.11	0.758
62	01023743-1-U	2.4	6.00	1.05E-05	167.47	37.59	N/A	0.766
63	01023745-1-U	2.4	6.04	1.05E-05	157.69	35.93	0.17	0.618
64	01023747-1-U	2.4	4.92	1.24E-06	264.26	35.91	0.15	N/A
65	01023747-3-U	2.4	4.80	1.15E-04	210.88	39.28	0.16	N/A
66	01023749-2-U	2.4	5.84	1.15E-06	157.6	37.24	0.21	0.767
67	01023750-U	2.4	4.54	1.21E-05	176.52	38.1	0.18	0.688
68	01023751-1-U	2.4	5.63	1.16E-07	176.95	34.51	0.17	0.597
69	01023754-2-U	2.4	4.45	1.40E-06	152.53	28.94	0.15	0.856
70	01023760-1-U	2.4	6.94	1.02E-05	126.12	34.08	0.13	0.855
71	01023760-2-U	2.4	5.45	9.85E-05	158.24	39.36	0.15	0.833
72	01025224-1-U	2.4	5.03	1.32E-04	209.32	35.06	0.12	0.845
73	01025224-3-U	2.4	6.12	1.06E-05	154.49	35.03	0.18	0.772
74	01025225-1-U	2.4	6.03	1.05E-04	196.68	37.47	0.17	0.759
75	01025225-2-U	2.4	6.14	1.16E-04	217.53	33.85	0.13	0.793

Table 2.2 (Continued)

76	01025226-1-U	2.4	4.99	1.29E-07	227.37	35.32	0.20	0.674
77	01025227-1-U	2.4	5.92	9.65E-04	189.27	38.93	0.2	0.684
78	01025227-2-U	2.4	4.25	8.85E-03	198.7	41.62	0.17	0.813
79	01025230-1-U	2.4	5.11	1.47E-06	209.46	29.28	0.12	0.744
80	01025230-2-U	2.4	4.90	1.16E-05	269.62	37.19	0.18	0.692
81	01025231-1-U	2.4	6.10	1.04E-05	142.85	35.72	0.16	0.670
82	01025231-2-U	2.4	6.67	8.72E-06	72.86	30.87	N/A	0.880
83	01025232-1-U	2.4	5.76	7.45E-03	215.84	38.22	0.15	0.743
84	01025233-1-U	2.4	6.89	1.01E-07	197.48	32.73	0.11	0.723
85	01025234-1-U	2.4	5.08	1.30E-05	291.64	36.32	0.16	1.039
86	01025235-1-U	2.4	4.89	1.24E-04	285.88	37.41	0.14	0.789
87	01025235-2-U	2.4	4.96	1.30E-06	229.75	35.87	0.16	0.661
88	01025259-1-U	2.4	6.08	1.10E-06	238.26	37.43	0.17	0.711
89	01025260-1-U	2.4	5.91	1.33E-06	212.17	32.86	0.14	0.718
90	01025261-1-U	2.4	5.61	1.07E-04	133.74	36.15	0.13	0.735
91	01025262-U	2.4	5.09	5.43E-03	272.85	43.22	0.17	0.727
92	01025263-U	2.4	6.62	8.75E-06	98.27	36.79	0.11	0.943
93	01025264-U	2.4	5.72	1.09E-07	119.22	35.42	0.15	0.775

Note: the DTN for the specimen information in this table is 018LM.001

* Moisture content is measured after testing.

CHAPTER 3 CREEP TESTING IN UNIAXIAL COMPRESSION

3.1 Introduction

Fourteen specimens have been tested in uniaxial creep. The specimens were collected from the middle nonlithphysal (Tptpmn), lower lithophysal (Tptpll) and lower nonlithophysal (Tptpln) units of Topopah Spring Tuff formation (Table 3.1).

Table 3.1 Source information of test specimens

Specimen ID	Borehole	Range in borehole (ft)	Unit
01014949-1-CU	UE-25 UZ#16	543.6-544.3	Tptpmn
01014951-1-CU	UE-25 UZ#16	545.0-546.2	Tptpmn
01014951-2-CU	UE-25 UZ#16	545.0-546.2	Tptpmn
01014733-2-CU	UE-25 UZ#16	817.9-818.8	Tptpll
01014756-1-CU	USW WZ-14	828.8 - 829.4	Tptpmn
01015022-1-CU	USW SD-12	737.6-738.6	Tptpmn
01015022-2-CU	USW SD-12	737.6-738.6	Tptpmn
01015465-CU	USW SD-12	1118.5-1118.8	Tptpln
01023361-1-CU	ESF-MD-NICHE 3107#7	10.6-11.4	Tptpmn
01023363-1-CU	ESF-MD-NICHE 3107#7	12.1-13.6	Tptpmn
01023363-3-CU	ESF-MD-NICHE 3107#7	12.1-13.6	Tptpmn
01023364-1-CU	ESF-MD-NICHE 3107#7	13.6-14.6	Tptpmn
01023582-3-CU	ESF-HD-WH-5	33.0 – 34.2	Tptpmn
01023665-2-CU	ESF-HD-WH-36	34.6-35.8	Tptpmn

Note: the DTN for the specimen information in this table is 018LM.003. The Unit column is Non-Q, for information only.

The purpose of creep testing is to study the long-term mechanical behavior of rock specimens under constant load. For a constant temperature, strain rate can be expressed as a function of stress level and time. A commonly recognized creep curve is shown in Fig. 3.1. Three stages describe the creep history: primary (transient), secondary (steady-state) and tertiary (accelerating) creep. In the primary creep, the specimen deforms at a decreasing strain rate. After this stage the strain rate tends to remain constant at a certain value, i.e. the test transits to the secondary stage. When the deformation of the specimen reaches a critical threshold value, the tertiary stage starts. After a short time, the specimen breaks.

For brittle rock, especially for rocks with extremely variable mechanical properties such as Yucca Mountain tuffs, it is difficult to predict the ultimate strength of a specimen. Thus it is difficult to complete a creep test in one stress level, because it is difficult to select a stress level that will assuredly give creep without instantaneously leading to failure. In this study, multiple stress levels are applied to each specimen until it fails. Each stress level is maintained for at least three days. The stress level increment ranges from 7 to 10 MPa. The tests took from 2 to 17 stress steps. All the tests are performed

under uniaxial compression at room temperature and humidity. The longest test lasted 1644.4 hours (68.5 days). Fig. 3.2 shows the complete stress-time and strain-time curves for the test 01023664-1-CU. The strain-time and stress-strain curves for other tests are shown in Figs. 3-I-1 through 3-I-13 in Appendix I.

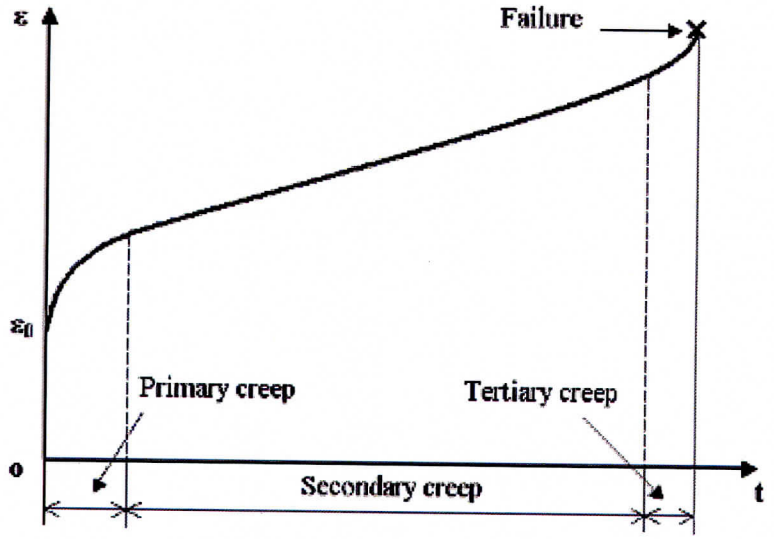

Figure 3.1 A commonly recognized creep curve (e.g. Jaeger and Cook, 1979, Fig. 11.1.1; Goodman, 1989, Fig. 6.16)

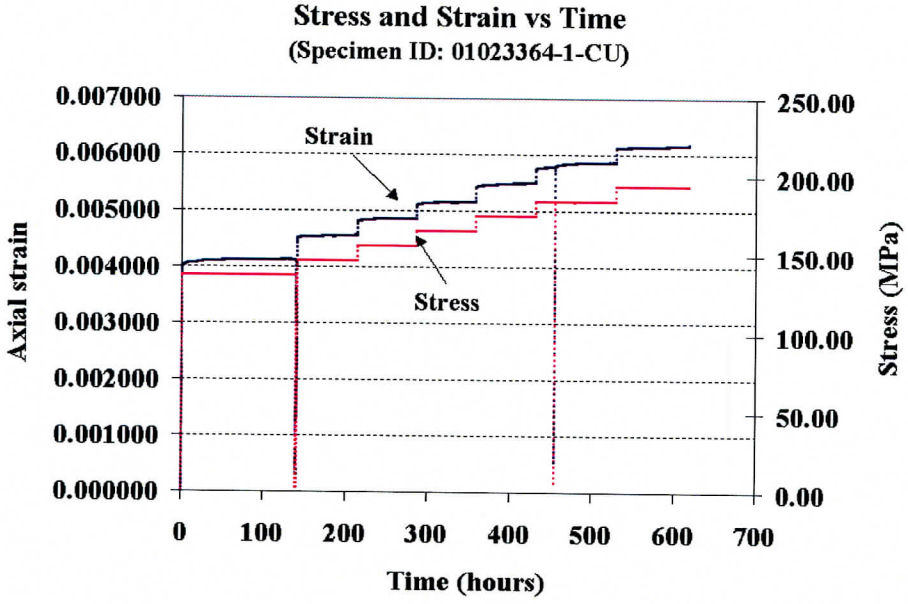

Figure 3.2 Experimental stress-time and strain-time curves for test 01023364-1-CU (from Tptpmn)

3.2 Experimental description

The specimens are selected so that they do not contain major lithophysae or visible fissures. Vapor-phase altered spots are common among the rock cores. Small vapor-phase altered inclusions are allowed in the specimens for creep testing. Fig. 3.3 shows a typical specimen used for a creep test, illustrating that a "flawless" specimen is "flawless" only when compared to a lithophysal sample, certainly not when compared to a uniform fine grained limestone or granite.

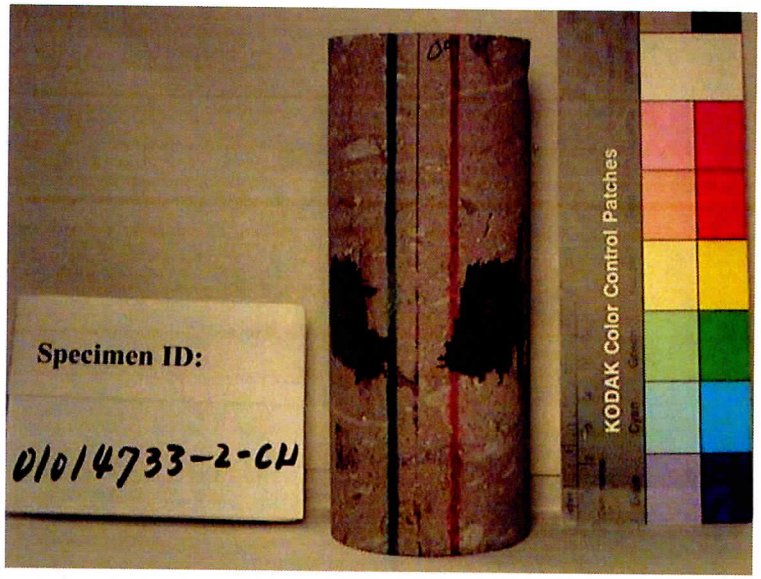

Figure 3.3 A typical specimen for creep testing, with strain gages installed (Specimen ID: 01014733-2-CU, from Tptpll)

All the test specimens are cut to a ratio of length to diameter of 1.9 – 2.5 (Table 3.2), to approximately meet ASTM D 4543-85. Moisture contents are measured after testing. Table 3.2 gives a summary of the test specimen geometries and moisture contents.

Strain is measured using 120-ohm electric resistance strain gages for most tests. For one test strain is measured using extensometers for the first half of the test and then with strain gages for the second half. For another test strain is measured using both extensometers and strain gages. When using extensometers, two axial ones are installed. The results are calculated by taking the average of the two measurements. Lateral strain is not measured in this case. For tests with strain gages, usually six strain gages are used. Four measure axial strain. Two measure lateral strain. All strain gages are cemented at about midheight of the specimen (Fig. 3.3). Strain in each direction is calculated by taking the average of all measurements in that direction.

Thermocouples are used to monitor the temperature for most of the tests. Significant temperature variation is observed. This is also reflected by strain gage measurements. The temperature variation comes from three sources: 1) alternation of days and nights; 2)

accumulated heat generated by the testing machine; 3) unexpected adjustment of room air conditioning. Of the above, 1) accompanied all the tests. The 3) happened several times during the creep testing. Seasonal temperature change is not obvious. Temperature change impairs strain gage readings. Not only does it affect the strain gage itself, but it affects the test specimen as well. In fact, the temperature effect on specimens is more serious than the one on strain gages (this can be observed by checking extensometer measurements). The deformations of both specimen and strain gage are recorded by the strain gage measurement. Applying the temperature-correction equations provided by the manufacturer of the strain gages to correct the strain gage measurements only eliminates the part of temperature effect accounted for by the strain gages. As a consequence a complementary measure is adopted. Each load step is maintained for not less than three days. Then it is not difficult to get a reasonable curve fitting for strain rate to eliminate the effects of temperature cycles.

Table 3.2 Summary of test specimen geometry and moisture content

Specimen ID	Diameter (in)	Length (in)	L/D ratio	Moisture content (%)
01014949-1-CU	2.39	5.95	2.5	0.29
01014951-1-CU	2.39	5.93	2.5	0.32
01014951-2-CU	2.39	4.55	1.9	0.30
01014733-2-CU	2.40	5.92	2.5	0.25
01014756-1-CU	2.41	5.24	2.2	0.47
01015022-1-CU	2.41	5.36	2.2	0.59
01015022-2-CU	2.41	5.61	2.3	0.47
01015465-CU	2.40	4.57	1.9	N/A
01023361-1-CU	1.78	4.21	2.4	0.41
01023363-1-CU	1.78	4.14	2.3	0.45
01023363-3-CU	1.78	4.05	2.3	0.42
01023364-1-CU	1.78	4.15	2.3	0.43
01023582-3-CU	2.40	5.71	2.4	0.72
01023665-2-CU	2.40	4.89	2.0	0.71
				Average: 0.45%

Note: the DTN for the specimen information in this table is 018LM.003.

3.3 Test results and Analysis

As shown in Table 3.3, the first stress levels are set at from 30% to 90% of the ultimate strengths of the specimens. Fig. 3.4 gives a stepwise strain-time curve under multiple constant stresses.

In a stepwise strain-time curve like the one in Fig. 3.4, primary creep and secondary creep exist at every stress level. In the last stress level, typically all three stages exist. For the special case where the specimen has been highly damaged, the secondary stage may not develop. A strain-time curve for one stress level in this study is shown in Fig. 3.5.

Table 3.3 Summary of all the creep tests

Specimen ID	Test duration (hours (days))	Number of stress levels	First stress level (MPa)	Ultimate strength (MPa)	First stress level/Ultimate strength
01014949-1-CU	480.7 (20.0)	6	62.17	96.74	0.6
01014951-1-CU	510.7 (21.3)	6	62.01	89.65	0.7
01014951-2-CU	332.1 (13.8)	2	55.09	61.98	0.9
01014733-2-CU	73.4 (3.1)	2	93.19	103.53	0.9
01014756-1-CU	655.4 (27.3)	7	61.16	91.75	0.7
01015022-1-CU	1644.4 (68.5)	13	61.05	187.45	0.3
01015022-2-CU	232.0 (9.7)	2	61.14	152.98	0.4
01015465-CU	287.7 (12.0)	3	102	143.93	0.7
01023361-1-CU	213.3 (8.9)	4	93.74	112.47	0.8
01023363-1-CU	1206.3 (50.3)	13	93.79	168.77	0.6
01023363-3-CU	1609.6 (67.1)	17	87.49	187.49	0.5
01023364-1-CU	617.7 (25.7)	7	137.53	193.77	0.7
01023582-3-CU	637.0 (26.5)	7	159.67	200.79	0.8
01023665-2-CU	1132.9 (47.2)	12	102	195.29	0.5

Note: the DTN for the specimen information in this table is 018LM.003.

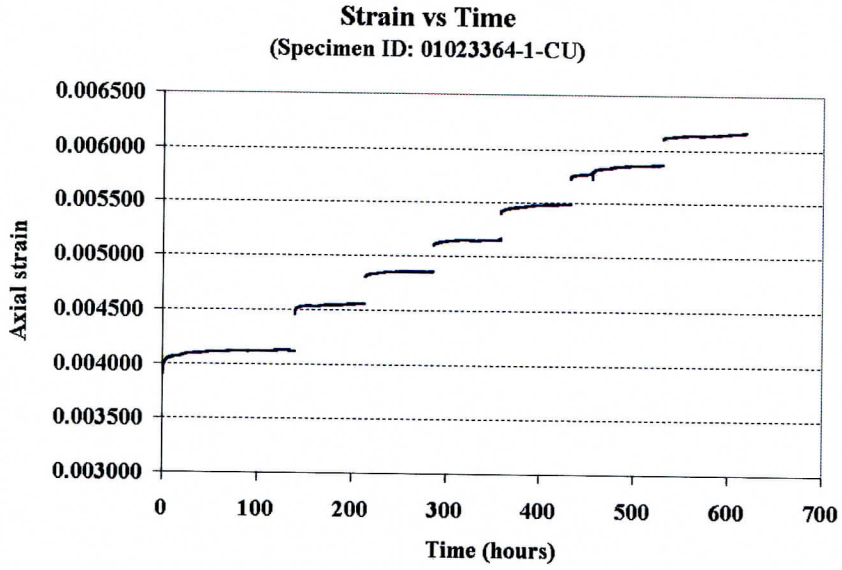

Figure 3.4 A stepwise experimental creep curve under multiple constant stresses (Specimen ID: 01023364-1-CU)

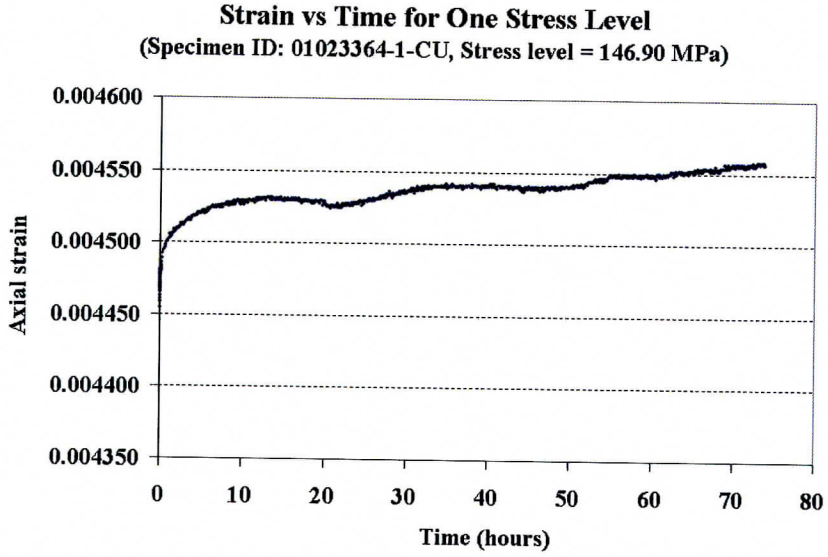

Figure 3.5 Experimental strain-time curve for one stress level (Specimen ID: 01023364-1-CU, Stress level = 146.90 MPa)

3.3.1 Primary creep

The primary creep stage normally takes 7 to 25 hours to complete. Fig. 3.6 shows an experimental strain-time plot and a fitting curve. For almost every stress level the strain-time primary creep stage observed in this study can be fit with an equation of the form

$$\varepsilon_{pr} = \varepsilon_0 + \alpha t^{\beta} \tag{3.1}$$

where ε_0 is the initial axial strain, α and β are constants. In the equation of the fitting curve in Fig. 3.6, α and β take the values of 4.67×10^{-5} and 0.22, respectively.

Taking the derivative of Eq. (3.1) with respect to time t, the strain rate for the primary creep is obtained as

$$\dot{\varepsilon}_{pr} = \alpha \times \beta \times t^{\beta - 1} \tag{3.2}$$

Eq. (3.2) has the same form as the empirical law for salt proposed by Andrade (1910) that was quoted by Dusseault (1993, p. 121) for primary creep. In Andrade's study, the exponent of t takes the value of –2/3. When Cruden (1974, p. 68) used Griggs' data for alabaster creep tests (1940) to fit the strain-time curve for primary creep, he found the same function as Eq. (3.2).

Applying Eq. (3.2), the strain rate during primary creep is calculated. The strain rate as a function of time is plotted in Fig. 3.7. The secant elastic modulus (determined from dividing axial stress by axial strain)-time curve is plotted in the same coordinate system.

As time goes on, both parameters decrease following the similar functions and at the similar trends. At the end of the stage, secant modulus-time curve stabilizes at a constant slope, strain rate-time curve tends to be flat. From this view it can be concluded that elastic modulus is highly related to strain rate in primary creep.

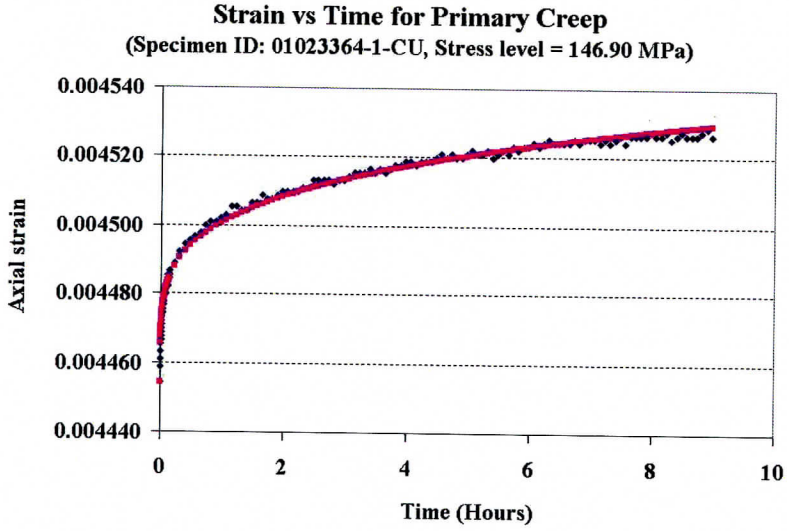

Figure 3.6 Experimental strain-time curve for primary creep and fitting curve (Specimen ID: 01023364-1-CU, Stress level = 146.90 MPa)

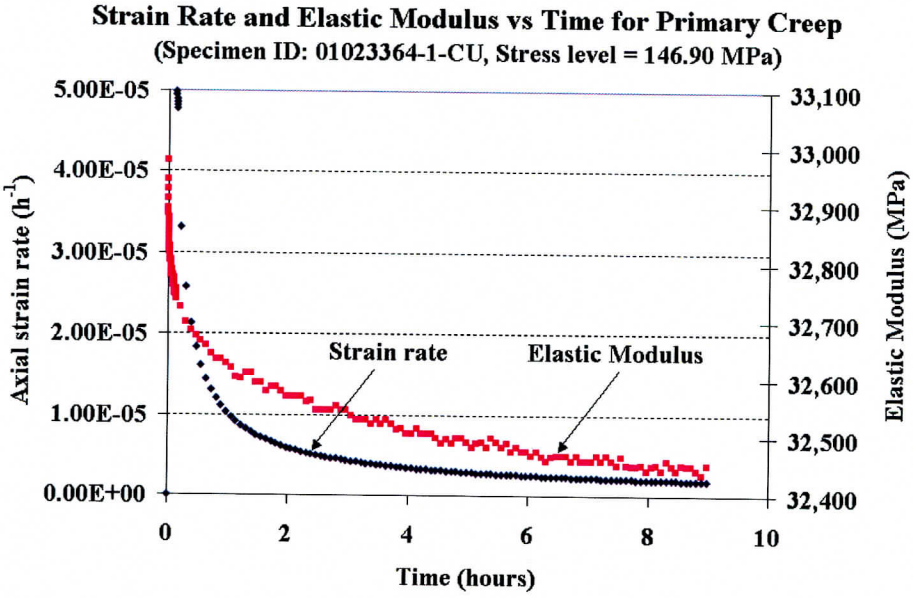

Figure 3.7 Strain rate-time and secant modulus-time curves for primary creep (Specimen ID: 01023364-1-CU, Stress level = 146.90 MPa)

Immediately after a load is applied or increased, axial stress in a specimen increases to a higher level. Meanwhile, the axial strain in the specimen increases with a high initial rate, this strain rate decelerates quickly with time, and following Eq. (3.2). Consequently the elastic modulus decreases with time until it stabilizes at an approximately constant value. This value is approximately the same for all stress levels within the elastic limit of the specimen. There might be complicated mechanisms in micro scale, which cause the primary creep, but the problem could be simplified if we consider the elastic modulus as a reflection of them. We can use the elastic modulus as an indicator of strain rate development in primary creep. It is widely believed that cracking is the mechanism responsible for creep of brittle rock (Costin, 1985, p. 26; Scholz, 1968b, p. 3300). However, it is still quite uncertain whether the three creep stages result from the same mechanism. In a study of time-dependence of quartz, Martin (1972, p. 1416) found that time-dependent cracking has an initial period of rapidly decelerating growth followed by what might be interpreted as a steady-state segment if the test is short. To prove that primary creep is dominated by microfracturing systematic experiments for brittle rocks are needed.

Picking the axial stress and axial strain at the transition point between primary and secondary creep for each stress level, plotting these points in a stress-strain coordinate, and connecting these points, forms the boundary between primary and secondary creep for each stress level (Fig. 3.8).

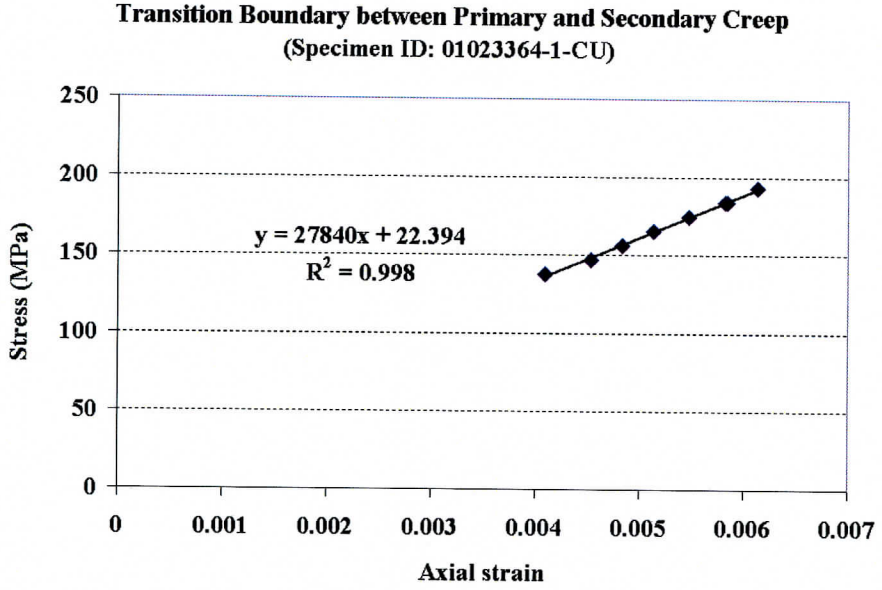

Figure 3.8 Plot of stress-strain magnitudes at which the transition takes place from primary to secondary creep at seven stress levels (Specimen ID: 01023364-1-CU)

Below the elastic limit, the plot, as shown in Fig. 3.8, appears approximately linear. To the upper-left side of the boundary, primary creep exists. To the lower-right of it, secondary creep takes place. Fig. 3.9 gives an example in which a nonlinear part occurs at

the end of the stress-strain plot. As shown in Fig. 3.9, the three points at the end of the plot deviate from the straight trend, indicating that the stress level has reached the tertiary creep level. This occurs when the specimen is near to failure. Before a specimen fails, a larger strain is generated. The elastic limit is exceeded. The rock is no longer elastic. Fig. 3.10 illustrates the transition boundary (AB) between primary and secondary creep, which describes how Figs. 3.8 and 3.9 are obtained.

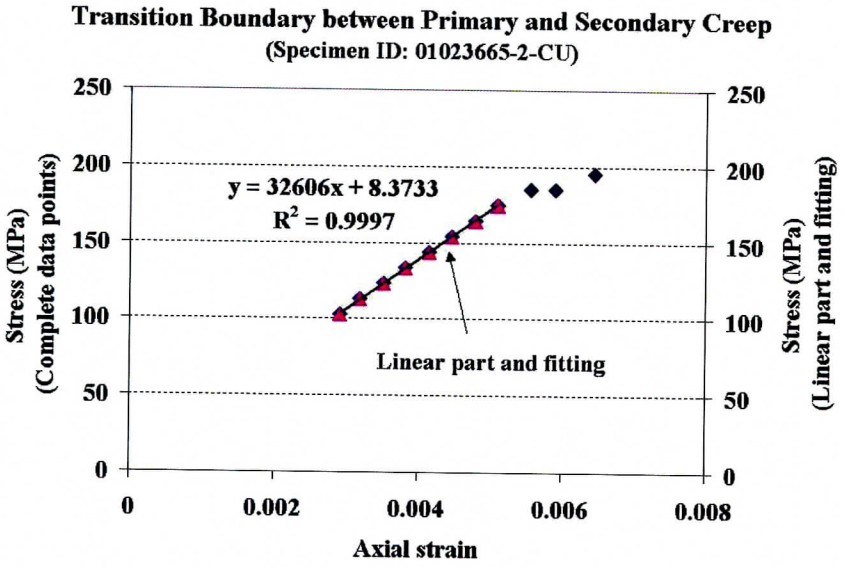

Figure 3.9 Plot of stress-strain position at which the transition takes place from primary to secondary creep at twelve stress levels (Specimen ID: 01023665-2-CU, from Tptpmn). At the highest stress levels tertiary creep has been reached.

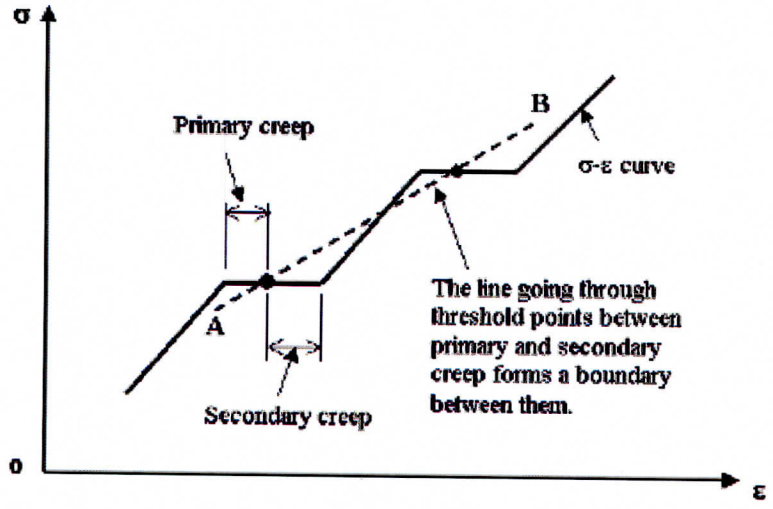

Figure 3.10 Diagram showing the stress-strain curve for creep under stepwise loading and the boundary (AB) between primary and secondary creep

3.3.2 Secondary creep

In this study the secondary creep is maintained from 2 to 7 days. Over this time the strain-time curves are approximately linear. Because of the temperature changes, only those strain-time curves are used from stress levels at which the secondary creep part has been maintained for at least three days. The slope of the straight line fit to a strain-time curve is the strain rate. Fig. 3.11 shows an example of how we obtained a strain rate for a secondary creep at a given stress level.

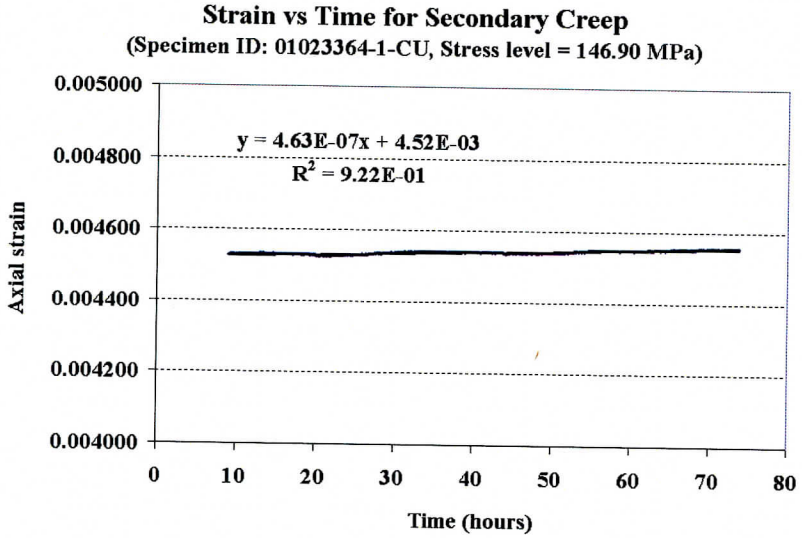

Figure 3.11 Experimental strain-time curve for secondary creep and best fit straight line (Specimen ID: 01023364-1-CU, Stress level = 146.90 MPa)

The strain rate cannot be calculated for some stress levels. This includes situations where: 1) the stress level was maintained constant for too short a time, i.e. less than three days; 2) temperature varies significantly, especially at the end of a strain-time curve; 3) test specimen was previously loaded higher than the current stress level. To study the stress dependence of a strain rate, a scatter plot of strain rate versus stress level is shown in Fig. 3.12.

A clear trend can be observed in Fig. 3.12. In this test, the starting stress is about 70% of the ultimate strength. If a starting stress is sufficiently low, the pattern of the strain rate-stress plot tends to be different (Figs. 3.13 and 3.14). Figs. 3.13 and 3.14 indicate that the points representing strain rate versus stress level show more scatter at low stress (left side of dashed lines). When the axial stress reaches a certain level, the distribution of the points follows the same trend as in Fig. 3.12. This trend can be described as a type of power function. The dashed lines are visually drawn boundaries. A critical stress level must be applied to define this boundary. Martin (1972) pointed out that above approximately half to two-thirds of the compressive strength, the dominant mode of deformation becomes the opening and subsequent growth of axial cracks. Martin (1972)

also referenced several authors (including Peng, 1970, Wawersik, 1968, Wawersik and Brace, 1971) who have shown that in granite microfracturing starts when the rock is stressed to about 60 % of its strength. This critical stress can be related to the critical stress intensity factor or fracture toughness, K_{IC} which is a material constant. K_{IC} is the maximum value of the stress intensity factor K_I for mode I (opening mode) crack.

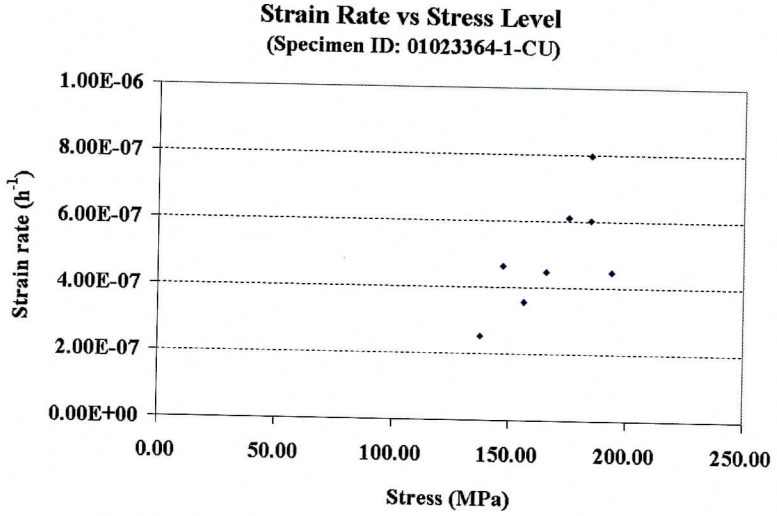

Figure 3.12 Plot of strain rate as a function of stress level showing stress dependence of secondary creep strain rate (Specimen ID: 01023364-1-CU)

Fig. 3.13 shows an example of a curve fit with the power function. Eq. (3.4) is rewritten from the one in Fig. 3.13, with real variables where $\dot{\varepsilon}_S$ denotes the strain rate during secondary creep. This equation agrees closely with the finding made by a number of investigators, which was quoted by Scholz (1968b, p. 3299): creep rate can often be given as a power function of stress, with the exponent greater than unity for moderate stresses and near unity for very small stresses. In a study of static fatigue of rock salt under uniaxial compression, Cruden (1974, p. 70) proposed the same form as Eq. (3.4) for the strain rate-stress relationship, where the exponent of σ is 2.7.

$$\dot{\varepsilon}_S = 8\times10^{-18}\times\sigma^{4.98} \tag{3.4}$$

To obtain an accurate function, more tests are needed. The strain rate at each stress level may depend on its entire creep history. If this is true, a relation obtained for strain rate and stress level under stepwise loading creep test may not be valid for predicting the time-dependence of a different specimen.

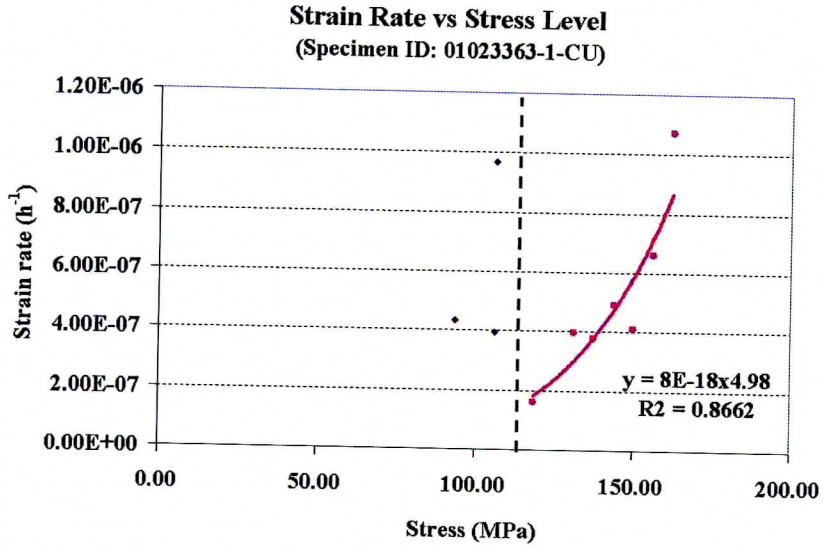

Figure 3.13 Plot of secondary creep strain rate as a function of stress level showing stress dependence of strain rate (Specimen ID: 01023363-1-CU, from Tptpmn)

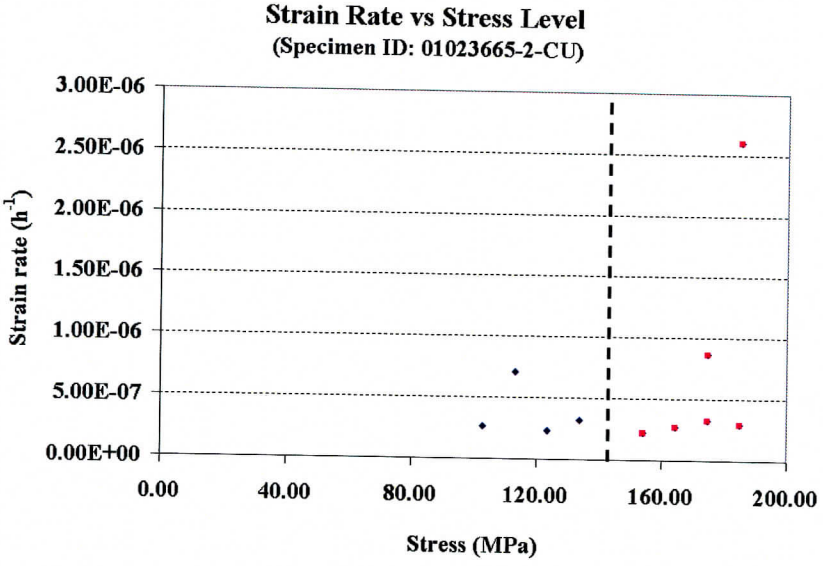

Figure 3.14 Plot of secondary strain rate as a function of stress level showing stress dependence of strain rate (Specimen ID: 01023665-2-CU)

3.3.3 Tertiary creep and specimen damage

This creep stage occurs during the final stress level for each test. However, when a specimen fails during or right after a loading increase, this stage may not occur. Tertiary creep progresses relatively quickly. It usually lasts for no longer than two hours. Fig. 3.15, which includes all three creep stages, is an example showing this stage. The tertiary

creep generates a large strain. At this stage, the elastic limit of the rock has been exceeded. Scholz (1968a), Cruden (1974), and Kranz and Scholz (1977, p. 4893) believed that tertiary creep starts when a critical crack density is reached. At this stage the specimen has been damaged to such an extent that it can no longer resist the applied load elastically. Once a rock has entered this stage it inevitably fails unless it is unloaded (Kranz and Scholz, 1977, p. 4893). Cruden (1974, p. 69) referenced the works by Potts (1964) and Hedley (1965). In their studies the strain before the onset of tertiary creep is considered as safe strain. To some extent, determining the critical point where the tertiary creep starts is more important than to study the detailed process of the tertiary creep stage. However, without a good understanding of the creep process in this stage, determining the critical point might be difficult.

Fig. 3.16 shows an example in which the secondary creep does not occur. The tertiary creep immediately follows the primary creep. Due to specimen damage, the primary creep is very short. This tertiary stage starts during the last loading step. It develops at the same time as the primary creep stage. The secondary creep does not occur.

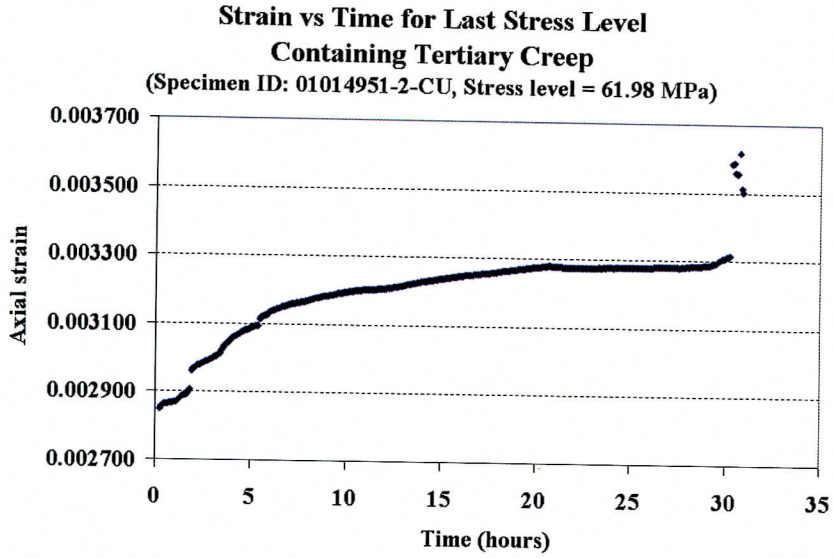

Figure 3.15 The last stress level, containing all three creep stages (Specimen ID: 01014951-2-CU, from Tptpmn)

Fig. 3.17 shows a case in which the tertiary creep starts during a loading increment. Its development progresses over the entire stress level. The creep curve in this case seems more complicated.

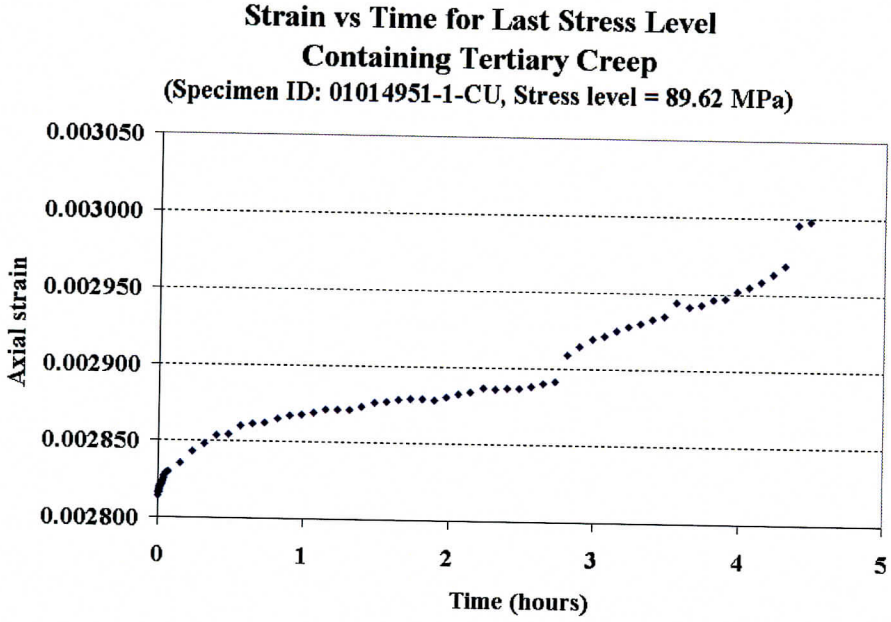

Figure 3.16 The last stress level, containing primary and tertiary creep only (Specimen ID: 01014951-1-CU, from Tptpmn)

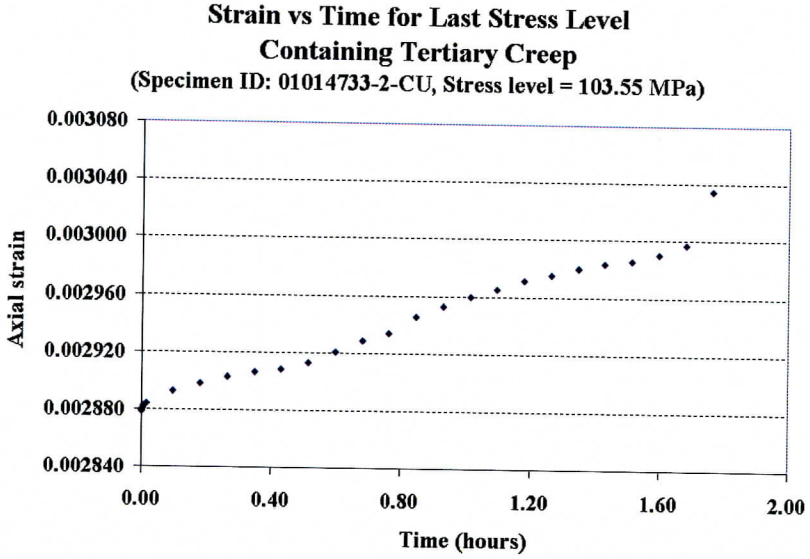

Figure 3.17 The last stress level showing that the tertiary creep develops over the course of an entire constant stress level. This case seems more complex (Specimen ID: 01014733-2-CU).

Between secondary and tertiary creep, there must exist another critical transition point. This point is analogous to the yield point for ductile materials. Beyond this point, the specimen loses its elasticity and enters a process where brittle failure develops.

Significant permanent deformation can start long before the tertiary creep obviously begins. The evidence can be found from Fig. 3.9 in which the nonlinear part of the stress-strain curve indicates a significant damage in the specimen. The critical points where deviations occur from the straight trend indicate that larger strains are generated. Fig. 3.18 is another example of such a case. A strain jump occurs at one point during the 175 MPa stress level. The last stress level for this specimen, i.e. the stress at which the specimen has failed, is 187.49 MPa.

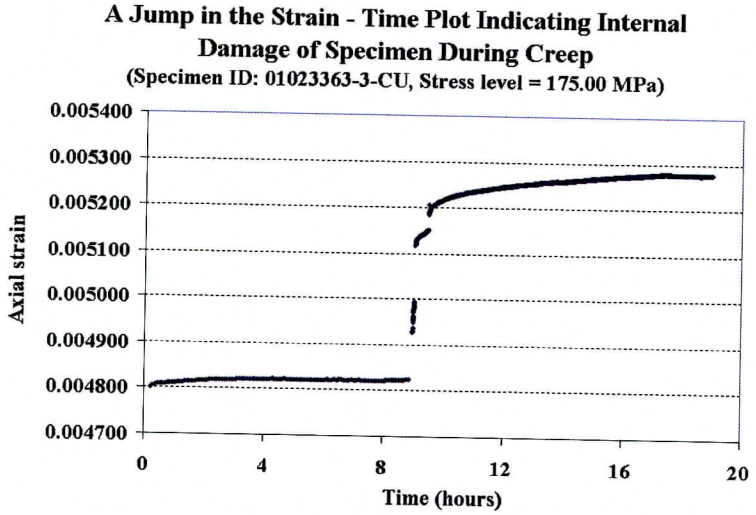

Figure 3.18 Internal damage of a specimen reflected in the strain-time curve at the next to last loading step in a series of constant axial stress steps (Specimen ID: 01023363-3-CU, from Tptpmn)

3.4 Significant findings:

1) **Transition from primary to secondary creep**. The transition points for each stress level define a boundary between primary and secondary creep. Elastic modulus is an indicator for this boundary. Whenever the load is increased to a higher level, primary creep starts developing. During this process, the elastic modulus decreases and tends to be stable. Below the elastic limit of a specimen, the elastic modulus does not vary much at the end of primary creep for each stress level.

2) **A critical stress exists, beyond which the secondary strain rate behaves as a defined function of stress**. When plotting strain rate as a function of the stress level for a given multiple stress level creep test, we find that a critical stress exists. Below this stress, the points of strain rate versus stress appear scattered. Beyond this stress, it obeys a power law distribution. This stress is a critical point which is defined by material property. In this report, we present three plots (Figs. 3.12-3.14) in which the critical stress is within a range of 110 – 145 MPa. This critical stress may be explained with the theory of fracture toughness, K_{IC}.

3) **Relation between strain rate and stress level for secondary creep**. A power law relation is found between strain rate and stress level for a multiple stress level creep test. This finding may be applicable to single stress level creep tests. To do this, a large number of tests are needed.

3.5 Recommendations

To deeply understand the long term behavior of the Yucca Mountain tuffs, an intensive and systematic study is essential. In this study a consistent test environment and a well conceived plan are required. The objective of the study should be focused on obtaining constitutive models for the tuffs. The following suggested tests give the main features for such a study plan:

- **Longer-term creep testing to test the linearity of secondary creep for different stress level**. This requires maintaining a stress level for a sufficiently long time and keeping the environment temperature constant or within a small range, i.e. ±1°C.

- **Static fatigue testing as a function of density (porosity)**.

- **Static fatigue testing as a function of moisture content**.

- **Static fatigue testing as a function of volume (size-dependency)**.

- **Triaxial creep testing**.

- **Acoustic emission monitoring**. For brittle rock, crack growth and development play an important or critical role in its damage. Observing the crack initiation and propagation under applied load and relating this progress to creep is an important step towards the creep study.

- **Fracture toughness testing**. This test may help determine the critical stress value described in item 2) of Section 3.4.

- **Elevated temperature creep testing**.

- **Determination of transition point between secondary and tertiary creep, for a range of conditions (stress, temperature, moisture content)**.

Appendix I

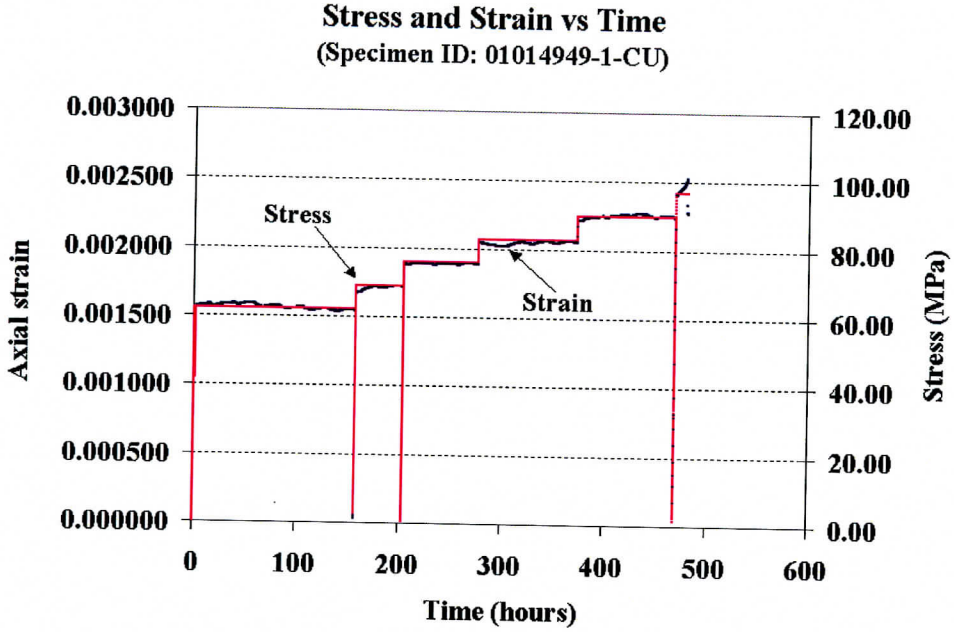

Figure 3-I-1 Plot of stress-time and strain-time for test 01014951-1-CU

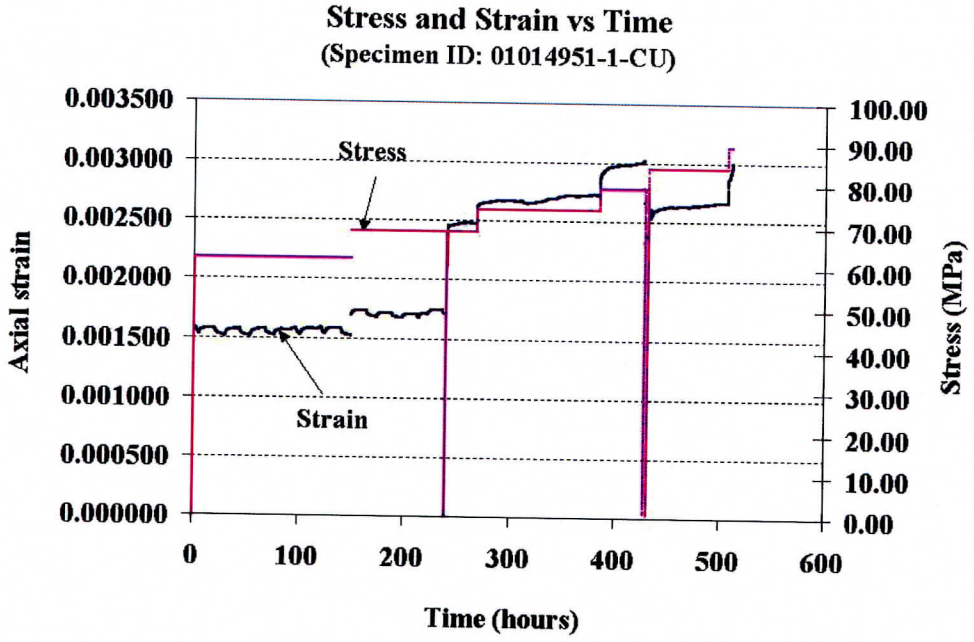

Figure 3-I-2 Plot of stress-time and strain-time for test 01014951-1-CU

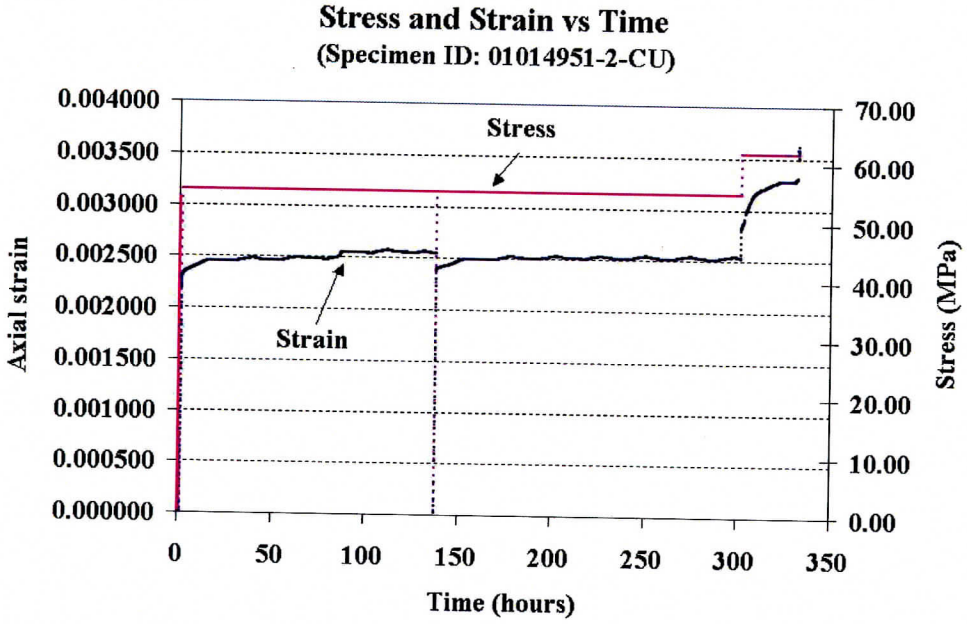

Figure 3-I-3 Plot of stress-time and strain-time for test 01014951-2-CU

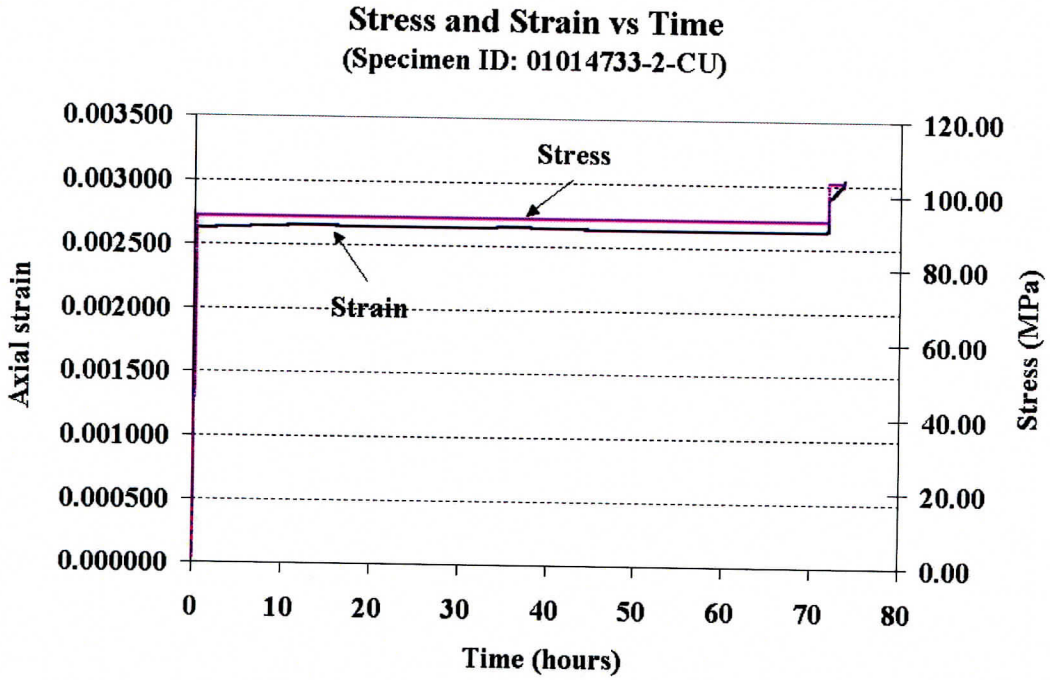

Figure 3-I-4 Plot of stress-time and strain-time for test 01014733-2-CU

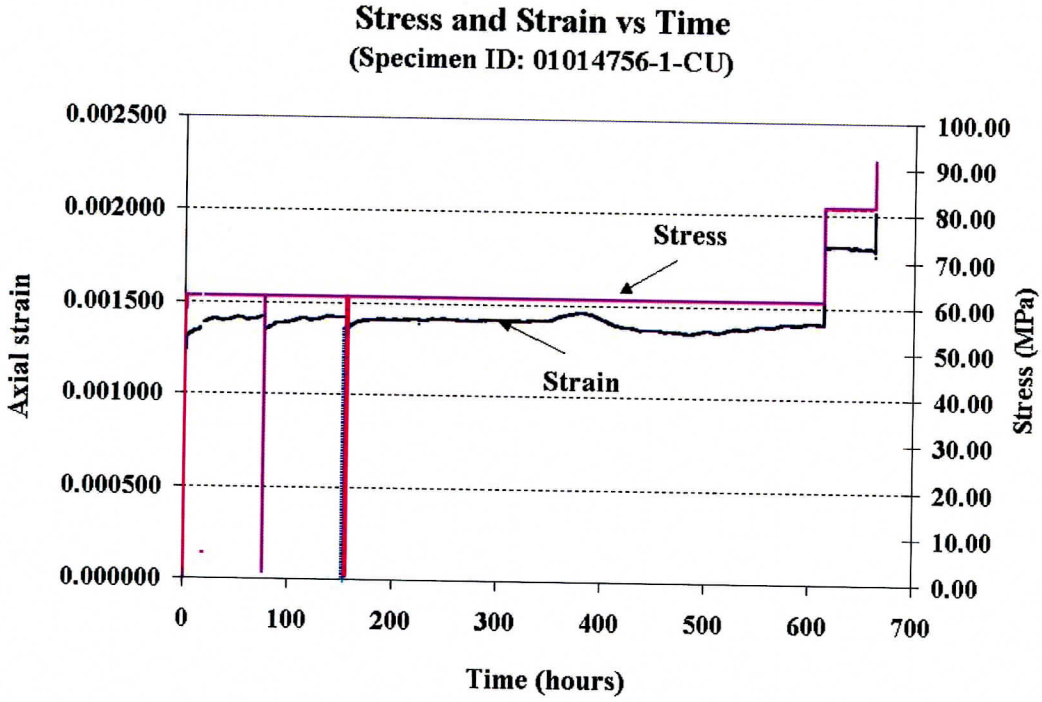

Figure 3-I-5 Plot of stress-time and strain-time for test 01014756-1-CU

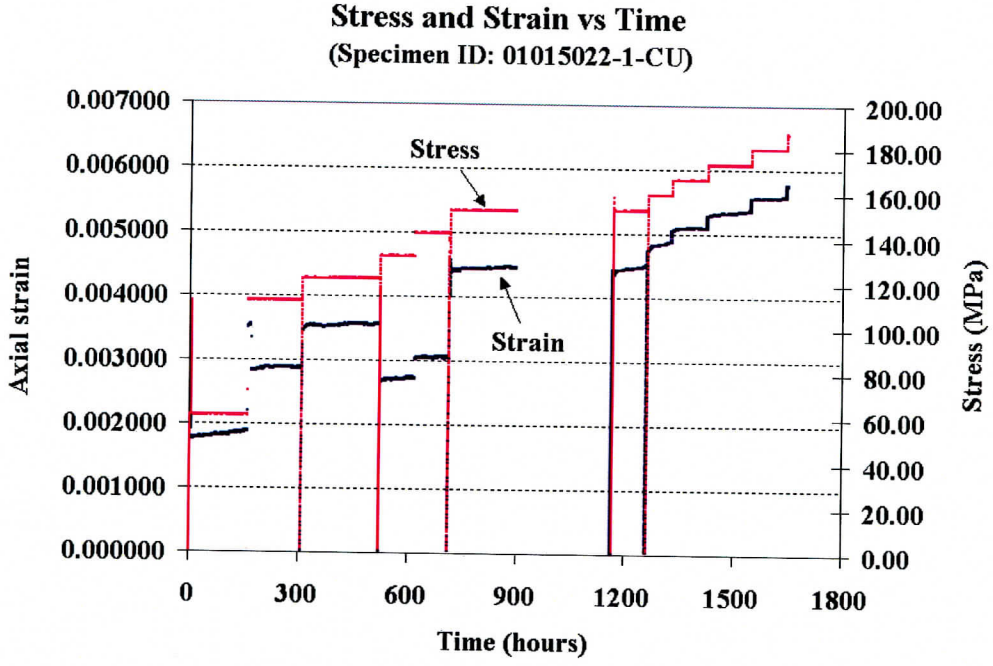

Figure 3-I-6 Plot of stress-time and strain-time for test 01015022-1-CU

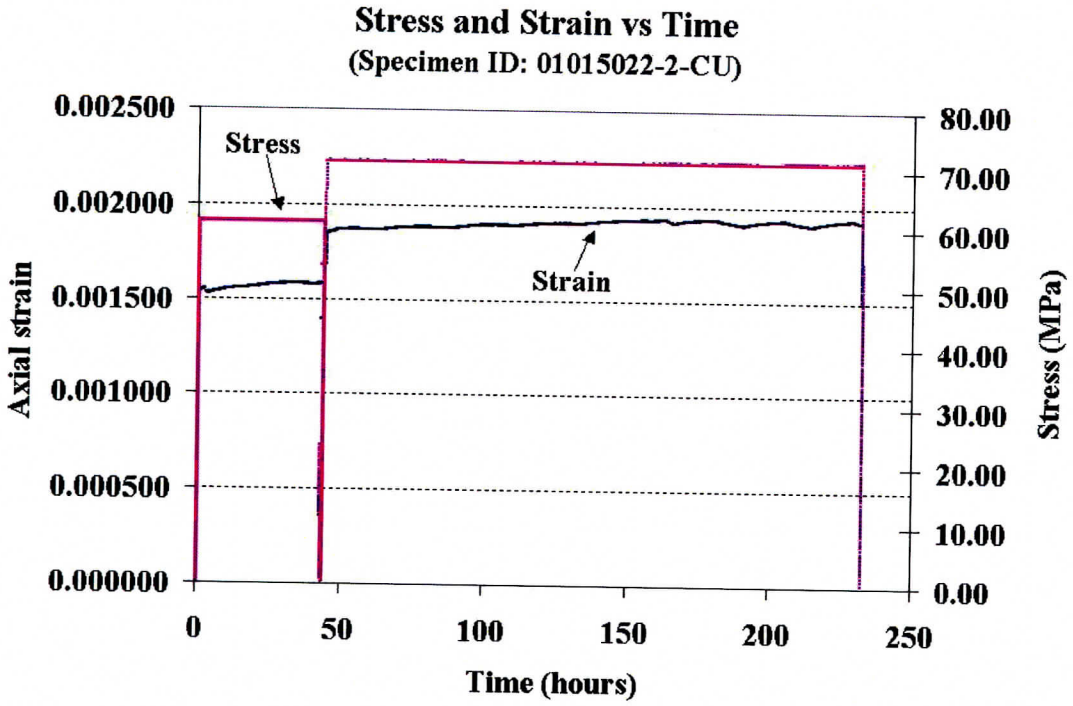

Figure 3-I-7 Plot of stress-time and strain-time for test 01015022-2-CU

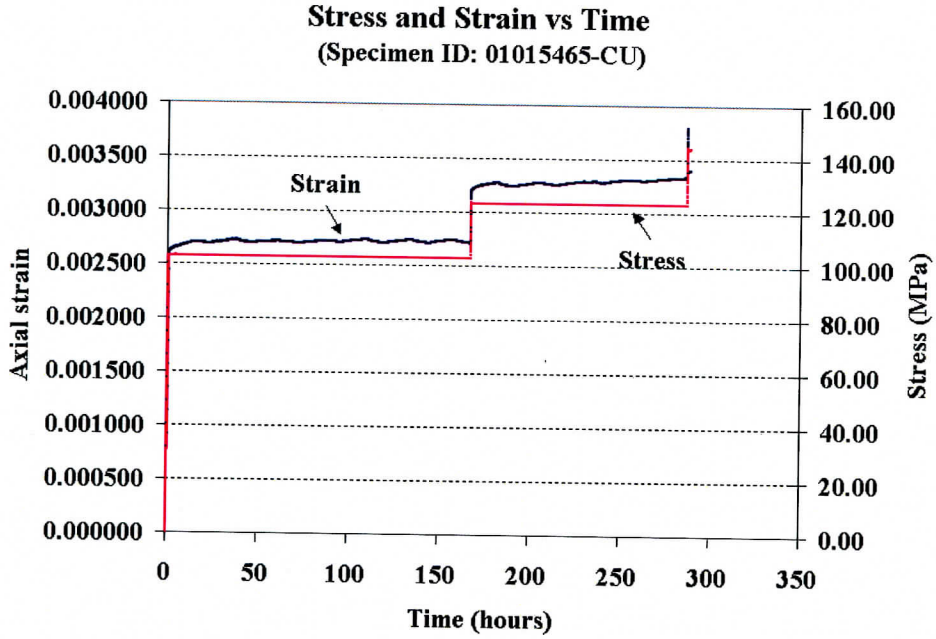

Figure 3-I-8 Plot of stress-time and strain-time for test 01015465-CU

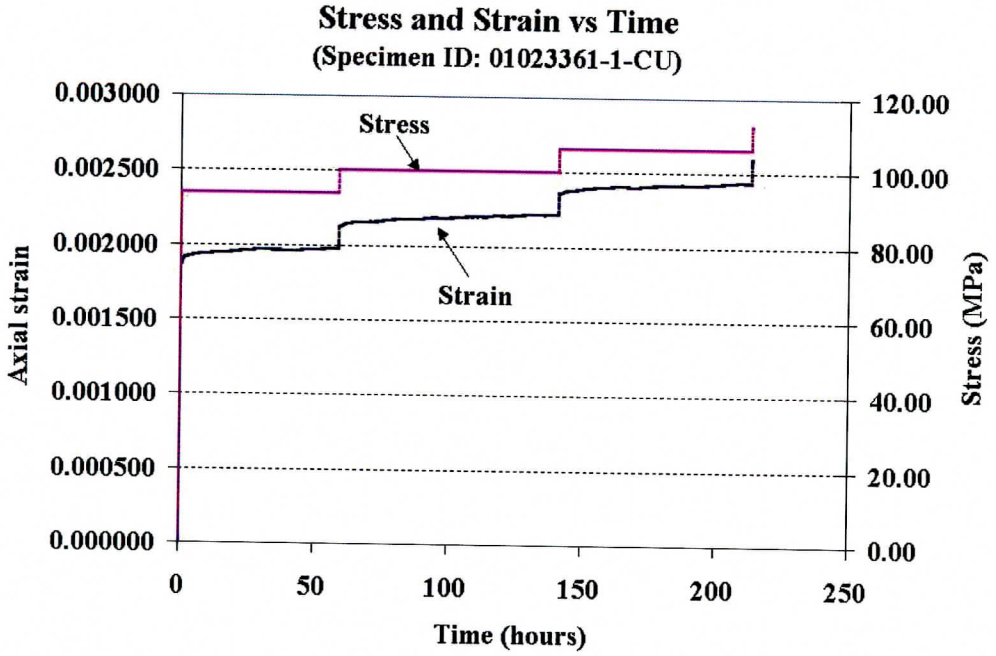

Figure 3-I-9 Plot of stress-time and strain-time for test 01023361-1-CU

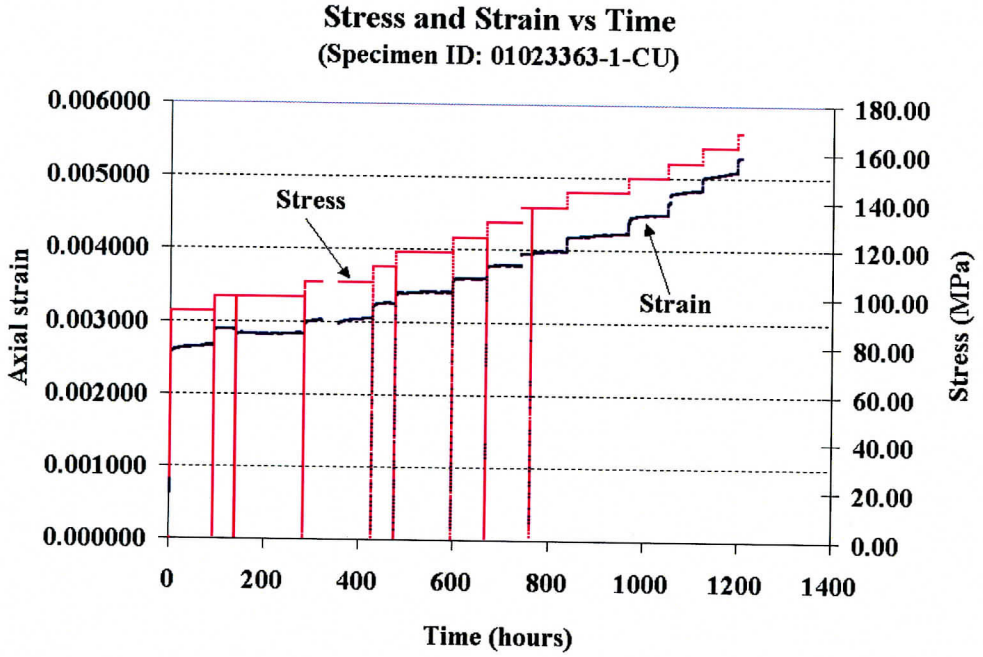

Figure 3-I-10 Plot of stress-time and strain-time for test 01023363-1-CU

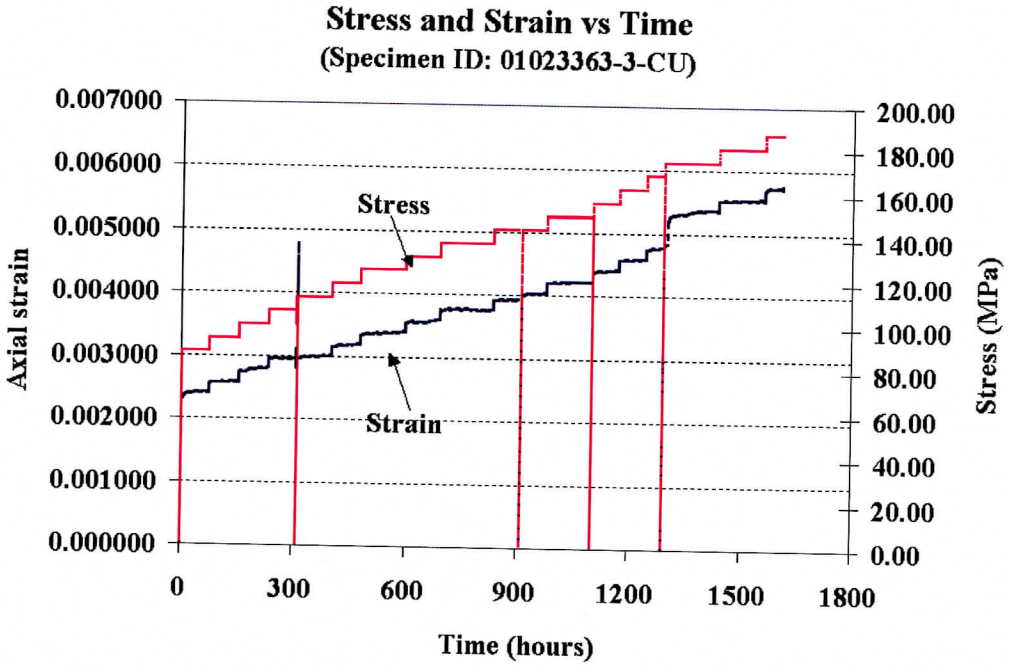

Figure 3-I-11 Plot of stress-time and strain-time for test 01023363-3-CU

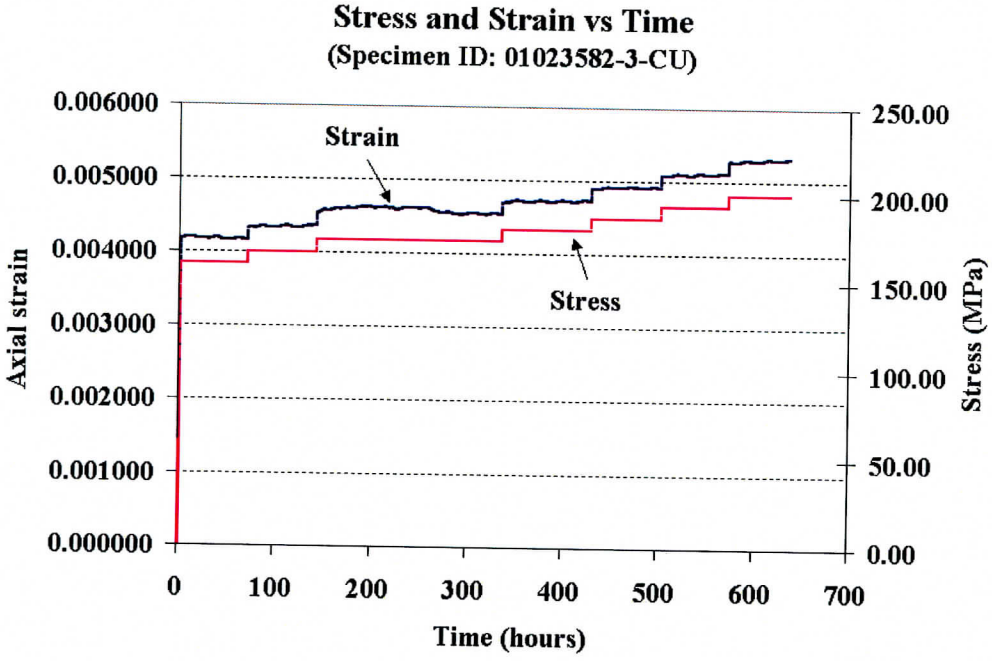

Figure 3-I-12 Plot of stress-time and strain-time for test 01023582-3-CU

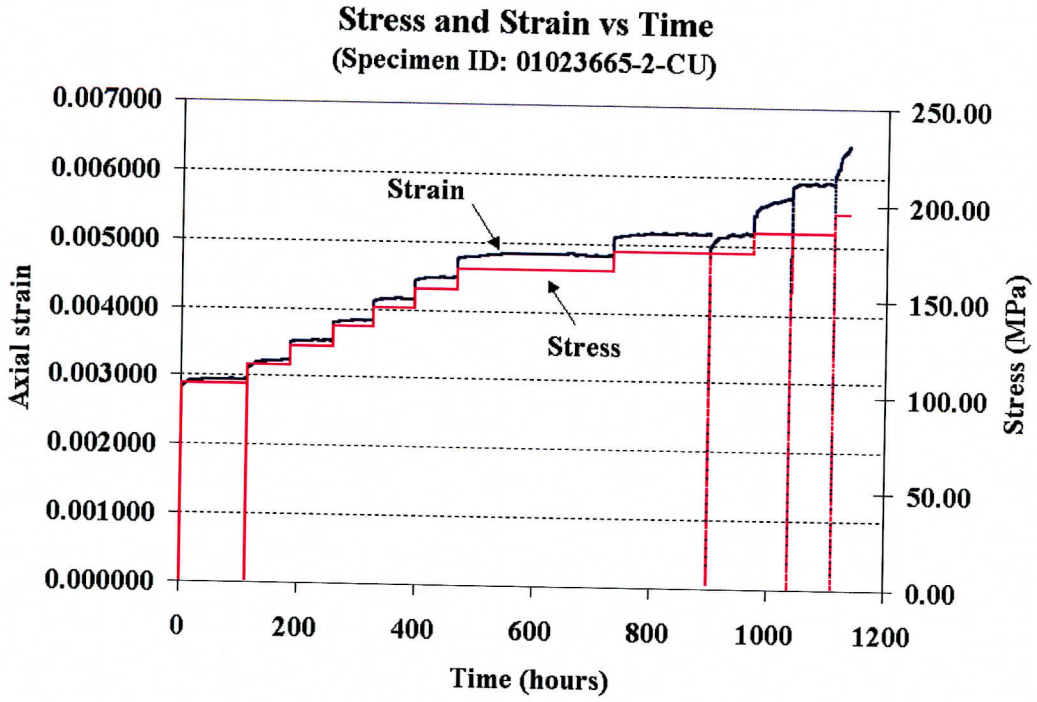

Figure 3-I-13 Plot of stress-time and strain-time for test 01023665-2-CU

CHAPTER 4 BRAZILIAN (INDIRECT SPLITTING TENSILE) TESTING, INCLUDING STRAIN-RATE DEPENDENT STRENGTH MEASUREMENTS

4.1 Experimental description

Brazilian (Indirect splitting tensile) tests have been performed on 158 specimens. Three specimens were collected from the lower lithophysal unit of the Topopah Spring Tuff formation (Tptpll). All others were collected from the middle nonlithophysal unit of the Topopah Spring Tuff formation (Tptpmn). The specimen source information and test results are given in Tables 4.1 and 4.2, respectively (at the end of this chapter). The test specimens are prepared from rock cores. Of the specimens, 146 have a nominal diameter of 2.4 inch (60.96 mm), 12 of 1.78 inch (45.21 mm). All the specimens are sawed and ground. The ratio of thickness to diameter is between 0.2 – 0.75, to meet ASTM D3967-95a. Moisture contents of 96 specimens have been measured before testing. The mean is 0.87% and standard deviation is 0.19%. Thirty four specimens have flaws. These flaws include lithophysal cavities and obvious vapor-phase altered inclusions.

Photographs of almost all specimens are included in the electronic database referenced in Section 1.1 of this part of the report.

All the tests are performed in an MTS testing machine. Load is measured using a load cell. Displacement is measured using the machine LVDT. The strain of a specimen is calculated by dividing the displacement (assumed equal to the diametrical compression) by the diameter of the specimen. The measured displacement is not only for the specimen, but also includes the deformation of steel platens and spacers, the machine frame deformation, and the deformation of each contact pair of specimen, platens, spacers and load cell. As a consequence, the calculated strain is not the true strain of the specimen. Given the low stress levels, and hence small maximum forces reached during these tests, we assume that the machine, platen, and spacer deformations are small, and essentially the same during all tests. All the tests follow ASTM D3967-95a and IPR-010, except for tests in which the applied displacement rate is intentionally changed (increases or reduced). Such accelerated or slowed down tests are performed in order to study strain rate dependency of rock strength. Fig. 4.1 shows a specimen in the frame for a Brazilian test.

The specimen sits between the bearing blocks. Bearing strips (cardboard) are used between the contact surfaces of the specimen and bearing blocks to transfer the load more evenly, and reduce the stress concentration on the contact surface of the specimen. This is more important for brittle rocks. Of the tests, fifteen did not use bearing strips in order to test the effect of the bearing strips. One specimen was broken accidentally before getting the results.

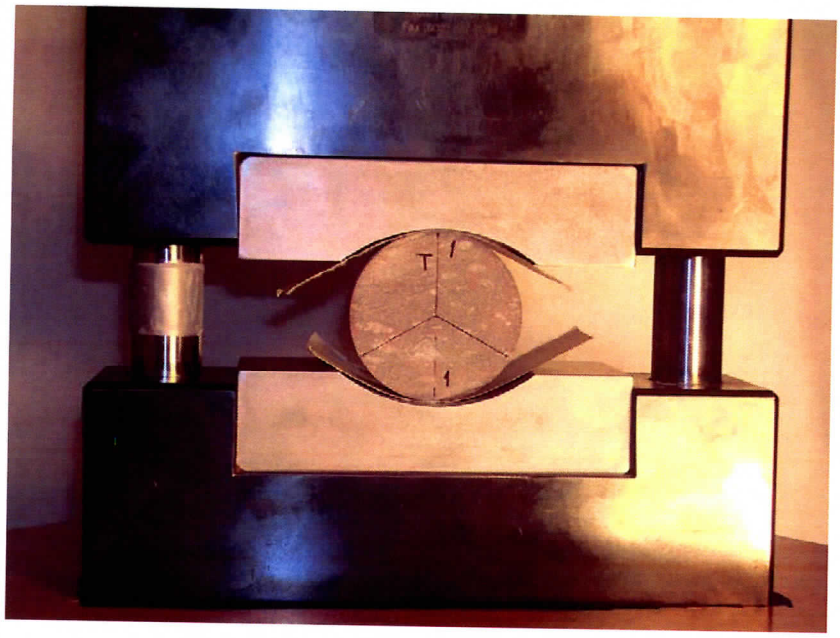

Figure 4.1 Example of a specimen considered not to contain major obvious flaws, although vapor altered "inclusions" ("spots") are clearly visible.

4.2 Test results and analysis

4.2.1 Tensile strength

The splitting tensile strength of a specimen is calculated from Eq (4.1) (ASTM D 3967-95a) if the failure is a true splitting failure, i.e. a tension crack running diametrically between the loading points.

$$\sigma_t = \frac{2 \times P}{\pi \times L \times D} \tag{4.1}$$

where:
σ_t = splitting (Brazilian) tensile strength, MPa (psi),
P = load at (splitting) failure, N (lbf),
L = average specimen thickness, mm (inch), and
D = diameter, mm (inch).

The tests are categorized into three groups. Group 1 refers to the tests for which bearing strips were used and for which the specimens do not contain major obvious flaws. One hundred and twelve tests fall in this group. Seventy seven of those are tested at the standard loading rate (the total test duration is between 1 and 10 minutes, as required by ASTM D 3967–95a). Group 2 includes the tests where we do not use bearing strips and for which the specimens are judged not to contain major flaws. Group 3 contains the tests for which no bearing strips were used, and for which there are flaws in the specimens.

Table 4.3 gives the strengths for the three groups for tests conducted at the standard loading rate.

Table 4.3 Statistical summary of Brazilian tests at standard loading rate

	Specimen ID in Database: 018LM.002	Group 1 (no flaws and with bearing strips)	Group 2 (no flaws and no bearing strips)	Group 3 (with flaws and with bearing strips)
Minimum	01014733-1-B, 01023693-2-B, 01023576-1-B	10.13	8.80	4.51
Maximum	01023755-2-B, 01025226-2-B, 01023666-2-B	22.69	19.46	21.61
Number of specimens		77	15	25
Mean		16.92	14.65	10.93
Median	01023581-3-B, 01023685-3-B, 01025229-1-B	16.85	14.71	10.93
Std Deviation		2.70	3.45	3.68

Note: the DTN for the information in this table is 018LM.002.

The mean strength of group 1 is the highest, and of group 3 the lowest. Group 1 has the lowest standard deviation. This comparison shows the effect of bearing strips and the effect of flaws in specimens. It appears that omitting the bearing strips slightly reduces the strength. It is clear that the presence of visible large flaws significantly reduces the strength.

Fig. 4.2 shows a typical failure pattern for the specimens of group 1. A main fracture runs between the loading points and close to the center of the specimen. In addition, two curved fractures symmetric about the main fracture are generated almost at the same time as the main fracture. The overwhelming majority of specimens in Group 1 show this classical (e.g. Andreev, 1995, Fig. 4.39) failure pattern.

The pattern shown in Fig. 4.3 also occurs very often: another two short fractures develop near one loading end of the specimen. This results from bending. The short fractures are generated after the three long fractures. After the three long fractures are formed, there is a strong tendency for the rock pieces at farthest left and farthest right to split away from the central vertical axis. At this moment the bearing block at the loading end is still moving down owing to inertia. As a consequence a heavy restriction is applied to the splitting rock pieces by the curved surface of the bearing block. The short fractures shown in Fig. 4.3 do not occur when running tests for smaller diameter (1.78 inch) specimens.

Figure 4.2 A typical failure pattern of specimens of Group1

Figure 4.3 A fracture pattern that occurs very often for 2.4 inch (60.96 mm) diameter specimens

Weakness inclusions affect the strength and failure pattern significantly. The vapor-phase altered spot on the left side of the specimen in Fig. 4.4 results in only one "diametrical" fracture developing. This type of asymmetric "diametrical" fracture, curving away from

the center of the specimen, has been observed fairly frequently. A secondary, probably bending, fracture has formed through the left half of the specimen, most likely as a result of a stress concentration at the edge of the vapor-altered weakened zone.

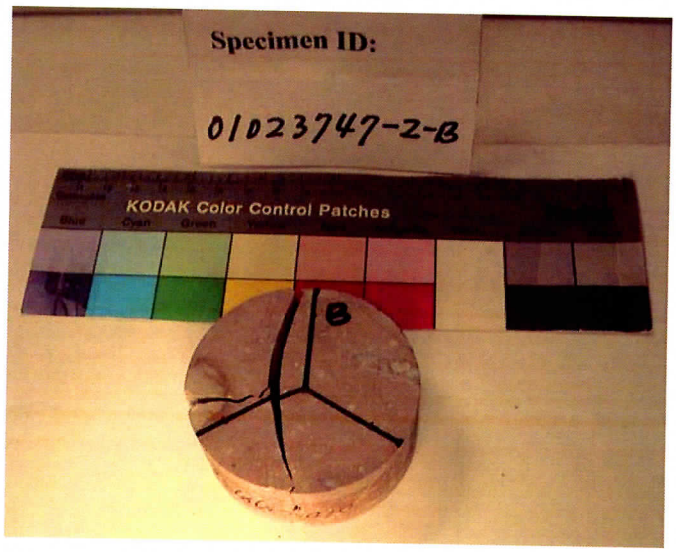

Figure 4.4 Effect of weakness inclusion on the failure pattern of a specimen: tensile failure of left part, assumed induced by weak (white) spot on left outer edge of specimen (Splitting tensile strength = 18.2 MPa).

Fig. 4.5 shows a case in which a vapor-phase altered zone was hidden inside and near the center of the specimen. In this example only one straight vertical fracture develops, through the weakness inclusion, and the specimen has a rather low strength.

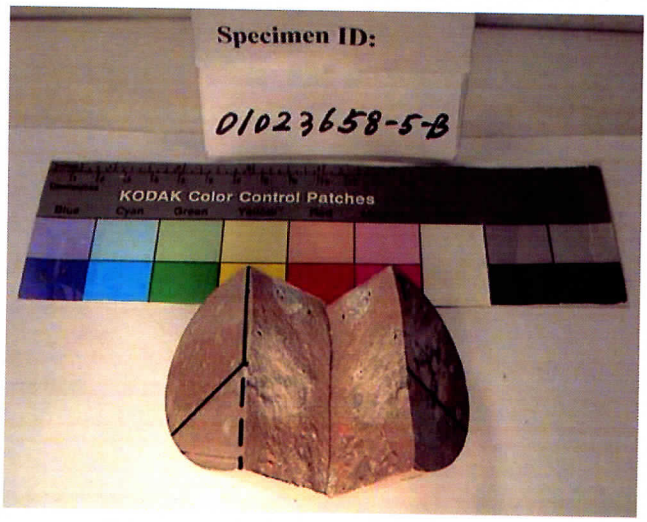

Figure 4.5 Effect of weakness inclusion on the failure pattern of a specimen (Splitting tensile strength = 8.5 MPa)

4.2.2 Strain rate dependence

The strain rate-dependence of tensile strength has been studied. Only the results of tests in Group 1 are used for this purpose. Fig. 4.6 shows a plot of tensile strength versus strain rate in logarithmic scale. As mentioned previously, the strain is not the true strain. Because the strain is calculated from a displacement that includes the test system deformation, the strain calculated and used here is somewhat larger than the actual strain. However, the strain rate should be very close to the actual diametrical strain rate. As a summary of strain rate-dependence, Fig. 4.6 is still valuable. The tensile strength decreases with a decrease of the strain rate. In other words, it decreases with an increase of test duration.

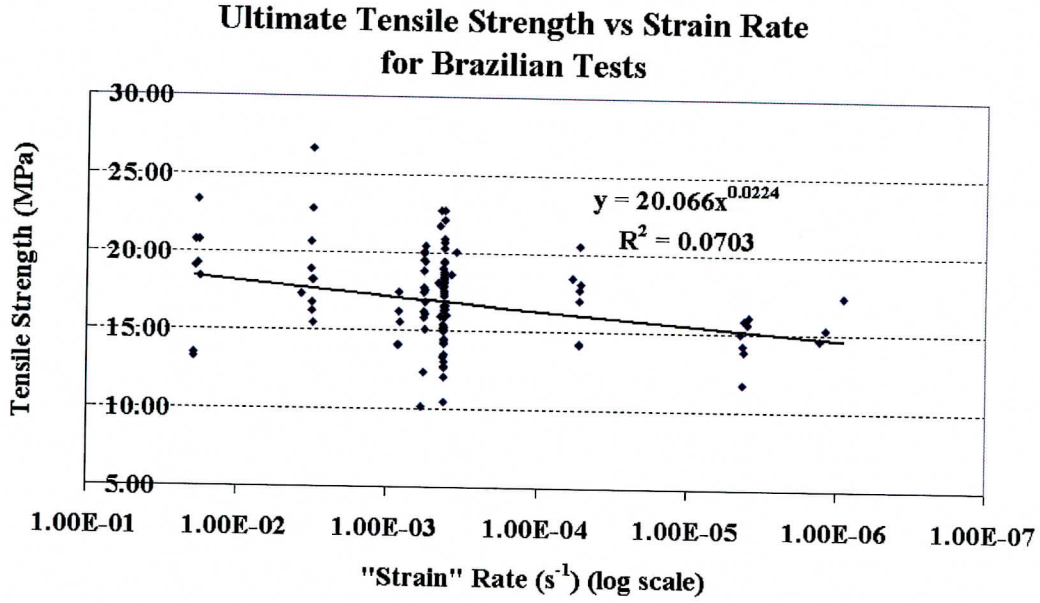

Figure 4.6 Tensile strength versus "strain rate" showing time-dependence of the tensile strength (Data used to construct the figure are in Summary of Brazilian Tests.xls)

4.3 Recommendations for further study

- Use Brazilian test data for spatial variability studies.
- Use Brazilian test data to analyze rock stiffness, possibly determine E.
- Perform static fatigue Brazilian tests.

- Study properties as a function of moisture content, density (porosity) and sample volume.

- Compare indirect tensile splitting strengths with uniaxial compressive strengths. Evaluate whether empirical relations in literature are acceptable for these tuffs, or whether they might need to be modified.

- Evaluate whether compressive and tensile strength (and stiffness) strain rate dependency can be (cor)related.

- Correlate Brazilian and lump test tensile strength results.

- Evaluate whether it is possible to evaluate numerically the influence of vapor altered spots on strength and stiffness.

- Perform numerical analyses of tests on specimens with modeled vapor altered spots, and performance sensitivity analyses.

- Evaluate whether it is possible to numerically reconcile strength and stiffness of specimens weakened and softened by vapor phase altered spots, by performing numerical simulations of such tests.

Table 4.1 Summary of Specimen Source Information for Brazilian tests

Serial #	Specimen ID	Borehole	Range in Borehole (ft)	Unit
1	01014733-1-B	UE-25 UZ#16	817.9-818.8	Tptpll
2	01014764-1-B	USW WZ-14	1076.1-1076.9	Tptpll
3	01014764-3-B	USW WZ-14	1076.1-1076.9	Tptpll
4	01023357-2-B	ESF-MD-NICHE 4788#1	3.3-3.8	Tptpmn
5	01023359-2-B	ESF-MD-NICHE 4788#1	15.7-16.5	Tptpmn
6	01023359-3-B	ESF-MD-NICHE 4788#1	15.7-16.5	Tptpmn
7	01023363-4-B	ESF-MD-NICHE 3107#7	12.1-13.6	Tptpmn
8	01023363-5-B	ESF-MD-NICHE 3107#7	12.1-13.6	Tptpmn
9	01023363-6-B	ESF-MD-NICHE 3107#7	12.1-13.7	Tptpmn
10	01023367-3-B	ESF-MD-NICHE 3107#7	8.1-9.6	Tptpmn
11	01023367-4-B	ESF-MD-NICHE 3107#7	8.1-9.6	Tptpmn
12	01023367-5-B	ESF-MD-NICHE 3107#7	8.1-9.6	Tptpmn
13	01023370-2-B	ESF-MD-NICHE 3107#7	20.9-21.5	Tptpmn
14	01023370-3-B	ESF-MD-NICHE 3107#7	20.9-21.5	Tptpmn
15	01023372-3-B	ESF-MD-NICHE 3107#7	22.7-23.4	Tptpmn
16	01023566-2-B	ESF-HD-WH-3	0.2-1.1	Tptpmn
17	01023567-2-B	ESF-HD-WH-3	2.0-2.9	Tptpmn
18	01023567-3-B	ESF-HD-WH-3	2.0-2.9	Tptpmn
19	01023567-4-B	ESF-HD-WH-3	2.0-2.9	Tptpmn
20	01023570-2-B	ESF-HD-WH-3	24.2-25.7	Tptpmn
21	01023570-3-B	ESF-HD-WH-3	24.2-25.7	Tptpmn
22	01023570-4-B	ESF-HD-WH-3	24.2-25.7	Tptpmn
23	01023571-1-B	ESF-HD-WH-3	27.2-27.9	Tptpmn
24	01023571-2-B	ESF-HD-WH-3	27.2-27.9	Tptpmn
25	01023571-3-B	ESF-HD-WH-3	27.2-27.9	Tptpmn
26	01023571-4-B	ESF-HD-WH-3	27.2-27.9	Tptpmn
27	01023574-1-B	ESF-HD-WH-4	15.6-16.3	Tptpmn
28	01023574-2-B	ESF-HD-WH-4	15.6-16.3	Tptpmn
29	01023574-3-B	ESF-HD-WH-4	15.6-16.3	Tptpmn
30	01023574-4-B	ESF-HD-WH-4	15.6-16.3	Tptpmn
31	01023574-5-B	ESF-HD-WH-4	15.6-16.3	Tptpmn
32	01023574-6-B	ESF-HD-WH-4	15.6-16.3	Tptpmn
33	01023574-7-B	ESF-HD-WH-4	15.6-16.3	Tptpmn
34	01023576-1-B	ESF-HD-WH-4	33.0-34.1	Tptpmn
35	01023579-2-B	ESF-HD-WH-5	12.4-13.0	Tptpmn
36	01023580-1-B	ESF-HD-WH-5	24.4-25.0	Tptpmn
37	01023581-1-B	ESF-HD-WH-5	27.7-28.4	Tptpmn
38	01023581-3-B	ESF-HD-WH-5	27.7-28.4	Tptpmn
39	01023581-4-B	ESF-HD-WH-5	27.7-28.4	Tptpmn
40	01023582-2-B	ESF-HD-WH-5	33.0-34.2	Tptpmn
41	01023585-1-B	ESF-HD-WH-6	28.2-28.9	Tptpmn

Table 4.1 (Continued)

42	01023585-2-B	ESF-HD-WH-6	28.2-28.9	Tptpmn
43	01023586-1-B	ESF-HD-WH-3	31.0-31.6	Tptpmn
44	01023586-2-B	ESF-HD-WH-3	31.0-31.6	Tptpmn
45	01023657-6-B	ESF-HD-WH-36	15.9-18.3	Tptpmn
46	01023657-7-B	ESF-HD-WH-36	15.6-18.3	Tptpmn
47	01023657-8-B	ESF-HD-WH-36	15.9-18.3	Tptpmn
48	01023658-1-B	ESF-HD-WH-36	18.8-20.2	Tptpmn
49	01023658-2-B	ESF-HD-WH-36	18.8-20.2	Tptpmn
50	01023658-3-B	ESF-HD-WH-36	18.8-20.2	Tptpmn
51	01023658-4-B	ESF-HD-WH-36	18.8-20.2	Tptpmn
52	01023658-5-B	ESF-HD-WH-36	18.8-20.2	Tptpmn
53	01023658-6-B	ESF-HD-WH-36	18.8-20.2	Tptpmn
54	01023661-1-B	ESF-HD-WH-36	30.5-31.8	Tptpmn
55	01023661-2-B	ESF-HD-WH-36	26.0-26.7	Tptpmn
56	01023661-3-B	ESF-HD-WH-36	26.0-26.7	Tptpmn
57	01023666-1-B	ESF-HD-WH-37	0.0-0.4	Tptpmn
58	01023666-2-B	ESF-HD-WH-37	0.0-0.4	Tptpmn
59	01023666-3-B	ESF-HD-WH-37	0.0-0.4	Tptpmn
60	01023666-4-B	ESF-HD-WH-37	0.0-0.4	Tptpmn
61	01023668-1-B	ESF-HD-WH-37	2.2-4.4	Tptpmn
62	01023668-2-B	ESF-HD-WH-37	2.2-4.4	Tptpmn
63	01023668-4-B	ESF-HD-WH-37	2.2-4.4	Tptpmn
64	01023668-5-B	ESF-HD-WH-37	2.2-4.4	Tptpmn
65	01023668-6-B	ESF-HD-WH-37	2.2-4.4	Tptpmn
66	01023668-7-B	ESF-HD-WH-37	2.2-4.4	Tptpmn
67	01023668-8-B	ESF-HD-WH-37	2.2-4.4	Tptpmn
68	01023685-1-B	ESF-HD-WH-37	9.8-11.0	Tptpmn
69	01023685-2-B	ESF-HD-WH-37	9.8-11.0	Tptpmn
70	01023685-3-B	ESF-HD-WH-37	9.8-11.0	Tptpmn
71	01023685-4-B	ESF-HD-WH-37	9.8-11.0	Tptpmn
72	01023685-5-B	ESF-HD-WH-37	9.8-11.0	Tptpmn
73	01023685-6-B	ESF-HD-WH-37	9.8-11.0	Tptpmn
74	01023685-7-B	ESF-HD-WH-37	9.8-11.0	Tptpmn
75	01023685-8-B	ESF-HD-WH-37	9.8-11.0	Tptpmn
76	01023689-3-B	ESF-HD-WH-37	19.6-21.1	Tptpmn
77	01023689-4-B	ESF-HD-WH-37	19.6-21.1	Tptpmn
78	01023689-5-B	ESF-HD-WH-37	19.6-21.1	Tptpmn
79	01023689-6-B	ESF-HD-WH-37	19.6-21.1	Tptpmn
80	01023689-7-B	ESF-HD-WH-37	19.6-21.1	Tptpmn
81	01023690-2-B	ESF-HD-WH-37	22.7-23.7	Tptpmn
82	01023690-3-B	ESF-HD-WH-37	22.7-23.7	Tptpmn
83	01023690-4-B	ESF-HD-WH-37	22.7-23.7	Tptpmn

Table 4.1 (Continued)

84	01023690-5-B	ESF-HD-WH-37	22.7-23.7	Tptpmn
85	01023693-1-B	ESF-HD-WH-37	27.6-28.1	Tptpmn
86	01023693-2-B	ESF-HD-WH-37	27.6-28.1	Tptpmn
87	01023697-2-B	ESF-HD-WH-50	4.8-6.0	Tptpmn
88	01023697-3-B	ESF-HD-WH-50	4.8-6.0	Tptpmn
89	01023697-4-B	ESF-HD-WH-50	4.8-6.0	Tptpmn
90	01023701-2-B	ESF-HD-WH-50	11.9-13.0	Tptpmn
91	01023701-3-B	ESF-HD-WH-50	11.9-13.0	Tptpmn
92	01023701-4-B	ESF-HD-WH-50	11.9-13.0	Tptpmn
93	01023702-1-B	ESF-HD-WH-50	15.1-16.2	Tptpmn
94	01023704-1-B	ESF-HD-WH-50	18.3-19.1	Tptpmn
95	01023704-3-B	ESF-HD-WH-50	18.3-19.1	Tptpmn
96	01023704-4-B	ESF-HD-WH-50	18.3-19.1	Tptpmn
97	01023704-5-B	ESF-HD-WH-50	18.3-19.1	Tptpmn
98	01023704-6-B	ESF-HD-WH-50	18.3-19.1	Tptpmn
99	01023704-7-B	ESF-HD-WH-50	18.3-19.1	Tptpmn
100	01023704-8-B	ESF-HD-WH-50	18.3-19.1	Tptpmn
101	01023704-9-B	ESF-HD-WH-50	18.3-19.1	Tptpmn
102	01023715-1-B	ESF-HD-WH-50	32.1-33.0	Tptpmn
103	01023715-2-B	ESF-HD-WH-50	32.1-33.0	Tptpmn
104	01023715-3-B	ESF-HD-WH-50	32.1-33.0	Tptpmn
105	01023715-4-B	ESF-HD-WH-50	32.1-33.0	Tptpmn
106	01023721-1-B	ESF-HD-WH-50	35.4-35.8	Tptpmn
107	01023721-2-B	ESF-HD-WH-50	35.4-35.8	Tptpmn
108	01023727-1-B	ESF-HD-WH-26	4.9-5.2	Tptpmn
109	01023727-2-B	ESF-HD-WH-26	4.9-5.2	Tptpmn
110	01023734-1-B	ESF-HD-WH-26	15.5-16.0	Tptpmn
111	01023734-2-B	ESF-HD-WH-26	15.5-16.0	Tptpmn
112	01023734-3-B	ESF-HD-WH-26	15.5-16.0	Tptpmn
113	01023734-4-B	ESF-HD-WH-26	15.5-16.0	Tptpmn
114	01023734-5-B	ESF-HD-WH-26	15.5-16.0	Tptpmn
115	01023735-1-B	ESF-HD-WH-26	14.1-14.4	Tptpmn
116	01023735-2-B	ESF-HD-WH-4	26.1-27.3	Tptpmn
117	01023735-3-B	ESF-HD-WH-26	14.1-14.4	Tptpmn
118	01023741-1-B	ESF-HD-WH-26	22.6-22.8	Tptpmn
119	01023741-2-B	ESF-HD-WH-26	22.6-22.8	Tptpmn
120	01023744-1-B	ESF-HD-WH-26	24.1-24.4	Tptpmn
121	01023744-2-B	ESF-HD-WH-26	24.1-24.4	Tptpmn
122	01023746-1-B	ESF-HD-WH-26	25.2-25.5	Tptpmn
123	01023746-2-B	ESF-HD-WH-26	25.2-25.5	Tptpmn
124	01023746-3-B	ESF-HD-WH-26	25.2-25.5	Tptpmn
125	01023747-2-B	ESF-HD-WH-26	25.7-26.8	Tptpmn

Table 4.1 (Continued)

126	01023747-4-B	ESF-HD-WH-26	25.7-26.8	Tptpmn
127	01023748-1-B	ESF-HD-WH-26	29.0-29.3	Tptpmn
128	01023748-2-B	ESF-HD-WH-26	29.0-29.3	Tptpmn
129	01023754-1-B	ESF-HD-WH-32	4.7-5.7	Tptpmn
130	01023754-3-B	ESF-HD-WH-32	4.7-5.7	Tptpmn
131	01023755-1-B	ESF-HD-WH-32	9.0-9.3	Tptpmn
132	01023755-2-B	ESF-HD-WH-32	9.0-9.3	Tptpmn
133	01023755-3-B	ESF-HD-WH-32	9.0-9.3	Tptpmn
134	01023756-1-B	ESF-HD-WH-32	9.6-9.7	Tptpmn
135	01023756-2-B	ESF-HD-WH-32	9.6-9.7	Tptpmn
136	01023757-1-B	ESF-HD-WH-32	9.9-10.2	Tptpmn
137	01023757-2-B	ESF-HD-WH-32	9.9-10.2	Tptpmn
138	01025222-B	ESF-HD-WH-32	16.1-16.2	Tptpmn
139	01025224-2-B	ESF-HD-WH-32	27.2-28.8	Tptpmn
140	01025224-3-B	ESF-HD-WH-32	27.2-28.8	Tptpmn
141	01025226-2-B	ESF-HD-WH-32	32.0-33.1	Tptpmn
142	01025226-3-B	ESF-HD-WH-32	32.0-33.1	Tptpmn
143	01025226-4-B	ESF-HD-WH-32	32.0-33.1	Tptpmn
144	01025226-5-B	ESF-HD-WH-32	32.0-33.1	Tptpmn
145	01025227-3-B	ESF-HD-WH-32	33.8-35.6	Tptpmn
146	01025227-4-B	ESF-HD-WH-32	33.8-35.6	Tptpmn
147	01025227-5-B	ESF-HD-WH-32	33.8-35.6	Tptpmn
148	01025228-1-B	ESF-HD-WH-32	37.4-37.6	Tptpmn
149	01025228-2-B	ESF-HD-WH-32	37.4-37.6	Tptpmn
150	01025228-3-B	ESF-HD-WH-32	37.4-37.6	Tptpmn
151	01025229-1-B	ESF-HD-WH-32	35.8-36.2	Tptpmn
152	01025229-2-B	ESF-HD-WH-32	35.8-36.2	Tptpmn
153	01025229-3-B	ESF-HD-WH-32	35.8-36.2	Tptpmn
154	01025229-4-B	ESF-HD-WH-32	35.8-36.2	Tptpmn
155	01025232-2-B	ESF-HD-WH-33	10.2-10.9	Tptpmn
156	01025232-3-B	ESF-HD-WH-33	10.2-10.9	Tptpmn
157	01025232-4-B	ESF-HD-WH-33	10.2-10.9	Tptpmn
158	01025261-3-B	ESF-HD-WH-33	25.8-26.5	Tptpmn

Note: the DTN for the specimen source information in this table is 018LM.002. The Unit column is Non-Q, for information only.

Tptpll = lower lithophysal unit of Topopah Spring Tuff,
Tptpmn = middle nonlithophysal unit of Topopah Spring Tuff.

Table data are in Summary of Brazilian Tests.xls.

Table 4.2 Analyses of Brazilian tests

Serial #	Specimen ID	Specimen Code *	Test Code **	Diameter (in)	Thickness (in)	Strength (MPa)	"Strain" Rate (/s)	Moisture Content (%)
1	01014733-1-B	0	0	2.40	0.99	10.13	0.000589	N/A
2	01014764-1-B	1	0	2.40	1.23	8.50	0.000418	N/A
3	01014764-3-B	1	0	2.40	1.31	6.87	0.000419	N/A
4	01023357-2-B	0	0	1.77	1.05	12.39	0.000575	N/A
5	01023359-2-B	0	0	1.77	0.95	16.22	0.000567	N/A
6	01023359-3-B	0	0	1.77	0.68	18.87	0.000569	N/A
7	01023363-4-B	0	0	1.78	0.82	15.12	0.000565	N/A
8	01023363-5-B	0	0	1.78	0.63	19.51	0.000573	N/A
9	01023363-6-B***	0	0	1.78	0.67	N/A	N/A	N/A
10	01023367-3-B	0	0	1.78	0.57	19.41	0.000566	N/A
11	01023367-4-B	0	0	1.78	0.59	17.49	0.000566	N/A
12	01023367-5-B	0	0	1.78	0.72	20.00	0.000570	N/A
13	01023370-2-B	0	0	1.78	0.64	20.43	0.000566	N/A
14	01023370-3-B	0	0	1.78	0.68	17.65	0.000565	N/A
15	01023372-3-B	0	0	1.78	0.68	15.87	0.000571	N/A
16	01023566-2-B	0	0	2.40	0.90	13.38	0.000425	0.652
17	01023567-2-B	0	0	2.40	1.06	17.73	0.000569	N/A
18	01023567-3-B	1	0	2.40	1.14	10.23	0.000559	N/A
19	01023567-4-B	1	0	2.40	1.14	11.21	0.000564	N/A
20	01023570-2-B	1	0	2.40	0.87	12.14	0.000421	N/A
21	01023570-3-B	0	0	2.38	1.01	20.04	0.000567	N/A
22	01023570-4-B	0	0	2.39	0.74	19.01	0.000423	N/A
23	01023571-1-B	0	0	2.40	1.04	15.67	0.000004	0.819
24	01023571-2-B	0	0	2.40	1.04	13.50	0.000419	0.901
25	01023571-3-B	0	0	2.40	1.10	16.25	0.003195	0.932
26	01023571-4-B	0	0	2.40	1.01	12.06	0.000421	0.952

Table 4.2 (Continued)

27	01023574-1-B	1	1	2.40	1.42	9.22	0.000419	0.679
28	01023574-2-B	0	0	2.40	1.00	16.03	0.000402	0.936
29	01023574-3-B	0	0	2.40	1.05	14.66	0.000001	0.816
30	01023574-4-B	0	0	2.40	0.87	18.47	0.000058	0.858
31	01023574-5-B	0	1	2.40	0.99	14.59	0.000418	1.008
32	01023574-6-B	0	0	2.40	0.96	18.63	0.000417	0.931
33	01023574-7-B	0	0	2.40	1.09	20.25	0.000423	0.808
34	01023576-1-B	1	0	2.40	1.30	4.51	0.000556	N/A
35	01023579-2-B	0	0	2.40	1.16	18.62	0.000373	N/A
36	01023580-1-B	0	0	2.40	1.17	15.41	0.000427	N/A
37	01023581-1-B	0	0	2.40	1.22	19.46	0.000418	N/A
38	01023581-3-B	0	0	2.40	1.16	16.85	0.000557	N/A
39	01023581-4-B	0	0	2.40	1.29	16.13	0.000564	N/A
40	01023582-2-B	0	0	2.40	0.98	20.06	0.000347	N/A
41	01023585-1-B	0	0	2.40	1.12	22.69	0.000419	0.552
42	01023585-2-B	0	0	2.40	1.08	20.71	0.017992	0.658
43	01023586-1-B	1	0	2.40	1.13	9.84	0.000423	N/A
44	01023586-2-B	0	0	2.31	1.00	15.91	0.000444	N/A
45	01023657-6-B	0	0	2.40	0.98	13.87	0.000004	0.864
46	01023657-7-B	0	0	2.40	0.93	14.27	0.000053	0.925
47	01023657-8-B	0	0	2.40	1.06	18.10	0.000420	0.801
48	01023658-1-B	0	0	2.40	0.68	15.47	0.003099	N/A
49	01023658-2-B	0	0	2.40	1.05	18.24	0.003153	N/A
50	01023658-3-B	0	0	2.40	0.85	19.04	0.019150	N/A
51	01023658-4-B	0	0	2.40	0.89	18.08	0.000051	N/A
52	01023658-5-B	1	0	2.40	1.24	8.47	0.003280	N/A
53	01023658-6-B	0	0	2.40	0.67	26.62	0.003194	N/A
54	01023661-1-B	0	1	2.40	1.09	15.67	0.000418	0.679

Table 4.2 (Continued)

55	01023661-2-B	0	0	2.40	1.08	12.72	0.000420	0.625
56	01023661-3-B	0	0	2.40	1.14	11.74	0.000004	0.662
57	01023666-1-B	1	0	2.40	1.08	16.93	0.000420	N/A
58	01023666-2-B	1	0	2.40	0.88	21.61	0.000418	N/A
59	01023666-3-B	0	0	2.40	0.85	23.31	0.018229	N/A
60	01023666-4-B	1	0	2.40	0.88	13.13	0.000421	N/A
61	01023668-1-B	0	0	2.40	1.24	15.59	0.000825	N/A
62	01023668-2-B	0	0	2.40	0.75	16.28	0.000843	N/A
63	01023668-4-B	0	0	2.40	0.85	17.37	0.000001	N/A
64	01023668-5-B	0	0	2.40	0.88	16.97	0.000052	N/A
65	01023668-6-B	1	0	2.40	1.00	11.68	0.000424	N/A
66	01023668-7-B	1	0	2.40	0.82	15.24	0.000414	N/A
67	01023668-8-B	0	0	2.40	0.87	22.81	0.003183	N/A
68	01023685-1-B	0	0	2.40	1.11	13.25	0.019444	0.943
69	01023685-2-B	0	0	2.40	0.94	20.68	0.003247	0.807
70	01023685-3-B	0	1	2.40	0.97	14.71	0.000418	0.948
71	01023685-4-B	0	0	2.40	1.08	18.27	0.000421	0.983
72	01023685-5-B	0	1	2.40	0.95	14.07	0.000402	0.988
73	01023685-6-B	1	0	2.40	0.90	7.85	0.000418	1.145
74	01023685-7-B	1	0	2.40	0.97	7.00	0.000418	1.221
75	01023685-8-B	0	1	2.40	0.95	18.89	0.000416	1.066
76	01023689-3-B	0	0	2.40	1.10	15.28	0.000418	0.708
77	01023689-4-B	0	0	2.40	1.11	16.57	0.000419	0.842
78	01023689-5-B	0	0	2.40	1.04	16.66	0.000419	0.924
79	01023689-6-B	1	0	2.40	1.06	13.27	0.000416	0.830
80	01023689-7-B	0	0	2.40	1.00	18.32	0.000416	0.734
81	01023690-2-B	0	0	2.40	1.11	14.23	0.000419	0.703
82	01023690-3-B	0	1	2.40	1.04	17.79	0.000413	0.814

Table 4.2 (Continued)

83	01023690-4-B	0	0	2.40	1.06	17.22	0.000420	0.722
84	01023690-5-B	0	0	2.40	1.06	18.04	0.000458	0.874
85	01023693-1-B	0	0	2.40	1.08	16.58	0.000417	0.818
86	01023693-2-B	1	1	2.40	1.09	8.80	0.000419	1.022
87	01023697-2-B	0	0	2.40	0.84	15.30	0.000001	0.806
88	01023697-3-B	0	1	2.40	0.84	17.32	0.000422	0.974
89	01023697-4-B	0	1	2.40	0.88	15.66	0.000414	0.992
90	01023701-2-B	0	0	2.40	1.04	16.34	0.000417	0.988
91	01023701-3-B	0	0	2.40	0.89	16.63	0.000414	1.030
92	01023701-4-B	0	0	2.40	0.97	17.74	0.000424	0.894
93	01023702-1-B	1	0	2.40	1.27	7.39	0.000415	0.921
94	01023704-1-B	0	0	2.40	1.19	14.52	0.000419	0.805
95	01023704-3-B	0	0	2.40	1.08	13.52	0.019360	N/A
96	01023704-4-B	0	0	2.40	0.86	14.09	0.000845	N/A
97	01023704-5-B	1	0	2.40	0.81	12.34	0.003108	N/A
98	01023704-6-B	0	0	2.40	0.80	14.15	0.000857	N/A
99	01023704-7-B	0	0	2.40	1.05	15.87	0.000004	N/A
100	01023704-8-B	0	0	2.40	0.73	14.19	0.000052	N/A
101	01023704-9-B	1	0	2.40	0.64	9.82	0.000421	N/A
102	01023715-1-B	0	0	2.40	1.06	16.41	0.000409	0.787
103	01023715-2-B	0	0	2.40	0.86	22.06	0.000420	0.635
104	01023715-3-B	0	0	2.40	0.83	14.44	0.000418	0.635
105	01023715-4-B	0	0	2.40	0.92	20.69	0.000420	0.693
106	01023721-1-B	0	0	2.40	1.01	20.49	0.000052	N/A
107	01023721-2-B	0	0	2.40	0.93	15.16	0.000423	0.676
108	01023727-1-B	0	0	2.40	1.05	10.48	0.000420	0.541
109	01023727-2-B	0	1	2.40	0.87	17.25	0.000406	0.609
110	01023734-1-B	1	0	2.40	1.06	14.36	0.000419	N/A

Table 4.2 (Continued)

111	01023734-2-B	1	0	2.40	0.78	11.81	0.000419	N/A
112	01023734-3-B	1	0	2.40	0.90	13.54	0.018836	N/A
113	01023734-4-B	0	0	2.40	0.94	18.39	0.017765	N/A
114	01023734-5-B	0	0	2.40	0.85	20.76	0.018964	N/A
115	01023735-1-B	0	0	2.40	0.98	19.33	0.000419	0.508
116	01023735-2-B	0	0	2.40	0.91	19.41	0.000419	0.474
117	01023735-3-B	0	0	2.40	1.29	14.27	0.000419	0.473
118	01023741-1-B	0	0	2.40	0.97	17.28	0.003721	0.747
119	01023741-2-B	0	0	2.40	0.85	14.47	0.000417	0.725
120	01023744-1-B	1	1	2.40	0.96	13.42	0.000413	0.761
121	01023744-2-B	0	0	2.40	0.79	15.05	0.000428	0.766
122	01023746-1-B	0	0	2.40	0.99	17.57	0.000420	0.776
123	01023746-2-B	0	0	2.40	0.86	18.63	0.000420	0.757
124	01023746-3-B	0	0	2.40	1.32	19.21	0.018188	0.677
125	01023747-2-B	0	0	2.40	1.22	18.24	0.003105	N/A
126	01023747-4-B	0	0	2.40	0.71	17.47	0.000837	N/A
127	01023748-1-B	0	0	2.40	1.04	21.74	0.000453	0.640
128	01023748-2-B	0	0	2.40	0.83	20.91	0.000421	0.630
129	01023754-1-B	0	0	2.40	0.99	18.45	0.000420	0.918
130	01023754-3-B	0	0	2.40	0.82	17.86	0.000419	0.921
131	01023755-1-B	1	0	2.40	1.04	8.62	0.000414	0.910
132	01023755-2-B	0	0	2.40	1.06	22.69	0.000441	0.997
133	01023755-3-B	1	0	2.40	1.22	10.67	0.000414	0.933
134	01023756-1-B	0	0	2.40	0.85	15.05	0.000004	0.847
135	01023756-2-B	0	0	2.40	0.88	16.09	0.000004	0.894
136	01023757-1-B	0	1	2.40	0.98	14.05	0.000409	0.868
137	01023757-2-B	1	0	2.40	0.93	11.94	0.000395	1.076
138	01025222-B	1	1	2.40	1.50	8.81	0.000421	0.697

Table 4.2 (Continued)

139	01025224-2-B	0	0	2.40	1.04	15.00	0.000419	1.260
140	01025224-3-B	1	0	2.40	0.92	8.87	0.000003	1.261
141	01025226-2-B	0	1	2.40	0.92	19.46	0.000420	1.368
142	01025226-3-B	0	0	2.40	0.93	16.77	0.003193	1.197
143	01025226-4-B	0	0	2.40	0.81	15.08	0.000418	1.241
144	01025226-5-B	0	0	2.40	0.93	17.39	0.000415	1.057
145	01025227-3-B	0	0	2.40	1.01	15.85	0.000419	1.034
146	01025227-4-B	0	0	2.40	0.91	18.91	0.003245	1.184
147	01025227-5-B	1	0	2.40	0.86	11.18	0.000418	1.369
148	01025228-1-B	0	0	2.40	1.02	18.77	0.000416	0.906
149	01025228-2-B	0	0	2.40	0.81	18.40	0.000417	0.929
150	01025228-3-B	0	0	2.40	0.90	15.05	0.000421	1.129
151	01025229-1-B	1	0	2.40	1.07	10.93	0.000422	0.945
152	01025229-2-B	1	0	2.40	0.90	13.24	0.003225	1.060
153	01025229-3-B	0	0	2.40	0.94	17.68	0.000053	1.148
154	01025229-4-B	0	0	2.40	0.97	12.68	0.000419	1.217
155	01025232-2-B	0	0	2.40	0.89	13.09	0.000420	0.852
156	01025232-3-B	0	0	2.40	0.92	18.12	0.000419	0.886
157	01025232-4-B	0	0	2.40	0.90	14.30	0.000004	0.828
158	01025261-3-B	1	0	2.40	1.15	6.43	0.000417	0.663

Note: the DTN for the specimen information in this table is 018LM.002.

* 0: no obvious major flaws and/or weakness inclusions, 1: visible obvious flaws and/or weakness inclusions.
** 0: with cardboard bearing strip, 1: without.
*** Broken accidentally before getting results

CHAPTER 5 UNIAXIAL COMPRESSIVE TESTING OF LITHOPHYSAL SPECIMENS

5.1 Experimental description

In this chapter, the uniaxial compression tests on specimens containing lithophysae are discussed (Tables 5.1 and 5.2). Nineteen tests fall into this category. These specimens were collected from the upper lithophysal (Tptpul) and lower lithophysal (Tptpll) units of the Topopah Spring Tuff. Another group of nine tests on specimens that do not contain lithophysae are listed in Tables 5.3 and 5.4 at the end of this chapter.

The nineteen specimens contain a significant number of lithophysae and large vapor-phase altered zones (Fig. 5.1). These weakness inclusions make these specimens much weaker. In some cases measuring the mechanical properties of a specimen becomes difficult or impossible. The main purpose of testing these specimens is to see how they fail. For only six specimens have we been able to measure strains and calculate some "nominal" Young's modulus as well as Poisson's ratio. Given that strains and stress in these specimens are highly nonuniform, these properties can be considered as some descriptor of local axial and lateral stiffness of the specimen. The force-displacement plots for these tests probably give a better measure of the stiffness of these specimens.

Table 5.1 Source information for the specimens containing lithophysae

Specimen ID	Borehole	Range in Borehole (ft)	Unit
01014755-U	USW UZ-14	828.8-828.4	Tptpll
01014979-U	UE-25 UZ#16	422.4-422.8	Tptpul
01014985-U	USW SD-12	442.0-442.4	Tptpul
01014994-U	USW SD-12	513.4-513.8	Tptpul
01015001-U	USW SD-12	600.3-600.6	Tptpul
01015004-U	USW SD-12	614.8-615.4	Tptpul
01015455-1-U	USW SD-12	519.4-520.1	Tptpul
01015456-U	USW SD-12	520.2-520.6	Tptpul
01014723-U	UE-25-UZ#16	785.8-786.3	Tptpll
01014759-U	USW UZ-14	990.4-990.8	Tptpll
01014760-U	USW UZ-14	992.2-992.9	Tptpll
01014765-U	USW UZ-14	1077.3-1077.7	Tptpll
01014779-1-U	USW UZ-14	1137.0-1137.5	Tptpll
01014780-U	USW UZ-14	1023.2-1023.6	Tptpll
01014947-1-U	UE-25 UZ#16	451.2-452.4	Tptpul
01014977-U	UE-25 UZ#16	420.5-420.9	Tptpul
01014986-U	USW SD-12	446.9-447.2	Tptpul
01015003-U	USW SD-12	613.2-613.6	Tptpul
01015453-U	USW SD-12	518.5-518.9	Tptpul

Note: the Unit column is Non-Q, for information only.

All nineteen specimens have a nominal diameter of 2.4 inch (60.96 mm). Moisture content is not measured. Fig. 5.1 shows two typical specimens.

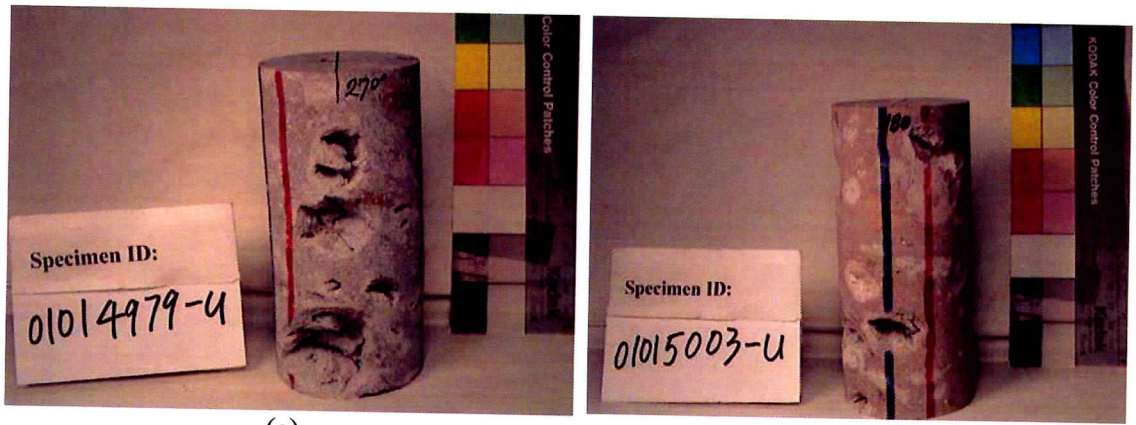

(a) (b)

Figure 5.1 Typical specimens containing lithophysae and vapor-phase altered zones

Strain gages have been installed on the specimen shown in Fig. 5.1 (b), but not on the one shown in Fig. 5.1 (a). Strain gage measurements may give some insight into strain distributions around lithophysae, and may assist in clarifying failure mechanisms.

Strains for the six specimens are measured using 350 ohms strain gages. Four strain gages are installed on each specimen. Two measure the axial strain and two measure the lateral strain.

Photographs of most specimens are included in the electronic database referenced in Section 1.1 of this part of the report.

5.2 Results

Test results are shown in Table 5.2. The specimens containing lithophysae do not break in a brittle mode. After initial failure they tend to retain considerable residual strength remains. Fig. 5.2 shows an example of a specimen after the first loading cycle, i.e. after the loading-unloading cycle shown in Fig. 5.3.

Table 5.2 Summary of dimensions and test results for the specimens containing lithophysae

Specimen ID	Nomimal Diameter (in)	Length (in)	Strength (MPa)	"Young's Modulus (GPa)" *	"Poisson's Ratio" *
01014755-U	2.4	5.047	30.88	N/A	N/A
01014979-U	2.4	4.961	25.73	N/A	N/A
01014985-U	2.4	4.818	12.01	N/A	N/A

Table 5.2 (Continued)

01014994-U	2.4	4.657	25.74	N/A	N/A
01015001-U	2.4	4.738	15.43	N/A	N/A
01015004-U	2.4	4.113	41.27	N/A	N/A
01015455-1-U	2.4	3.981	18.89	N/A	N/A
01015456-U	2.4	3.917	39.49	N/A	N/A
01014723-U	2.4	4.544	98.8	25.73	0.13
01014759-U	2.4	4.936	58.54	N/A	N/A
01014760-U	2.4	5.712	44.02	20.91	0.22
01014765-U	2.4	4.211	57.11	N/A	N/A
01014779-1-U	2.4	5.588	92.94	22.77	0.13
01014780-U	2.4	4.949	94.31	N/A	N/A
01014947-1-U	2.4	3.981	49.55	29.59	0.24
01014977-U	2.4	4.876	30.97	N/A	N/A
01014986-U	2.4	3.912	75.7	26.03	0.2
01015003-U	2.4	5.323	30.96	28.29	0.14
01015453-U	2.4	4.648	33.03	N/A	N/A

Note: the DTN for the specimen information in this table is 018LM.001.

* These properties should be considered as nominal values, given the fact that strain and stress distributions in these specimens were strongly nonuniform.

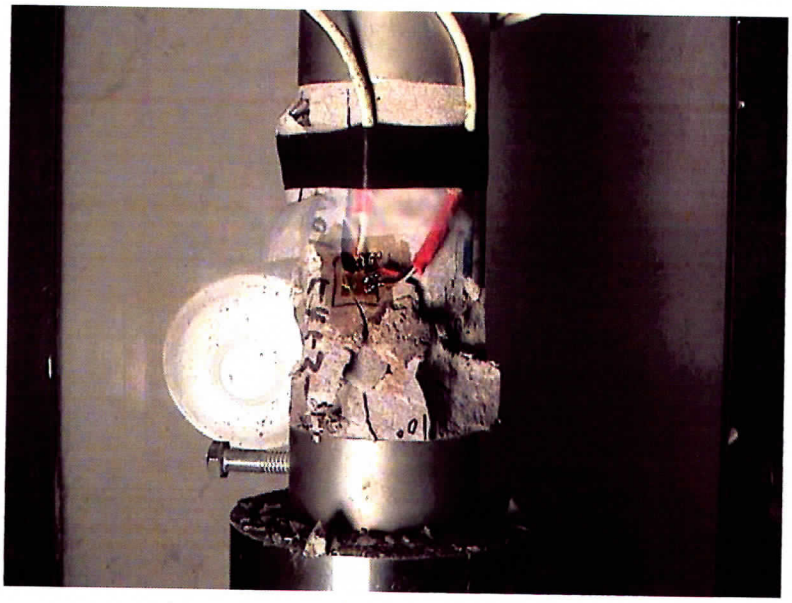

Figure 5.2 A specimen can be loaded again after failure (Specimen ID: 01015453-U, after completion of the loading-unloading cycle shown in Fig. 5.3).

Figs. 5.3 – 5.6 shows load-displacement plots for four loading-unloading cycles for the specimen shown in Fig. 5.2. The observations from these plots can be summarized as: 1) the significant nonlinear load-displacement relation during loading indicates a large nonlinear compression of the specimen; 2) the "peak" load (or at least a fairly large stress fairly close to the maximum) can be sustained over a large strain range; 3) the maximum load for any subsequent cycle is lower but close to the unloading level of the current cycle. The rock "memorizes" its previous peak strength; 4) when the specimen is unloaded to zero stress, a significant strain remains as a permanent deformation; 5) significant residual strength remains even after very large deformation (Fig. 5.6). The permanent deformation increases significantly with each loading-unloading cycle.

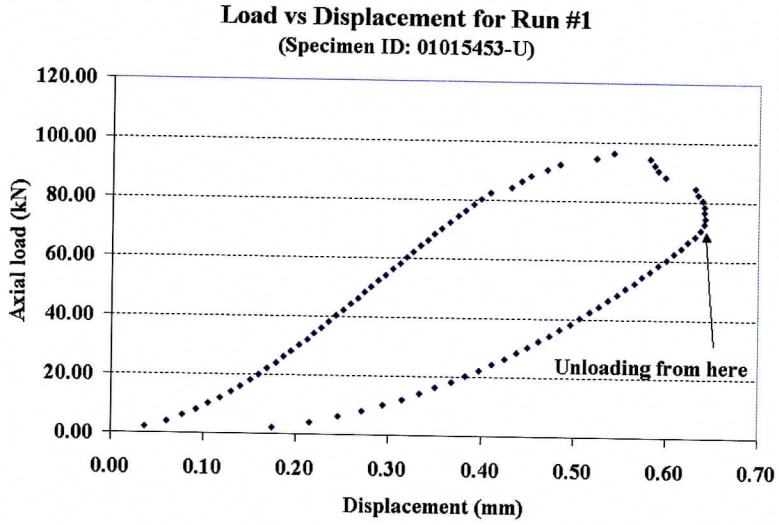

Figure 5.3 Plot of load versus displacement (Specimen ID: 01015453-U, 1st run)

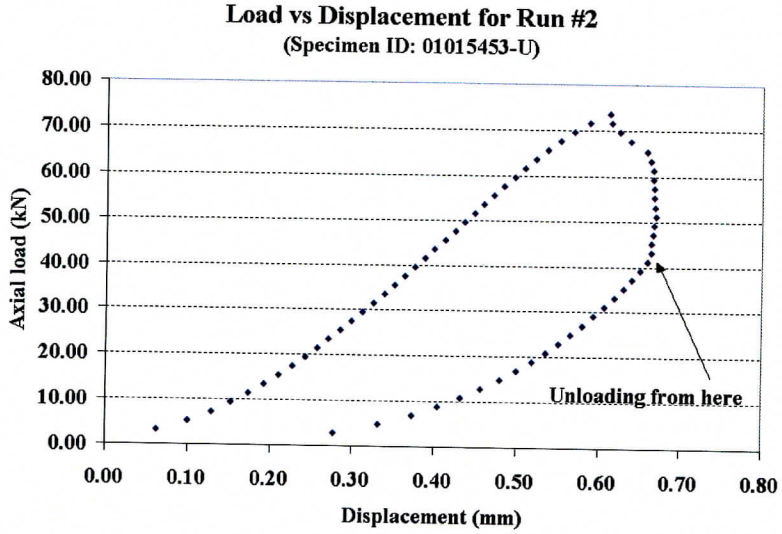

Figure 5.4 Plot of load versus displacement (Specimen ID: 01015453-U, 2nd run)

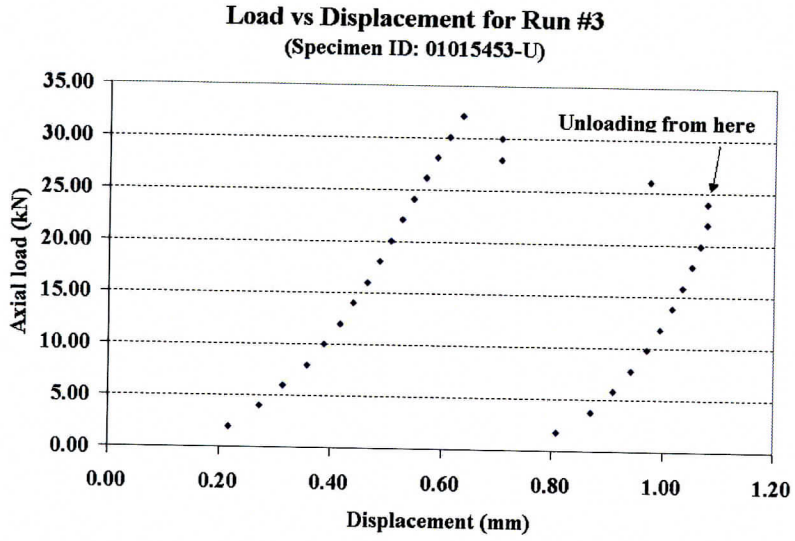

Figure 5.5 Plot of load versus displacement (Specimen ID: 01015453-U, 3rd run)

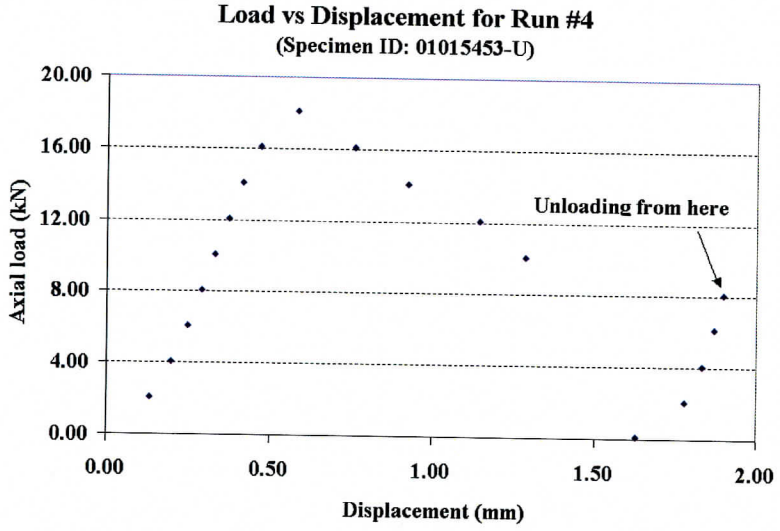

Figure 5.6 Plot of load versus displacement (Specimen ID: 01015453-U, 4th run)

5.3 Future work

Laboratory testing of lithophysal specimens can provide considerable insight into potential failure modes of excavations in lithophysal formations, but probably requires much more detailed and comprehensive analysis if one is to derive the full benefit of such tests. Striking is the non-brittle slow and gradual progress towards collapse as compared to the exceedingly brittle failure of virtual all nonlithophysal specimens tested. It is possible that a comparison of collapse mechanisms of these lithophysal samples with those of highly porous materials might be a productive avenue for further investigation

into the failure of lithophysal rock, recognizing that on the scale on which we test these samples we deal with a very small number of relatively large cavities, rather than with a very large number of very small cavities more typical for pore collapse analysis mechanics.

A first step in such a test program would be the installation of strain gages at judiciously chosen positions around lithophysal cavities (and/or using a noncontact displacement monitoring system). The purpose would be to obtain a database that can be analyzed through numerical modeling.

Videorecording of failure initiation/propagation.

Numerical analysis/simulation of failure initiation and propagation.

A/E monitoring of failure initiation and propagation should assist in identifying the location of failure events, and the stress/deformation levels at which they occur. It is of concern that the highly nonuniform, and unknown, distribution of voids in the specimens is likely to complicate the interpretation and analysis.

Table 5.3 Source information for the specimens not containing lithophysae

Specimen ID	Borehole	Range in Borehole (ft)	Unit
01014764-2-CU(U)	USW WZ-14	1076.1-1076.9	Tptpll
01014950-U	UE-25 UZ#16	544.6-544.9	Tptpmn
01015013-1-U	USW SD-12	781.7-782.5	Tptpmn
01023357-1-U	ESF-MD-NICHE 4788#1	3.3-3.8	Tptpmn
01023359-1-U	ESF-MD-NICHE 4788#1	15.7-16.5	Tptpmn
01023363-2-U	ESF-MD-NICHE 3107#7	12.1-13.6	Tptpmn
01023372-1-U	ESF-MD-NICHE 3107#7	22.7-23.4	Tptpmn
01023567-CU(U)	ESF-HD-WH-3	2.0-2.9	Tptpmn
01025234-2-U	ESF-HD-WH-33	18.0-19.1	Tptpmn

Note: the Unit column is Non-Q, for information only.

Table 5.4 Summary of dimensions and test results for the specimens not containing lithophysae

Specimen ID	Nominal diameter (in)	Length of Specimen (in)	Loading Rate (MPa/s)	Strength (MPa)	Young's Modulus (GPa)	Poisson's Ratio	Moisture content (%)
01014764-2-CU(U)	2.4	5.945	0.31	80.53	46.9	0.24	N/A
01014950-U	2.4	3.709	0.35	133.55	29.57	0.18	0.332*
01015013-1-U	2.4	4.256	0.44	263.06	34.1	N/A	0.441*
01023357-1-U	1.78	4.29	5.23E-06 /s**	224.42	35.95	0.16	0.335*
01023359-1-U	1.78	4.187	0.37	203.57	30.68	0.15	0.344*
01023363-2-U	1.78	4.29	0.31	116.99	32.61	0.16	0.470*
01023372-1-U	1.78	4.23	0.42	140.49	31.98	0.16	0.497*
01023567-CU(U)	2.4	5.46	3.69E-06 /s**	91.07	46.65	0.22	0.533*
01025234-2-U***	2.4	4.65	N/A	N/A	N/A	N/A	1.065

Note: the DTN for the information in this table is 018LM.001.

* Moisture content is measured after testing; ** Displacement control is used when testing; *** Specimen was broken accidentally before getting result.

CHAPTER 6 REFERENCES AND BIBLIOGRAPHY

6.1 References

Ameen, M. S., Edit, 1995, *Fractography: Fracture Topography as a Tool in Fracture Mechanics and Stress Analysis*, Geological Society Special Publication No. 92, London.

ASTM D 2938-95, "Standard Test Method for Unconfined Compressive Strength of Intact Rock Core Specimens," *Annual Book of ASTM Standards*, Section 4, Construction, Volume 04.08 Soil and Rock, Building Stones, American Society for Testing and Materials, Philadelphia.

ASTM D3967-95a, "Standard Test Method for Splitting Tensile Strength of Intact Rock Core Specimens," *Annual Book of ASTM Standards*, Section 4, Construction, Volume 04.08 Soil and Rock; Building Stones. American Society for Testing and Materials, Philadelphia.

ASTM D 4543-85 (Reapproved 1991), "Standard Practice for Preparing Rock Core Specimens and Determining Dimensional and Shape Tolerances," *Annual Book of ASTM Standards*, Section 4, Construction, Volume 04.08 Soil and Rock; Building Stones. American Society for Testing and Materials, Philadelphia.

Costin, L. S. "Time-Dependent Damage and Creep of Brittle Rock." *Damage Mechanics and Continuum Modeling*, Proceedings of 2 Sessions Sponsored by the Engineering Mechanics Division of the American Society of Civil Engineers in Conjunction with the ASCE Convention, Detroit, Michigan, Stubbs, N. and D. Krajcinovic Ed. Oct. 22, 1985.

Dusseault, M. B. and C. J. Fordham. "Time-dependent Behavior of Rocks." in *Comprehensive Rock Engineering, Principles, Practice and Projects*, PERGAMON PRESS, Oxford 1993, Editor-in-Chief J. A. Hudson, Vol.3, pp. 119-149.

Goodman, R. E., 1989, *Introduction to Rock Mechanics*, Second Edition, John Wiley & Sons, New York.

Griggs, D., "Experimental flow of rocks under conditions favoring recrystallization." *Bull. Geol. Soc. Amer.* Vol. 51, pp. 1001-1022, July 1, 1940.

Hudson, J. A. "Rock Properties, Testing Methods and Site Characterization." in *Comprehensive Rock Engineering, Principles, Practice and Projects*, PERGAMON PRESS, Oxford 1993, Editor-in-Chief J. A. Hudson, Vol.3, pp. 1-39.

Jaeger, J. C. and N. G. W. Cook, 1979, *Fundamentals of Rock Mechanics*, 3rd Ed. Chapman and Hall, London, UK.

Kranz, R. L. and C. H. Scholz, "Critical Dilatant Volume of Rocks at the Onset of Tertiary Creep", *Journal of Geophysical Research*, Vol. 82, No. 30, pp. 4893-4898, Oct.

10, 1977.

Martin, III, R. J, "Time-Dependent Crack Growth in Quartz and Its Application to the Creep of Rocks." *Journal. of Geophysical Research.* Vol. 77, No. 8, March 10 1972.

Martin, III, R. J., Price, R. H., Boyd, P. J. and J. S. Noel. "The Influence of Strain Rate and Sample Inhomogeneity on the Moduli and Strength of Welded Tuff." *Int. J. Rock Mech. Min. Sci. & Geomech. Abstr.* Vol. 30, No. 7, pp. 1507-1510, 1993.

Sholtz, C. H., "Mechanism of Creep in Brittle Rock." *Journal of Geophysical Research.* Vol. 73, No. 10, 1968b.

6.2 Bibliography

Andreev, G. E.1995. *Brittle Failure of Rock Materials- Tests Results and Constitutive Models.* A.A. Balkema, P.O.Box 1675, 3000 BR Rotterdam, Netherlands.

Brace, W. F., "A note on Brittle Crack Growth in Compression." *Journal of Geophysical Research.* Vol. 68, No. 12. pp. 3709-3713. June 15, 1963.

Brace, W. F., Silver, E., Hadley, K. and C. Goetze. "Crack and Pores: A Closer Look." *Science*, Vol. 178, No. 4058. Oct. 13, 1972.

Budynas, R. G. 1999. Advanced Strength and Applied Stress Analysis, 2nd Edition. McGraw-Hill, NY, USA.

Costin, L. S. "A Microcrack Model for the Deformation and Failure of Brittle Rock." *Journal of Geophysical Research*, Vol. 88 No. B11, pp 9485-9492, Nov. 10, 1983.

Costin, L. S. and D. J. Holcomb. "A Continuum Model of Inelasticity Deformed Brittle Rock Based on the Mechanics of Microcracks." *Constitutive Laws for Engineering Materials Theory and Application.* Proceedings of the International Conference. Desai, C. S. and R. H. Gallagher Ed. Tucson, Arizona, USA, January 10-14, 1983.

Cristescu, N. D. and U. Hunsche. 1998. *Time Effects in Rock Mechanics.* John Wiley & Sons Ltd, Baffins Lane, Chichester, West Sussex PO19 1 UD, England.

Cruden, D. M., "The Form of the Creep Law for Rock Under Uniaxial Compression." *Int. J. Rock Mech. Min. Sci.*, Vol. 8, pp. 105-126, 1971.

Farmer, I., 1983, *Engineering Behaviour of Rocks*, 2nd Edition, Chapman and Hall, London.

Griggs, D., "Creep of Rocks", *Journal of Geology*, Vol. 48, No. 3, April-May, 1939.

Kranz, R. L., "Crack Growth and Development During Creep of Barre Granite", *Int. J. Rock Mech. Min. Sci. & Geomech. Abstr.* Vol. 16, pp. 23-35.

Ladanyi, B. "Time-dependent Response of Rock Around Tunnels." in *Comprehensive Rock Engineering, Principles, Practice and Projects*, PERGAMON PRESS, Oxford 1993, Editor-in-Chief J. A. Hudson, Vol.3, pp. 77-112.

Martin, III, R. J., Price, R. H., Boyd, P. J. and J. S. Noel. *Creep in Topopah Spring Member Welded Tuff*. SAND94-2585, UC-814. Sandia National Laboratories, 1995.

Martin, R. J., Noel, J. S., Boyd, P. J and R. H. Price. "Creep Properties of the Paintbrush Tuff Recoved from Borehole USW NRG-7/7A: Data Report." SAND95-1759, UC-814. Sandia National Laboratories, 1997.

Meerschaert, M. M., 1999, *Mathematical Modeling*, 2nd Ed, Academic Press, San Diego, USA.

Munson, D. E. and P. R. Dawson. "Constitutive Model for the Low Temperature Creep of Salt (with Application to WIPP)," SAND79-1853. Sandia National Laboratories, 1979.

Schmidtke, R. H. and E. Z. Lajtai, "The Long-term Strength of Lac du Bonnet Granite." *Int. J. Rock Mech. Min. Sci. & Geomech. Abstr*. Vol. 22, No. 6, pp. 461-465, 1985.

Walsh, J. B., "The Effect of Cracks on the Uniaxial Elastic Compression of Rocks." *Journal of Geophysical Research*, Vol. 70, No. 2. pp. 399-411. Jan. 15, 1965.

Exhibit Computer Program and Source Information

1. Computer Program Used in The Part of the Technical Report:

Microsoft Word 2000
Microsoft Excel 2000
Microsoft Paint 2000

2. Source Information for Tables and Figures in the Part of the Technical Report:

Figure or Table #	DTN #	Source file within TDA	Scientific Notebook
Fig. 2.1	018LM.001	01023703-1-U (LabVIEW).xls; 01023702-2-U (LabVIEW).xls; 01025235-2-U (LabVIEW).xls	UCCSN-UNR-024 Vol. 10, p. 74; UCCSN-UNR-024 Vol. 10, p. 91; UCCSN-UNR-024 Vol. 13, p. 5
Fig. 2.2	018LM.001	01014764-2-CU(U) (LabVIEW).xls	UCCSN-UNR-024 Vol. 5, pp. 88-91
Table 2.3	018LM.001	01023582-1-U (LabVIEW).xls; 01023657-1-U (LabVIEW).xls; 01023657-3-U (LabVIEW).xls; 01023664-U (LabVIEW).xls; 01023701-1-U (LabVIEW).xls; 01023687-1-U (LabVIEW).xls; 01023740-1-U (LabVIEW).xls; 01025224-3-U (LabVIEW).xls; 01025230-2-U (LabVIEW).xls; 01023695-2-U (LabVIEW).xls; 01025234-1-U (LabVIEW).xls; 01023702-2-U (LabVIEW).xls; 01023579-1-U (LabVIEW).xls; 01023657-4-U (LabVIEW).xls; 01023707-3-U (LabVIEW).xls;	UCCSN-UNR-024 Vol. 10, pp. 15-16; UCCSN-UNR-024 Vol. 10, pp. 47-48; UCCSN-UNR-024 Vol. 10, pp. 60-61; UCCSN-UNR-024 Vol. 10, pp. 64-65; UCCSN-UNR-024 Vol. 10, pp. 66-67; UCCSN-UNR-024 Vol. 10, p. 82; UCCSN-UNR-024 Vol. 10, p. 83; UCCSN-UNR-024 Vol. 10, p. 84; UCCSN-UNR-024 Vol. 10, p. 85; UCCSN-UNR-024 Vol. 10, p. 94; UCCSN-UNR-024 Vol. 10, p. 95; UCCSN-UNR-024 Vol. 13, p. 5; UCCSN-UNR-024 Vol. 13, p. 30; UCCSN-UNR-024 Vol. 13, p. 21; UCCSN-UNR-024 Vol. 13, p. 23;

		01023732-U (LabVIEW).xls; 01023743-1-U (LabVIEW).xls; 01023760-2-U (LabVIEW).xls	UCCSN-UNR-024 Vol. 13, p. 40; UCCSN-UNR-024 Vol. 13, p. 28; UCCSN-UNR-024 Vol. 13, p. 45;
Fig. 2.3	018LM.001	01023576-3-U_broken2.jpg	A summary of the test is in UCCSN-UNR-024 Vol. 10, p. 29-30; The photo is in TDA only.
Fig. 2.4	018LM.001	01023664-U (LabVIEW) .xls	UCCSN-UNR-024 Vol. 10, pp. 64-65
Fig. 2.5	018LM.001	01023570-U (LabVIEW) .xls; 01023662-3-U (LabVIEW) .xls; 01023682-3-U (LabVIEW) .xls; 01023691-2-U (LabVIEW) .xls; 01023694-1-U (LabVIEW) .xls; 01023740-2-U (LabVIEW) .xls; 01023745-1-U (LabVIEW) .xls; 01023750-U (LabVIEW) .xls; 01023760-1-U (LabVIEW) .xls; 01025231-2-U (LabVIEW) .xls; 01025263-U (LabVIEW) .xls; 01023582-1-U (LabVIEW) .xls; 01023657-1-U (LabVIEW) .xls; 01023657-3-U (LabVIEW) .xls; 01023662-2-U (LabVIEW) .xls; 01023664-U (LabVIEW) .xls; 01023701-1-U (LabVIEW) .xls; 01025225-1-U (LabVIEW) .xls; 01023687-1-U (LabVIEW) .xls; 01023740-1-U (LabVIEW) .xls; 01025224-3-U (LabVIEW) .xls; 01025230-2-U (LabVIEW) .xls; 01023695-2-U (LabVIEW) .xls;	UCCSN-UNR-024 Vol. 13, p. 20; UCCSN-UNR-024 Vol. 13, p. 25; UCCSN-UNR-024 Vol. 13, p. 39; UCCSN-UNR-024 Vol. 13, p. 26; UCCSN-UNR-024 Vol. 13, p. 22; UCCSN-UNR-024 Vol. 13, p. 27; UCCSN-UNR-024 Vol. 13, p. 29; UCCSN-UNR-024 Vol. 13, p. 24; UCCSN-UNR-024 Vol. 13, p. 31; UCCSN-UNR-024 Vol. 13, p. 32; UCCSN-UNR-024 Vol. 13, p. 33; UCCSN-UNR-024 Vol. 10, pp. 15-16; UCCSN-UNR-024 Vol. 10, pp. 47-48; UCCSN-UNR-024 Vol. 10, pp. 60-61; UCCSN-UNR-024 Vol. 10, pp. 62-63; UCCSN-UNR-024 Vol. 10, pp. 64-65; UCCSN-UNR-024 Vol. 10, pp. 66-67; UCCSN-UNR-024 Vol. 10, p. 79; UCCSN-UNR-024 Vol. 10, p. 82; UCCSN-UNR-024 Vol. 10, p. 83; UCCSN-UNR-024 Vol. 10, p. 84; UCCSN-UNR-024 Vol. 10, p. 85; UCCSN-UNR-024 Vol. 10, p. 94;

		01025234-1-U (LabVIEW) .xls; 01023702-2-U (LabVIEW) .xls; 01023657-4-U (LabVIEW) .xls; 01023707-3-U (LabVIEW) .xls; 01023732-U (LabVIEW) .xls; 01023743-1-U (LabVIEW) .xls; 01023760-2-U (LabVIEW) .xls	UCCSN-UNR-024 Vol. 10, p. 95; UCCSN-UNR-024 Vol. 13, p. 5; UCCSN-UNR-024 Vol. 13, p. 21; UCCSN-UNR-024 Vol. 13, p. 23; UCCSN-UNR-024 Vol. 13, p. 40; UCCSN-UNR-024 Vol. 13, p. 28; UCCSN-UNR-024 Vol. 13, p. 45
Fig. 2.6	018LM.001	01025231-2-U_180deg.jpg; 01025263-U_180deg.jpg	A summary of the test is in UCCSN-UNR-024 Vol. 13, p. 32; The photo is in TDA only. A summary of the test is in UCCSN-UNR-024 Vol. 13, p. 33; The photo is in TDA only.
Fig. 2.7	018LM.001	01023575-2-U (LabVIEW) .xls; 01023582-1-U (LabVIEW) .xls; 01023580-U (LabVIEW) .xls; 01023576-2-U (LabVIEW) .xls; 01023576-3-U (LabVIEW) .xls; 01023586-3-U (LabVIEW) .xls; 01023660-1-U (LabVIEW) .xls; 01023668-3-U (LabVIEW) .xls; 01023657-1-U (LabVIEW) .xls; 01023697-1-U (LabVIEW) .xls; 01023697-4-U (LabVIEW) .xls; 01023657-3-U (LabVIEW) .xls; 01023662-2-U (LabVIEW) .xls; 01023664-U (LabVIEW) .xls; 01023701-1-U (LabVIEW) .xls; 01023689-2-U (LabVIEW) .xls; 01023692-U (LabVIEW) .xls;	UCCSN-UNR-024 Vol. 10, pp. 39-40; UCCSN-UNR-024 Vol. 10, pp. 15-16; UCCSN-UNR-024 Vol. 10, pp. 19-20; UCCSN-UNR-024 Vol. 10, pp. 21-22; UCCSN-UNR-024 Vol. 10, pp. 29-30; UCCSN-UNR-024 Vol. 10, pp. 31-32; UCCSN-UNR-024 Vol. 10, pp. 43-44; UCCSN-UNR-024 Vol. 10, pp. 45-46; UCCSN-UNR-024 Vol. 10, pp. 47-48; UCCSN-UNR-024 Vol. 10, pp. 53-54; UCCSN-UNR-024 Vol. 10, pp. 55-56; UCCSN-UNR-024 Vol. 10, pp. 60-61; UCCSN-UNR-024 Vol. 10, pp. 62-63; UCCSN-UNR-024 Vol. 10, pp. 64-65; UCCSN-UNR-024 Vol. 10, pp. 66-67; UCCSN-UNR-024 Vol. 10, p. 72; UCCSN-UNR-024 Vol. 10, p. 73;

		01023703-1-U (LabVIEW) .xls;	UCCSN-UNR-024 Vol. 10, p. 74;
		01025224-1-U (LabVIEW) .xls;	UCCSN-UNR-024 Vol. 10, p. 75;
		01023690-1-U (LabVIEW) .xls;	UCCSN-UNR-024 Vol. 10, p. 76;
		01025235-1-U (LabVIEW) .xls;	UCCSN-UNR-024 Vol. 10, p. 78;
		01025225-1-U (LabVIEW) .xls;	UCCSN-UNR-024 Vol. 10, p. 79;
		01025225-2-U (LabVIEW) .xls;	UCCSN-UNR-024 Vol. 10, p. 80;
		01023703-2-U (LabVIEW) .xls;	UCCSN-UNR-024 Vol. 10, p. 81;
		01023687-1-U (LabVIEW) .xls;	UCCSN-UNR-024 Vol. 10, p. 82;
		01023740-1-U (LabVIEW) .xls;	UCCSN-UNR-024 Vol. 10, p. 83;
		01025224-3-U (LabVIEW) .xls;	UCCSN-UNR-024 Vol. 10, p. 84;
		01025230-2-U (LabVIEW) .xls;	UCCSN-UNR-024 Vol. 10, p. 85;
		01023667-1-U (LabVIEW) .xls;	UCCSN-UNR-024 Vol. 10, p. 87;
		01025259-1-U (LabVIEW) .xls;	UCCSN-UNR-024 Vol. 10, p. 88;
		01025230-1-U (LabVIEW) .xls;	UCCSN-UNR-024 Vol. 10, p. 89;
		01023722-2-U (LabVIEW) .xls;	UCCSN-UNR-024 Vol. 10, p. 90;
		01025235-2-U (LabVIEW) .xls;	UCCSN-UNR-024 Vol. 10, p. 91;
		01023687-2-U (LabVIEW) .xls;	UCCSN-UNR-024 Vol. 10, p. 92;
		01023686-2-U (LabVIEW) .xls;	UCCSN-UNR-024 Vol. 10, p. 93;
		01023695-2-U (LabVIEW) .xls;	UCCSN-UNR-024 Vol. 10, p. 94;
		01025234-1-U (LabVIEW) .xls;	UCCSN-UNR-024 Vol. 10, p. 95;
		01023702-2-U (LabVIEW) .xls;	UCCSN-UNR-024 Vol. 13, p. 5;
		01023691-1-U (LabVIEW) .xls;	UCCSN-UNR-024 Vol. 13, p. 7;
		01023707-1-U (LabVIEW) .xls;	UCCSN-UNR-024 Vol. 13, p. 2;
		01023686-1-U (LabVIEW) .xls;	UCCSN-UNR-024 Vol. 13, p. 8;
		01025260-1-U (LabVIEW) .xls;	UCCSN-UNR-024 Vol. 13, p. 11;
		01023694-2-U (LabVIEW) .xls;	UCCSN-UNR-024 Vol. 13, p. 10;
		01023662-1-U (LabVIEW) .xls;	UCCSN-UNR-024 Vol. 13, p. 9;
		01025226-1-U (LabVIEW) .xls;	UCCSN-UNR-024 Vol. 13, p. 12;
		01025264-U (LabVIEW) .xls;	UCCSN-UNR-024 Vol. 13, p. 13;
		01023682-2-U (LabVIEW) .xls;	UCCSN-UNR-024 Vol. 13, p. 14;
		01023579-1-U (LabVIEW) .xls;	UCCSN-UNR-024 Vol. 13, p. 30;

		01023657-4-U (LabVIEW) .xls; 01023687-3-U (LabVIEW) .xls; 01023706-1-U (LabVIEW) .xls; 01023707-3-U (LabVIEW) .xls; 01023732-U (LabVIEW) .xls; 01023743-1-U (LabVIEW) .xls; 01023747-1-U (LabVIEW) .xls; 01023747-3-U (LabVIEW) .xls; 01023749-2-U (LabVIEW) .xls; 01023750-U (LabVIEW) .xls; 01023751-1-U (LabVIEW) .xls; 01023760-2-U (LabVIEW) .xls; 01025233-1-U (LabVIEW) .xls; 01025227-1-U (LabVIEW) .xls; 01025227-2-U (LabVIEW) .xls; 01025232-1-U (LabVIEW) .xls; 01025262-U (LabVIEW) .xls	UCCSN-UNR-024 Vol. 13, p. 21; UCCSN-UNR-024 Vol. 13, p. 55; UCCSN-UNR-024 Vol. 13, p. 59; UCCSN-UNR-024 Vol. 13, p. 23; UCCSN-UNR-024 Vol. 13, p. 40; UCCSN-UNR-024 Vol. 13, p. 28; UCCSN-UNR-024 Vol. 13, p. 41; UCCSN-UNR-024 Vol. 13, p. 42; UCCSN-UNR-024 Vol. 13, p. 43; UCCSN-UNR-024 Vol. 13, p. 24; UCCSN-UNR-024 Vol. 13, p. 56; UCCSN-UNR-024 Vol. 13, p. 45; UCCSN-UNR-024 Vol. 13, p. 57; UCCSN-UNR-024 Vol. 13, p. 61; UCCSN-UNR-024 Vol. 13, p. 62; UCCSN-UNR-024 Vol. 13, p. 63; UCCSN-UNR-024 Vol. 13, p. 64
Fig. 2.8	018LM.001	01025230-2-U (LabVIEW) .xls; 01023722-2-U (LabVIEW) .xls; 01023686-2-U (LabVIEW) .xls	UCCSN-UNR-024 Vol. 10, p. 85; UCCSN-UNR-024 Vol. 10, p. 90; UCCSN-UNR-024 Vol. 10, p. 93
Fig. 2.9	018LM.001	01023582-1-U (LabVIEW) .xls; 01023580-U (LabVIEW) .xls; 01023657-1-U (LabVIEW) .xls; 01023657-3-U (LabVIEW) .xls; 01023662-2-U (LabVIEW) .xls; 01023664-U (LabVIEW) .xls; 01023701-1-U (LabVIEW) .xls; 01023689-2-U (LabVIEW) .xls; 01023692-U (LabVIEW) .xls; 01023703-1-U (LabVIEW) .xls; 01025224-1-U (LabVIEW) .xls;	UCCSN-UNR-024 Vol. 10, pp. 15-16; UCCSN-UNR-024 Vol. 10, pp. 19-20; UCCSN-UNR-024 Vol. 10, pp. 47-48; UCCSN-UNR-024 Vol. 10, pp. 60-61; UCCSN-UNR-024 Vol. 10, pp. 62-63; UCCSN-UNR-024 Vol. 10, pp. 64-65; UCCSN-UNR-024 Vol. 10, pp. 66-67; UCCSN-UNR-024 Vol. 10, p. 72; UCCSN-UNR-024 Vol. 10, p. 73; UCCSN-UNR-024 Vol. 10, p. 74; UCCSN-UNR-024 Vol. 10, p. 75;

		01023690-1-U (LabVIEW) .xls;	UCCSN-UNR-024 Vol. 10, p. 76;
		01025235-1-U (LabVIEW) .xls;	UCCSN-UNR-024 Vol. 10, p. 78;
		01025225-1-U (LabVIEW) .xls;	UCCSN-UNR-024 Vol. 10, p. 79;
		01025225-2-U (LabVIEW) .xls;	UCCSN-UNR-024 Vol. 10, p. 80;
		01023703-2-U (LabVIEW) .xls;	UCCSN-UNR-024 Vol. 10, p. 81;
		01023687-1-U (LabVIEW) .xls;	UCCSN-UNR-024 Vol. 10, p. 82;
		01023740-1-U (LabVIEW) .xls;	UCCSN-UNR-024 Vol. 10, p. 83;
		01025224-3-U (LabVIEW) .xls;	UCCSN-UNR-024 Vol. 10, p. 84;
		01025230-2-U (LabVIEW) .xls;	UCCSN-UNR-024 Vol. 10, p. 85;
		01023667-1-U (LabVIEW) .xls;	UCCSN-UNR-024 Vol. 10, p. 87;
		01025259-1-U (LabVIEW) .xls;	UCCSN-UNR-024 Vol. 10, p. 88;
		01025230-1-U (LabVIEW) .xls;	UCCSN-UNR-024 Vol. 10, p. 89;
		01025235-2-U (LabVIEW) .xls;	UCCSN-UNR-024 Vol. 10, p. 91;
		01023687-2-U (LabVIEW) .xls;	UCCSN-UNR-024 Vol. 10, p. 92;
		01023686-2-U (LabVIEW) .xls;	UCCSN-UNR-024 Vol. 10, p. 93;
		01023695-2-U (LabVIEW) .xls;	UCCSN-UNR-024 Vol. 10, p. 94;
		01025234-1-U (LabVIEW) .xls;	UCCSN-UNR-024 Vol. 10, p. 95;
		01023702-2-U (LabVIEW) .xls;	UCCSN-UNR-024 Vol. 13, p. 5;
		01023691-1-U (LabVIEW) .xls;	UCCSN-UNR-024 Vol. 13, p. 7;
		01023707-1-U (LabVIEW) .xls;	UCCSN-UNR-024 Vol. 13, p. 2;
		01023686-1-U (LabVIEW) .xls;	UCCSN-UNR-024 Vol. 13, p. 8;
		01025260-1-U (LabVIEW) .xls;	UCCSN-UNR-024 Vol. 13, p. 11;
		01023694-2-U (LabVIEW) .xls;	UCCSN-UNR-024 Vol. 13, p. 10;
		01023662-1-U (LabVIEW) .xls;	UCCSN-UNR-024 Vol. 13, p. 9;
		01025226-1-U (LabVIEW) .xls;	UCCSN-UNR-024 Vol. 13, p. 12;
		01025264-U (LabVIEW) .xls;	UCCSN-UNR-024 Vol. 13, p. 13;
		01023682-2-U (LabVIEW) .xls;	UCCSN-UNR-024 Vol. 13, p. 14;
		01023579-1-U (LabVIEW) .xls;	UCCSN-UNR-024 Vol. 13, p. 30;
		01023657-4-U (LabVIEW) .xls;	UCCSN-UNR-024 Vol. 13, p. 21;
		01023687-3-U (LabVIEW) .xls;	UCCSN-UNR-024 Vol. 13, p. 55;
		01023706-1-U (LabVIEW) .xls;	UCCSN-UNR-024 Vol. 13, p. 59;

		01023707-3-U (LabVIEW) .xls; 01023747-1-U (LabVIEW) .xls; 01023747-3-U (LabVIEW) .xls; 01023750-U (LabVIEW) .xls; 01023751-1-U (LabVIEW) .xls; 01023760-2-U (LabVIEW) .xls; 01025233-1-U (LabVIEW) .xls; 01025227-1-U (LabVIEW) .xls; 01025227-2-U (LabVIEW) .xls; 01025232-1-U (LabVIEW) .xls; 01025262-U (LabVIEW) .xls	UCCSN-UNR-024 Vol. 13, p. 23; UCCSN-UNR-024 Vol. 13, p. 41; UCCSN-UNR-024 Vol. 13, p. 42; UCCSN-UNR-024 Vol. 13, p. 24; UCCSN-UNR-024 Vol. 13, p. 56; UCCSN-UNR-024 Vol. 13, p. 45; UCCSN-UNR-024 Vol. 13, p. 57; UCCSN-UNR-024 Vol. 13, p. 61; UCCSN-UNR-024 Vol. 13, p. 62; UCCSN-UNR-024 Vol. 13, p. 63; UCCSN-UNR-024 Vol. 13, p. 64
Figs. 2.10, 2.11 and 2.12	018LM.001	01023575-2-U (LabVIEW) .xls; 01023582-1-U (LabVIEW) .xls; 01023580-U (LabVIEW) .xls; 01023576-2-U (LabVIEW) .xls; 01023576-3-U (LabVIEW) .xls; 01023586-3-U (LabVIEW) .xls; 01023660-1-U (LabVIEW) .xls; 01023668-3-U (LabVIEW) .xls; 01023657-1-U (LabVIEW) .xls; 01023697-1-U (LabVIEW) .xls; 01023697-4-U (LabVIEW) .xls; 01023657-3-U (LabVIEW) .xls; 01023662-2-U (LabVIEW) .xls; 01023664-U (LabVIEW) .xls; 01023701-1-U (LabVIEW) .xls; 01023689-2-U (LabVIEW) .xls; 01023692-U (LabVIEW) .xls; 01023703-1-U (LabVIEW) .xls; 01025224-1-U (LabVIEW) .xls; 01023690-1-U (LabVIEW) .xls;	UCCSN-UNR-024 Vol. 10, pp. 39-40; UCCSN-UNR-024 Vol. 10, pp. 15-16; UCCSN-UNR-024 Vol. 10, pp. 19-20; UCCSN-UNR-024 Vol. 10, pp. 21-22; UCCSN-UNR-024 Vol. 10, pp. 29-30; UCCSN-UNR-024 Vol. 10, pp. 31-32; UCCSN-UNR-024 Vol. 10, pp. 43-44; UCCSN-UNR-024 Vol. 10, pp. 45-46; UCCSN-UNR-024 Vol. 10, pp. 47-48; UCCSN-UNR-024 Vol. 10, pp. 53-54; UCCSN-UNR-024 Vol. 10, pp. 55-56; UCCSN-UNR-024 Vol. 10, pp. 60-61; UCCSN-UNR-024 Vol. 10, pp. 62-63; UCCSN-UNR-024 Vol. 10, pp. 64-65; UCCSN-UNR-024 Vol. 10, pp. 66-67; UCCSN-UNR-024 Vol. 10, p. 72; UCCSN-UNR-024 Vol. 10, p. 73; UCCSN-UNR-024 Vol. 10, p. 74; UCCSN-UNR-024 Vol. 10, p. 75; UCCSN-UNR-024 Vol. 10, p. 76;

		01025235-1-U (LabVIEW) .xls;	UCCSN-UNR-024 Vol. 10, p. 78;
		01025225-1-U (LabVIEW) .xls;	UCCSN-UNR-024 Vol. 10, p. 79;
		01025225-2-U (LabVIEW) .xls;	UCCSN-UNR-024 Vol. 10, p. 80;
		01023703-2-U (LabVIEW) .xls;	UCCSN-UNR-024 Vol. 10, p. 81;
		01023687-1-U (LabVIEW) .xls;	UCCSN-UNR-024 Vol. 10, p. 82;
		01023740-1-U (LabVIEW) .xls;	UCCSN-UNR-024 Vol. 10, p. 83;
		01025224-3-U (LabVIEW) .xls;	UCCSN-UNR-024 Vol. 10, p. 84;
		01025230-2-U (LabVIEW) .xls;	UCCSN-UNR-024 Vol. 10, p. 85;
		01023667-1-U (LabVIEW) .xls;	UCCSN-UNR-024 Vol. 10, p. 87;
		01025259-1-U (LabVIEW) .xls;	UCCSN-UNR-024 Vol. 10, p. 88;
		01025230-1-U (LabVIEW) .xls;	UCCSN-UNR-024 Vol. 10, p. 89;
		01023722-2-U (LabVIEW) .xls;	UCCSN-UNR-024 Vol. 10, p. 90;
		01025235-2-U (LabVIEW) .xls;	UCCSN-UNR-024 Vol. 10, p. 91;
		01023687-2-U (LabVIEW) .xls;	UCCSN-UNR-024 Vol. 10, p. 92;
		01023686-2-U (LabVIEW) .xls;	UCCSN-UNR-024 Vol. 10, p. 93;
		01023695-2-U (LabVIEW) .xls;	UCCSN-UNR-024 Vol. 10, p. 94;
		01025234-1-U (LabVIEW) .xls;	UCCSN-UNR-024 Vol. 10, p. 95;
		01023702-2-U (LabVIEW) .xls;	UCCSN-UNR-024 Vol. 13, p. 5;
		01023691-1-U (LabVIEW) .xls;	UCCSN-UNR-024 Vol. 13, p. 7;
		01023707-1-U (LabVIEW) .xls;	UCCSN-UNR-024 Vol. 13, p. 2;
		01023686-1-U (LabVIEW) .xls;	UCCSN-UNR-024 Vol. 13, p. 8;
		01025260-1-U (LabVIEW) .xls;	UCCSN-UNR-024 Vol. 13, p. 11;
		01023694-2-U (LabVIEW) .xls;	UCCSN-UNR-024 Vol. 13, p. 10;
		01023662-1-U (LabVIEW) .xls;	UCCSN-UNR-024 Vol. 13, p. 9;
		01025226-1-U (LabVIEW) .xls;	UCCSN-UNR-024 Vol. 13, p. 12;
		01025264-U (LabVIEW) .xls;	UCCSN-UNR-024 Vol. 13, p. 13;
		01023682-2-U (LabVIEW) .xls;	UCCSN-UNR-024 Vol. 13, p. 14;
		01023579-1-U (LabVIEW) .xls;	UCCSN-UNR-024 Vol. 13, p. 30;
		01023657-4-U (LabVIEW) .xls;	UCCSN-UNR-024 Vol. 13, p. 21;
		01023687-3-U (LabVIEW) .xls;	UCCSN-UNR-024 Vol. 13, p. 55;
		01023706-1-U (LabVIEW) .xls;	UCCSN-UNR-024 Vol. 13, p. 59;

		01023707-3-U (LabVIEW) .xls; 01023732-U (LabVIEW) .xls; 01023743-1-U (LabVIEW) .xls; 01023747-1-U (LabVIEW) .xls; 01023747-3-U (LabVIEW) .xls; 01023749-2-U (LabVIEW) .xls; 01023750-U (LabVIEW) .xls; 01023751-1-U (LabVIEW) .xls; 01023760-2-U (LabVIEW) .xls; 01025233-1-U (LabVIEW) .xls; 01025227-1-U (LabVIEW) .xls; 01025227-2-U (LabVIEW) .xls; 01025232-1-U (LabVIEW) .xls; 01025262-U (LabVIEW) .xls	UCCSN-UNR-024 Vol. 13, p. 23; UCCSN-UNR-024 Vol. 13, p. 40; UCCSN-UNR-024 Vol. 13, p. 28; UCCSN-UNR-024 Vol. 13, p. 41; UCCSN-UNR-024 Vol. 13, p. 42; UCCSN-UNR-024 Vol. 13, p. 43; UCCSN-UNR-024 Vol. 13, p. 24; UCCSN-UNR-024 Vol. 13, p. 56; UCCSN-UNR-024 Vol. 13, p. 45; UCCSN-UNR-024 Vol. 13, p. 57; UCCSN-UNR-024 Vol. 13, p. 61; UCCSN-UNR-024 Vol. 13, p. 62; UCCSN-UNR-024 Vol. 13, p. 63; UCCSN-UNR-024 Vol. 13, p. 64
Fig. 2.13		Diagram. Not based on QA data.	
Fig. 2.14		Based on Eq. (2.8) and Fig. 2.13.	
Table 2.1	018LM.001	Summary of 01023358-U.doc; Summary of 01023362-U.doc; Summary of 01023367-1-U.doc; Summary of 01023367-2-U.doc; Summary of 01023370-1-U.doc; Summary of 01023568-1-CU(U).doc; Summary of 01023570-1-U.doc; Summary of 01023570-U.doc; Summary of 01023575-1-U.doc; Summary of 01023575-2-U.doc; Summary of 01023576-2-U.doc; Summary of 01023576-3-U.doc; Summary of 01023579-1-U.doc; Summary of 01023580-U.doc; Summary of 01023581-2-U.doc;	Attachment 4 of UCCSN-UNR-024 Vol. 5; Attachment 4 of UCCSN-UNR-024 Vol. 5; Attachment 4 of UCCSN-UNR-024 Vol. 5; Attachment 4 of UCCSN-UNR-024 Vol. 5; Attachment 4 of UCCSN-UNR-024 Vol. 5; Attachment 1 of UCCSN-UNR-024 Vol. 10; Attachment 1 of UCCSN-UNR-024 Vol. 10; Attachment 1 of UCCSN-UNR-024 Vol. 10; Attachment 1 of UCCSN-UNR-024 Vol. 10; Attachment 1 of UCCSN-UNR-024 Vol. 10; Attachment 1 of UCCSN-UNR-024 Vol. 10; Attachment 1 of UCCSN-UNR-024 Vol. 10; Attachment 1 of UCCSN-UNR-024 Vol. 10; Attachment 1 of UCCSN-UNR-024 Vol. 10; Attachment 1 of UCCSN-UNR-024 Vol. 10;

		Summary of 01023582-1-U.doc;	Attachment 1 of UCCSN-UNR-024 Vol. 10;
		Summary of 01023586-3-U.doc;	Attachment 1 of UCCSN-UNR-024 Vol. 10;
		Summary of 01023657-1-U.doc;	Attachment 1 of UCCSN-UNR-024 Vol. 10;
		Summary of 01023657-3-U.doc;	Attachment 1 of UCCSN-UNR-024 Vol. 10;
		Summary of 01023657-4-U.doc;	Attachment 1 of UCCSN-UNR-024 Vol. 10;
		Summary of 01023660-1-U.doc;	Attachment 1 of UCCSN-UNR-024 Vol. 10;
		Summary of 01023662-1-U.doc;	Attachment 1 of UCCSN-UNR-024 Vol. 10;
		Summary of 01023662-2-U.doc;	Attachment 1 of UCCSN-UNR-024 Vol. 10;
		Summary of 01023662-3-U.doc;	Attachment 1 of UCCSN-UNR-024 Vol. 10;
		Summary of 01023663-1-U.doc;	Attachment 1 of UCCSN-UNR-024 Vol. 10;
		Summary of 01023663-2-U.doc;	Attachment 1 of UCCSN-UNR-024 Vol. 10;
		Summary of 01023664-U.doc;	Attachment 1 of UCCSN-UNR-024 Vol. 10;
		Summary of 01023667-1-U.doc;	Attachment 1 of UCCSN-UNR-024 Vol. 10;
		Summary of 01023667-2-U.doc;	Attachment 1 of UCCSN-UNR-024 Vol. 10;
		Summary of 01023668-3-U.doc;	Attachment 1 of UCCSN-UNR-024 Vol. 10;
		Summary of 01023682-2-U.doc;	Attachment 1 of UCCSN-UNR-024 Vol. 10;
		Summary of 01023682-3-U.doc;	Attachment 1 of UCCSN-UNR-024 Vol. 10;
		Summary of 01023686-1-U.doc;	Attachment 1 of UCCSN-UNR-024 Vol. 10;
		Summary of 01023686-2-U.doc;	Attachment 1 of UCCSN-UNR-024 Vol. 10;
		Summary of 01023687-1-U.doc;	Attachment 1 of UCCSN-UNR-024 Vol. 10;
		Summary of 01023687-2-U.doc;	Attachment 1 of UCCSN-UNR-024 Vol. 10;
		Summary of 01023687-3-U.doc;	Attachment 1 of UCCSN-UNR-024 Vol. 10;
		Summary of 01023689-2-U.doc;	Attachment 1 of UCCSN-UNR-024 Vol. 10;
		Summary of 01023690-1-U.doc;	Attachment 1 of UCCSN-UNR-024 Vol. 10;
		Summary of 01023691-1-U.doc;	Attachment 1 of UCCSN-UNR-024 Vol. 10;
		Summary of 01023691-2-U.doc;	Attachment 1 of UCCSN-UNR-024 Vol. 10;
		Summary of 01023692-U.doc;	Attachment 1 of UCCSN-UNR-024 Vol. 10;
		Summary of 01023694-1-U.doc;	Attachment 1 of UCCSN-UNR-024 Vol. 10;
		Summary of 01023694-2-U.doc;	Attachment 1 of UCCSN-UNR-024 Vol. 10;
		Summary of 01023695-1-U.doc;	Attachment 1 of UCCSN-UNR-024 Vol. 10;
		Summary of 01023695-2-U.doc;	Attachment 1 of UCCSN-UNR-024 Vol. 10;

		Summary of 01023697-1-U.doc;	Attachment 1 of UCCSN-UNR-024 Vol. 10;
		Summary of 01023697-4-U.doc;	Attachment 1 of UCCSN-UNR-024 Vol. 10;
		Summary of 01023701-1-U.doc;	Attachment 1 of UCCSN-UNR-024 Vol. 10;
		Summary of 01023702-2-U.doc;	Attachment 1 of UCCSN-UNR-024 Vol. 10;
		Summary of 01023702-3-U.doc;	Attachment 1 of UCCSN-UNR-024 Vol. 10;
		Summary of 01023703-1-U.doc;	Attachment 1 of UCCSN-UNR-024 Vol. 10;
		Summary of 01023703-2-U.doc;	Attachment 1 of UCCSN-UNR-024 Vol. 10;
		Summary of 01023706-1-U.doc;	Attachment 1 of UCCSN-UNR-024 Vol. 10;
		Summary of 01023707-1-U.doc;	Attachment 1 of UCCSN-UNR-024 Vol. 10;
		Summary of 01023707-2-U.doc;	Attachment 1 of UCCSN-UNR-024 Vol. 10;
		Summary of 01023707-3-U.doc;	Attachment 1 of UCCSN-UNR-024 Vol. 10;
		Summary of 01023722-2-U.doc;	Attachment 1 of UCCSN-UNR-024 Vol. 10;
		Summary of 01023732-U.doc;	Attachment 1 of UCCSN-UNR-024 Vol. 10;
		Summary of 01023740-1-U.doc;	Attachment 1 of UCCSN-UNR-024 Vol. 10;
		Summary of 01023740-2-U.doc;	Attachment 1 of UCCSN-UNR-024 Vol. 10;
		Summary of 01023743-1-U.doc;	Attachment 1 of UCCSN-UNR-024 Vol. 10;
		Summary of 01023745-1-U.doc;	Attachment 1 of UCCSN-UNR-024 Vol. 10;
		Summary of 01023747-1-U.doc;	Attachment 1 of UCCSN-UNR-024 Vol. 10;
		Summary of 01023747-3-U.doc;	Attachment 1 of UCCSN-UNR-024 Vol. 10;
		Summary of 01023749-2-U.doc;	Attachment 1 of UCCSN-UNR-024 Vol. 10;
		Summary of 01023750-U.doc;	Attachment 1 of UCCSN-UNR-024 Vol. 10;
		Summary of 01023751-1-U.doc;	Attachment 1 of UCCSN-UNR-024 Vol. 10;
		Summary of 01023754-2-U.doc;	Attachment 1 of UCCSN-UNR-024 Vol. 10;
		Summary of 01023760-1-U.doc;	Attachment 1 of UCCSN-UNR-024 Vol. 10;
		Summary of 01023760-2-U.doc;	Attachment 1 of UCCSN-UNR-024 Vol. 10;
		Summary of 01025224-1-U.doc;	Attachment 1 of UCCSN-UNR-024 Vol. 10;
		Summary of 01025224-3-U.doc;	Attachment 1 of UCCSN-UNR-024 Vol. 10;
		Summary of 01025225-1-U.doc;	Attachment 1 of UCCSN-UNR-024 Vol. 10;
		Summary of 01025225-2-U.doc;	Attachment 1 of UCCSN-UNR-024 Vol. 10;
		Summary of 01025226-1-U.doc;	Attachment 1 of UCCSN-UNR-024 Vol. 10;
		Summary of 01025227-1-U.doc;	Attachment 1 of UCCSN-UNR-024 Vol. 10;

		Summary of 01025227-2-U.doc; Summary of 01025230-1-U.doc; Summary of 01025230-2-U.doc; Summary of 01025231-1-U.doc; Summary of 01025231-2-U.doc; Summary of 01025232-1-U.doc; Summary of 01025233-1-U.doc; Summary of 01025234-1-U.doc; Summary of 01025235-1-U.doc; Summary of 01025235-2-U.doc; Summary of 01025259-1-U.doc; Summary of 01025260-1-U.doc; Summary of 01025261-1-U.doc; Summary of 01025262-U.doc; Summary of 01025263-U.doc; Summary of 01025264-U.doc	Attachment 1 of UCCSN-UNR-024 Vol. 10; Attachment 1 of UCCSN-UNR-024 Vol. 10; Attachment 1 of UCCSN-UNR-024 Vol. 10; Attachment 1 of UCCSN-UNR-024 Vol. 10; Attachment 1 of UCCSN-UNR-024 Vol. 10; Attachment 1 of UCCSN-UNR-024 Vol. 10; Attachment 1 of UCCSN-UNR-024 Vol. 10; Attachment 1 of UCCSN-UNR-024 Vol. 10; Attachment 1 of UCCSN-UNR-024 Vol. 10; Attachment 1 of UCCSN-UNR-024 Vol. 10; Attachment 1 of UCCSN-UNR-024 Vol. 10; Attachment 1 of UCCSN-UNR-024 Vol. 10; Attachment 1 of UCCSN-UNR-024 Vol. 10; Attachment 1 of UCCSN-UNR-024 Vol. 10; Attachment 1 of UCCSN-UNR-024 Vol. 10; Attachment 1 of UCCSN-UNR-024 Vol. 10
Table 2.2	018LM.001	Summary of 01023358-U.doc; Summary of 01023362-U.doc; Summary of 01023367-1-U.doc; Summary of 01023367-2-U.doc; Summary of 01023370-1-U.doc; Summary of 01023568-1-CU(U).doc; Summary of 01023570-1-U.doc; Summary of 01023570-U.doc; Summary of 01023575-1-U.doc; Summary of 01023575-2-U.doc; Summary of 01023576-2-U.doc; Summary of 01023576-3-U.doc; Summary of 01023579-1-U.doc; Summary of 01023580-U.doc; Summary of 01023581-2-U.doc;	UCCSN-UNR-024 Vol. 13, p. 34; UCCSN-UNR-024 Vol. 13, p. 35; UCCSN-UNR-024 Vol. 13, p. 36; UCCSN-UNR-024 Vol. 13, p. 37; UCCSN-UNR-024 Vol. 13, p. 38; UCCSN-UNR-024 Vol. 10, pp. 27-28; UCCSN-UNR-024 Vol. 10, pp. 17-18; UCCSN-UNR-024 Vol. 13, p. 20; UCCSN-UNR-024 Vol. 10, pp. 35-36; UCCSN-UNR-024 Vol. 10, pp. 39-40; UCCSN-UNR-024 Vol. 10, pp. 21-22; UCCSN-UNR-024 Vol. 10, pp. 29-30; UCCSN-UNR-024 Vol. 13, p. 30; UCCSN-UNR-024 Vol. 10, pp. 19-20; UCCSN-UNR-024 Vol. 10, pp. 37-38;

		Summary of 01023582-1-U.doc;	UCCSN-UNR-024 Vol. 10, pp. 15-16;
		Summary of 01023586-3-U.doc;	UCCSN-UNR-024 Vol. 10, pp. 31-32;
		Summary of 01023657-1-U.doc;	UCCSN-UNR-024 Vol. 10, pp. 47-48;
		Summary of 01023657-3-U.doc;	UCCSN-UNR-024 Vol. 10, pp. 60-61;
		Summary of 01023657-4-U.doc;	UCCSN-UNR-024 Vol. 13, p. 21;
		Summary of 01023660-1-U.doc;	UCCSN-UNR-024 Vol. 10, pp. 43-44;
		Summary of 01023662-1-U.doc;	UCCSN-UNR-024 Vol. 13, p. 9;
		Summary of 01023662-2-U.doc;	UCCSN-UNR-024 Vol. 10, pp. 62-63;
		Summary of 01023662-3-U.doc;	UCCSN-UNR-024 Vol. 13, p. 25;
		Summary of 01023663-1-U.doc;	UCCSN-UNR-024 Vol. 10, pp. 49-50;
		Summary of 01023663-2-U.doc;	UCCSN-UNR-024 Vol. 10, pp. 40-41;
		Summary of 01023664-U.doc;	UCCSN-UNR-024 Vol. 10, pp. 64-65;
		Summary of 01023667-1-U.doc;	UCCSN-UNR-024 Vol. 13, p. 87;
		Summary of 01023667-2-U.doc;	UCCSN-UNR-024 Vol. 10, pp. 51-52;
		Summary of 01023668-3-U.doc;	UCCSN-UNR-024 Vol. 10, pp. 45-46;
		Summary of 01023682-2-U.doc;	UCCSN-UNR-024 Vol. 13, p. 14;
		Summary of 01023682-3-U.doc;	UCCSN-UNR-024 Vol. 13, p. 39;
		Summary of 01023686-1-U.doc;	UCCSN-UNR-024 Vol. 13, p. 8;
		Summary of 01023686-2-U.doc;	UCCSN-UNR-024 Vol. 10, p. 93;
		Summary of 01023687-1-U.doc;	UCCSN-UNR-024 Vol. 10, p. 82;
		Summary of 01023687-2-U.doc;	UCCSN-UNR-024 Vol. 10, p. 92;
		Summary of 01023687-3-U.doc;	UCCSN-UNR-024 Vol. 13, p. 55;
		Summary of 01023689-2-U.doc;	UCCSN-UNR-024 Vol. 10, p. 72;
		Summary of 01023690-1-U.doc;	UCCSN-UNR-024 Vol. 10, p. 76;
		Summary of 01023691-1-U.doc;	UCCSN-UNR-024 Vol. 13, p. 7;
		Summary of 01023691-2-U.doc;	UCCSN-UNR-024 Vol. 13, p. 26;
		Summary of 01023692-U.doc;	UCCSN-UNR-024 Vol. 10, p. 73;
		Summary of 01023694-1-U.doc;	UCCSN-UNR-024 Vol. 13, p. 22;
		Summary of 01023694-2-U.doc;	UCCSN-UNR-024 Vol. 13, p. 10;
		Summary of 01023695-1-U.doc;	UCCSN-UNR-024 Vol. 10, p. 77;
		Summary of 01023695-2-U.doc;	UCCSN-UNR-024 Vol. 10, p. 94;

		Summary of 01023697-1-U.doc;	UCCSN-UNR-024 Vol. 10, pp. 53-54;
		Summary of 01023697-4-U.doc;	UCCSN-UNR-024 Vol. 10, pp. 55-56;
		Summary of 01023701-1-U.doc;	UCCSN-UNR-024 Vol. 13, p. 3;
		Summary of 01023702-2-U.doc;	UCCSN-UNR-024 Vol. 13, p. 5;
		Summary of 01023702-3-U.doc;	UCCSN-UNR-024 Vol. 10, p. 86;
		Summary of 01023703-1-U.doc;	UCCSN-UNR-024 Vol. 10, p. 74;
		Summary of 01023703-2-U.doc;	UCCSN-UNR-024 Vol. 10, p. 81
		Summary of 01023706-1-U.doc;	UCCSN-UNR-024 Vol. 13, p. 59;
		Summary of 01023707-1-U.doc;	UCCSN-UNR-024 Vol. 13, p. 2;
		Summary of 01023707-2-U.doc;	UCCSN-UNR-024 Vol. 13, p. 58;
		Summary of 01023707-3-U.doc;	UCCSN-UNR-024 Vol. 13, p. 23;
		Summary of 01023722-2-U.doc;	UCCSN-UNR-024 Vol. 10, p. 90;
		Summary of 01023732-U.doc;	UCCSN-UNR-024 Vol. 13, p. 40;
		Summary of 01023740-1-U.doc;	UCCSN-UNR-024 Vol. 10, p. 83;
		Summary of 01023740-2-U.doc;	UCCSN-UNR-024 Vol. 13, p. 27;
		Summary of 01023743-1-U.doc;	UCCSN-UNR-024 Vol. 13, p. 28;
		Summary of 01023745-1-U.doc;	UCCSN-UNR-024 Vol. 13, p. 29;
		Summary of 01023747-1-U.doc;	UCCSN-UNR-024 Vol. 13, p. 41;
		Summary of 01023747-3-U.doc;	UCCSN-UNR-024 Vol. 13, p. 42;
		Summary of 01023749-2-U.doc;	UCCSN-UNR-024 Vol. 13, p. 43;
		Summary of 01023750-U.doc;	UCCSN-UNR-024 Vol. 13, p. 24;
		Summary of 01023751-1-U.doc;	UCCSN-UNR-024 Vol. 13, p. 56;
		Summary of 01023754-2-U.doc;	UCCSN-UNR-024 Vol. 13, p. 44;
		Summary of 01023760-1-U.doc;	UCCSN-UNR-024 Vol. 13, p. 31;
		Summary of 01023760-2-U.doc;	UCCSN-UNR-024 Vol. 13, p. 45;
		Summary of 01025224-1-U.doc;	UCCSN-UNR-024 Vol. 10, p. 75;
		Summary of 01025224-3-U.doc;	UCCSN-UNR-024 Vol. 10, p. 84;
		Summary of 01025225-1-U.doc;	UCCSN-UNR-024 Vol. 10, p. 79;
		Summary of 01025225-2-U.doc;	UCCSN-UNR-024 Vol. 10, p. 80;
		Summary of 01025226-1-U.doc;	UCCSN-UNR-024 Vol. 13, p. 12;
		Summary of 01025227-1-U.doc;	UCCSN-UNR-024 Vol. 13, p. 61;

		Summary of 01025227-2-U.doc; Summary of 01025230-1-U.doc; Summary of 01025230-2-U.doc; Summary of 01025231-1-U.doc; Summary of 01025231-2-U.doc; Summary of 01025232-1-U.doc; Summary of 01025233-1-U.doc; Summary of 01025234-1-U.doc; Summary of 01025235-1-U.doc; Summary of 01025235-2-U.doc; Summary of 01025259-1-U.doc; Summary of 01025260-1-U.doc; Summary of 01025261-1-U.doc; Summary of 01025262-U.doc; Summary of 01025263-U.doc; Summary of 01025264-U.doc	UCCSN-UNR-024 Vol. 13, p. 62; UCCSN-UNR-024 Vol. 10, p. 89; UCCSN-UNR-024 Vol. 10, p. 85; UCCSN-UNR-024 Vol. 13, p. 6; UCCSN-UNR-024 Vol. 13, p. 32; UCCSN-UNR-024 Vol. 13, p. 63; UCCSN-UNR-024 Vol. 13, p. 57; UCCSN-UNR-024 Vol. 10, p. 95; UCCSN-UNR-024 Vol. 10, p. 78; UCCSN-UNR-024 Vol. 10, p. 91; UCCSN-UNR-024 Vol. 10, p. 88; UCCSN-UNR-024 Vol. 13, p. 11; UCCSN-UNR-024 Vol. 13, p. 46; UCCSN-UNR-024 Vol. 13, p. 64; UCCSN-UNR-024 Vol. 13, p. 33; UCCSN-UNR-024 Vol. 13, p. 13
Table 3.1	018LM.003	Summary of 01014949-1-CU.doc; Summary of 01014951-1-CU.doc; Summary of 01014951-2-CU.doc; Summary of 01014733-2-CU.doc; Summary of 01014756-1-CU.doc; Summary of 01015022-1-CU.doc; Summary of 01015022-2-CU.doc; Summary of 01015465-CU.doc; Summary of 01023361-1-CU.doc; Summary of 01023363-1-CU.doc; Summary of 01023363-3-CU.doc; Summary of 01023364-1-CU.doc; Summary of 01023582-3-CU.doc; Summary of 01023665-2-CU.doc	Attachment 1 of UCCSN-UNR-024 Vol. 5; Attachment 1 of UCCSN-UNR-024 Vol. 5; Attachment 1 of UCCSN-UNR-024 Vol. 5; Attachment 4 of UCCSN-UNR-024 Vol. 5; Attachment 1 of UCCSN-UNR-024 Vol. 5; Attachment 4 of UCCSN-UNR-024 Vol. 5; Attachment 4 of UCCSN-UNR-024 Vol. 5; Attachment 4 of UCCSN-UNR-024 Vol. 5; Attachment 4 of UCCSN-UNR-024 Vol. 5; Attachment 4 of UCCSN-UNR-024 Vol. 5; Attachment 4 of UCCSN-UNR-024 Vol. 5; Attachment 4 of UCCSN-UNR-024 Vol. 5; Attachment 1 of UCCSN-UNR-024 Vol. 10; Attachment 1 of UCCSN-UNR-024 Vol. 10

Fig. 3.1		Diagram. Not based on QA data.	
Fig. 3.2	018LM.003	01023364-1-CU (LabVIEW).xls	UCCSN-UNR-024 Vol. 10, pp. 13-14
Fig. 3.3	018LM.003	01014733-2-CU_0deg.jpg	A summary of the test is in UCCSN-UNR-024 Vol. 10, pp. 33-34; The photo is in TDA only.
Tables 3.2 and 3.3	018LM.003	Summary of 01014949-1-CU.doc; Summary of 01014951-1-CU.doc; Summary of 01014951-2-CU.doc; Summary of 01014733-2-CU.doc; Summary of 01014756-1-CU.doc; Summary of 01015022-1-CU.doc; Summary of 01015022-2-CU.doc; Summary of 01015465-CU.doc; Summary of 01023361-1-CU.doc; Summary of 01023363-1-CU.doc; Summary of 01023363-3-CU.doc; Summary of 01023364-1-CU.doc; Summary of 01023582-3-CU.doc; Summary of 01023665-2-CU.doc	UCCSN-UNR-024 Vol. 5, pp. 93-94; UCCSN-UNR-024 Vol. 10, pp. 1-2; UCCSN-UNR-024 Vol. 10, pp. 11-12; UCCSN-UNR-024 Vol. 10, pp. 33-34; UCCSN-UNR-024 Vol. 5, pp. 69-75; UCCSN-UNR-024 Vol. 5, pp. 95-97; UCCSN-UNR-024 Vol. 10, pp. 58-59; UCCSN-UNR-024 Vol. 13, p. 60; UCCSN-UNR-024 Vol. 10, pp. 3-4; UCCSN-UNR-024 Vol. 10, pp. 9-10; UCCSN-UNR-024 Vol. 10, pp. 6-7; UCCSN-UNR-024 Vol. 10, pp. 13-14; UCCSN-UNR-024 Vol. 10, pp. 23-24; UCCSN-UNR-024 Vol. 13, p. 3
Figs. 3.4 - 3.8	018LM.003	01023364-1-CU (LabVIEW).xls	UCCSN-UNR-024 Vol. 10, pp. 13-14
Fig. 3.9	018LM.003	01023365-2-CU (LabVIEW).xls	UCCSN-UNR-024 Vol. 13, p. 3
Fig. 3.10		Diagram. Not based on QA data.	
Figs. 3.11 and 3.12	018LM.003	01023364-1-CU (LabVIEW).xls	UCCSN-UNR-024 Vol. 10, pp. 13-14
Fig. 3.13	018LM.003	01023363-1-CU (LabVIEW).xls	UCCSN-UNR-024 Vol. 10, pp. 9-10
Fig. 3.14	018LM.003	01023365-2-CU (LabVIEW).xls	UCCSN-UNR-024 Vol. 13, p. 3
Fig. 3.15	018LM.003	01014951-2-CU (LabVIEW).xls	UCCSN-UNR-024 Vol. 10, pp. 11-12
Fig. 3.16	018LM.003	01014951-1-CU (LabVIEW).xls	UCCSN-UNR-024 Vol. 10, pp. 1-2
Fig. 3.17	018LM.003	01014733-2-CU (LabVIEW).xls	UCCSN-UNR-024 Vol. 10, pp. 33-34
Fig. 3.18	018LM.003	01023363-3-CU (LabVIEW).xls	UCCSN-UNR-024 Vol. 10, pp. 6-7
Fig. 3-I-1	018LM.003	01014949-1-CU (LabVIEW).xls	UCCSN-UNR-024 Vol. 5, pp. 93-94

Fig. 3-I-2	018LM.003	01014951-1-CU (LabVIEW).xls	UCCSN-UNR-024 Vol. 10, pp. 1-2
Fig. 3-I-3	018LM.003	01014951-2-CU (LabVIEW).xls	UCCSN-UNR-024 Vol. 10, pp. 11-12
Fig. 3-I-4	018LM.003	01014733-2-CU (LabVIEW).xls	UCCSN-UNR-024 Vol. 10, pp. 33-34
Fig. 3-I-5	018LM.003	01014756-1-CU (LabVIEW).xls	UCCSN-UNR-024 Vol. 5, pp. 69-75
Fig. 3-I-6	018LM.003	01015022-1-CU (LabVIEW).xls	UCCSN-UNR-024 Vol. 5, pp. 95-97
Fig. 3-I-7	018LM.003	01015022-2-CU (LabVIEW).xls	UCCSN-UNR-024 Vol. 10, pp. 58-59
Fig. 3-I-8	018LM.003	01015465-CU (LabVIEW).xls	UCCSN-UNR-024 Vol. 13, p. 60
Fig. 3-I-9	018LM.003	01023361-1-CU (LabVIEW).xls	UCCSN-UNR-024 Vol. 10, pp. 3-4;
Fig. 3-I-10	018LM.003	01023363-1-CU (LabVIEW).xls	UCCSN-UNR-024 Vol. 10, pp. 9-10
Fig. 3-I-11	018LM.003	01023363-3-CU (LabVIEW).xls	UCCSN-UNR-024 Vol. 10, pp. 6-7
Fig. 3-I-12	018LM.003	01023582-3-CU (LabVIEW).xls	UCCSN-UNR-024 Vol. 10, pp. 23-24
Fig. 3-I-13	018LM.003	01023665-2-CU (LabVIEW).xls	UCCSN-UNR-024 Vol. 13, p. 3
Fig. 4.1	018LM.002	Machine picture. Not based on QA data.	
Table 4.3	018LM.002	The data for this table is contained in the file Summary of Brazilian Tests.xls. The following 117 tests are used to construct the table. 01023570-3-B; 01023576-1-B; 01023581-4-B; 01023581-3-B; 01023582-2-B; 01023581-1-B; 01023580-1-B; 01023570-4-B; 01023586-2-B; 01023579-2-B; 01023567-4-B;	UCCSN-UNR-024 Vol. 13, pp. 15-19

		01023567-3-B; 01023567-2-B; 01014733-1-B; 01023357-2-B; 01023359-2-B; 01023359-3-B; 01023363-4-B; 01023367-5-B; 01023363-5-B; 01023370-3-B; 01023372-3-B; 01023370-2-B; 01023367-3-B; 01023367-4-B; 01023690-5-B; 01023574-2-B; 01023755-2-B; 01023748-1-B; 01023757-2-B; 01023685-4-B; 01023701-3-B; 01023715-1-B; 01023685-5-B; 01023727-2-B; 01023690-3-B; 01023757-1-B; 01023744-1-B; 01023685-8-B; 01025222-B; 01025226-2-B; 01023685-3-B;	

		01023574-1-B; 01023693-2-B; 01023697-4-B; 01023697-3-B; 01023661-1-B; 01023574-7-B; 01023574-5-B; 01023735-2-B; 01023715-2-B; 01023693-1-B; 01023715-3-B; 01023585-1-B; 01023701-2-B; 01023685-7-B; 01023689-5-B; 01025228-1-B; 01023571-4-B; 01023685-6-B; 01023702-1-B; 01023574-6-B; 01025227-3-B; 01025227-5-B; 01023566-2-B; 01023741-2-B; 01023748-2-B; 01023689-6-B; 01025232-3-B; 01023690-2-B; 01023701-4-B; 01023727-1-B; 01023754-1-B;	

		01023704-1-B; 01023744-2-B; 01025261-3-B; 01023715-4-B; 01023690-4-B; 01023571-2-B; 01023746-2-B; 01023735-1-B; 01023755-1-B; 01023689-7-B; 01025224-2-B; 01025226-4-B; 01025232-2-B; 01023721-2-B; 01023735-3-B; 01023661-2-B; 01023754-3-B; 01023755-3-B; 01023689-4-B; 01023746-1-B; 01025226-5-B; 01023657-8-B; 01025228-3-B; 01025229-4-B; 01025228-2-B; 01025229-1-B; 01023689-3-B; 01023734-1-B; 01023734-2-B; 01023666-1-B; 01023666-4-B;	

		01014764-1-B; 01014764-3-B; 01023570-2-B; 01023586-1-B; 01023666-2-B; 01023668-6-B; 01023668-7-B; 01023704-9-B; 01023668-1-B; 01023668-2-B; 01023704-4-B; 01023704-6-B; 01023747-4-B	
Fig. 4.2	018LM.002	01025224-2-B_broken.jpg	A summary of the test is in UCCSN-UNR-024 Vol. 13, pp. 15-19; The photo is in TDA only.
Fig. 4.3	018LM.002	01023685-4-B_broken.jpg	A summary of the test is in UCCSN-UNR-024 Vol. 13, pp. 15-19; The photo is in TDA only.
Fig. 4.4	018LM.002	01023747-2-B_broken.jpg	A summary of the test is in UCCSN-UNR-024 Vol. 13, pp. 15-19; The photo is in TDA only.
Fig. 4.5	018LM.002	01023658-5-B_broken.jpg	A summary of the test is in UCCSN-UNR-024 Vol. 13, pp. 15-19; The photo is in TDA only.
Fig. 4.6	018LM.002	The data for this figure is contained in the file Summary of Brazilian Tests.xls. The following 112 tests are used to construct the figure. 01023570-3-B;	UCCSN-UNR-024 Vol. 13, pp. 15-19

		01023581-4-B; 01023581-3-B; 01023582-2-B; 01023581-1-B; 01023580-1-B; 01023570-4-B; 01023586-2-B; 01023579-2-B; 01023567-2-B; 01014733-1-B; 01023357-2-B; 01023359-2-B; 01023359-3-B; 01023363-4-B; 01023367-5-B; 01023363-5-B; 01023370-3-B; 01023372-3-B; 01023370-2-B; 01023367-3-B; 01023367-4-B; 01023690-5-B; 01023574-2-B; 01023755-2-B; 01023748-1-B; 01023685-4-B; 01023701-3-B; 01023715-1-B; 01023574-7-B; 01023735-2-B; 01023715-2-B;	

		01023693-1-B; 01023715-3-B; 01023585-1-B; 01023697-2-B; 01023701-2-B; 01023689-5-B; 01025228-1-B; 01023571-4-B; 01023574-6-B; 01025227-3-B; 01023566-2-B; 01023741-2-B; 01023748-2-B; 01025232-3-B; 01023574-3-B; 01023690-2-B; 01023701-4-B; 01023727-1-B; 01023754-1-B; 01023704-1-B; 01023744-2-B; 01023715-4-B; 01023690-4-B; 01023571-2-B; 01023746-2-B; 01023741-1-B; 01023685-2-B; 01023571-1-B; 01025226-3-B; 01023571-3-B; 01025227-4-B;	

		01023685-1-B; 01023657-7-B; 01023585-2-B; 01023756-2-B; 01023746-3-B; 01023756-1-B; 01023735-1-B; 01023689-7-B; 01023657-6-B; 01025224-2-B; 01023574-4-B; 01025226-4-B; 01025232-2-B; 01025232-4-B; 01023721-2-B; 01023735-3-B; 01023661-2-B; 01023754-3-B; 01023721-1-B; 01023661-3-B; 01023689-4-B; 01023746-1-B; 01025226-5-B; 01023657-8-B; 01025229-3-B; 01025228-3-B; 01025229-4-B; 01025228-2-B; 01023689-3-B; 01023734-4-B; 01023734-5-B;	

		01023666-3-B; 01023668-8-B; 01023658-1-B; 01023658-6-B; 01023704-8-B; 01023704-7-B; 01023668-5-B; 01023668-4-B; 01023668-1-B; 01023668-2-B; 01023704-3-B; 01023704-4-B; 01023704-6-B; 01023658-2-B; 01023658-3-B; 01023658-4-B; 01023747-4-B; 01023747-2-B	
Table 4.1	018LM.002	This table contains the following 158 specimens, which are available in the file Summary of Brazilian Tests.xls in TDA. 01014733-1-B 01014764-1-B 01014764-3-B 01023357-2-B 01023359-2-B 01023359-3-B 01023363-4-B 01023363-5-B 01023363-6-B	 Attachment 1 of UCCSN-UNR-024 Vol. 5; Attachment 1 of UCCSN-UNR-024 Vol. 5; Attachment 1 of UCCSN-UNR-024 Vol. 5; Attachment 4 of UCCSN-UNR-024 Vol. 5; Attachment 4 of UCCSN-UNR-024 Vol. 5; Attachment 4 of UCCSN-UNR-024 Vol. 5; Attachment 4 of UCCSN-UNR-024 Vol. 5; Attachment 4 of UCCSN-UNR-024 Vol. 5; Attachment 4 of UCCSN-UNR-024 Vol. 5;

		01023367-3-B	Attachment 4 of UCCSN-UNR-024 Vol. 5;
		01023367-4-B	Attachment 4 of UCCSN-UNR-024 Vol. 5;
		01023367-5-B	Attachment 4 of UCCSN-UNR-024 Vol. 5;
		01023370-2-B	Attachment 4 of UCCSN-UNR-024 Vol. 5;
		01023370-3-B	Attachment 4 of UCCSN-UNR-024 Vol. 5;
		01023372-3-B	Attachment 4 of UCCSN-UNR-024 Vol. 5;
		01023566-2-B	Attachment 1 of UCCSN-UNR-024 Vol. 10;
		01023567-2-B	Attachment 1 of UCCSN-UNR-024 Vol. 10;
		01023567-3-B	Attachment 1 of UCCSN-UNR-024 Vol. 10;
		01023567-4-B	Attachment 1 of UCCSN-UNR-024 Vol. 10;
		01023570-2-B	Attachment 1 of UCCSN-UNR-024 Vol. 10;
		01023570-3-B	Attachment 1 of UCCSN-UNR-024 Vol. 10;
		01023570-4-B	Attachment 1 of UCCSN-UNR-024 Vol. 10;
		01023571-1-B	Attachment 1 of UCCSN-UNR-024 Vol. 10;
		01023571-2-B	Attachment 1 of UCCSN-UNR-024 Vol. 10;
		01023571-3-B	Attachment 1 of UCCSN-UNR-024 Vol. 10;
		01023571-4-B	Attachment 1 of UCCSN-UNR-024 Vol. 10;
		01023574-1-B	Attachment 1 of UCCSN-UNR-024 Vol. 10;
		01023574-2-B	Attachment 1 of UCCSN-UNR-024 Vol. 10;
		01023574-3-B	Attachment 1 of UCCSN-UNR-024 Vol. 10;
		01023574-4-B	Attachment 1 of UCCSN-UNR-024 Vol. 10;
		01023574-5-B	Attachment 1 of UCCSN-UNR-024 Vol. 10;
		01023574-6-B	Attachment 1 of UCCSN-UNR-024 Vol. 10;
		01023574-7-B	Attachment 1 of UCCSN-UNR-024 Vol. 10;
		01023576-1-B	Attachment 1 of UCCSN-UNR-024 Vol. 10;
		01023579-2-B	Attachment 1 of UCCSN-UNR-024 Vol. 10;
		01023580-1-B	Attachment 1 of UCCSN-UNR-024 Vol. 10;
		01023581-1-B	Attachment 1 of UCCSN-UNR-024 Vol. 10;
		01023581-3-B	Attachment 1 of UCCSN-UNR-024 Vol. 10;
		01023581-4-B	Attachment 1 of UCCSN-UNR-024 Vol. 10;
		01023582-2-B	Attachment 1 of UCCSN-UNR-024 Vol. 10;

		01023585-1-B	Attachment 1 of UCCSN-UNR-024 Vol. 10;
		01023585-2-B	Attachment 1 of UCCSN-UNR-024 Vol. 10;
		01023586-1-B	Attachment 1 of UCCSN-UNR-024 Vol. 10;
		01023586-2-B	Attachment 1 of UCCSN-UNR-024 Vol. 10;
		01023657-6-B	Attachment 1 of UCCSN-UNR-024 Vol. 10;
		01023657-7-B	Attachment 1 of UCCSN-UNR-024 Vol. 10;
		01023657-8-B	Attachment 1 of UCCSN-UNR-024 Vol. 10;
		01023658-1-B	Attachment 1 of UCCSN-UNR-024 Vol. 10;
		01023658-2-B	Attachment 1 of UCCSN-UNR-024 Vol. 10;
		01023658-3-B	Attachment 1 of UCCSN-UNR-024 Vol. 10;
		01023658-4-B	Attachment 1 of UCCSN-UNR-024 Vol. 10;
		01023658-5-B	Attachment 1 of UCCSN-UNR-024 Vol. 10;
		01023658-6-B	Attachment 1 of UCCSN-UNR-024 Vol. 10;
		01023661-1-B	Attachment 1 of UCCSN-UNR-024 Vol. 10;
		01023661-2-B	Attachment 1 of UCCSN-UNR-024 Vol. 10;
		01023661-3-B	Attachment 1 of UCCSN-UNR-024 Vol. 10;
		01023666-1-B	Attachment 1 of UCCSN-UNR-024 Vol. 10;
		01023666-2-B	Attachment 1 of UCCSN-UNR-024 Vol. 10;
		01023666-3-B	Attachment 1 of UCCSN-UNR-024 Vol. 10;
		01023666-4-B	Attachment 1 of UCCSN-UNR-024 Vol. 10;
		01023668-1-B	Attachment 1 of UCCSN-UNR-024 Vol. 10;
		01023668-2-B	Attachment 1 of UCCSN-UNR-024 Vol. 10;
		01023668-4-B	Attachment 1 of UCCSN-UNR-024 Vol. 10;
		01023668-5-B	Attachment 1 of UCCSN-UNR-024 Vol. 10;
		01023668-6-B	Attachment 1 of UCCSN-UNR-024 Vol. 10;
		01023668-7-B	Attachment 1 of UCCSN-UNR-024 Vol. 10;
		01023668-8-B	Attachment 1 of UCCSN-UNR-024 Vol. 10;
		01023685-1-B	Attachment 1 of UCCSN-UNR-024 Vol. 10;
		01023685-2-B	Attachment 1 of UCCSN-UNR-024 Vol. 10;
		01023685-3-B	Attachment 1 of UCCSN-UNR-024 Vol. 10;
		01023685-4-B	Attachment 1 of UCCSN-UNR-024 Vol. 10;

		01023685-5-B	Attachment 1 of UCCSN-UNR-024 Vol. 10;
		01023685-6-B	Attachment 1 of UCCSN-UNR-024 Vol. 10;
		01023685-7-B	Attachment 1 of UCCSN-UNR-024 Vol. 10;
		01023685-8-B	Attachment 1 of UCCSN-UNR-024 Vol. 10;
		01023689-3-B	Attachment 1 of UCCSN-UNR-024 Vol. 10;
		01023689-4-B	Attachment 1 of UCCSN-UNR-024 Vol. 10;
		01023689-5-B	Attachment 1 of UCCSN-UNR-024 Vol. 10;
		01023689-6-B	Attachment 1 of UCCSN-UNR-024 Vol. 10;
		01023689-7-B	Attachment 1 of UCCSN-UNR-024 Vol. 10;
		01023690-2-B	Attachment 1 of UCCSN-UNR-024 Vol. 10;
		01023690-3-B	Attachment 1 of UCCSN-UNR-024 Vol. 10;
		01023690-4-B	Attachment 1 of UCCSN-UNR-024 Vol. 10;
		01023690-5-B	Attachment 1 of UCCSN-UNR-024 Vol. 10;
		01023693-1-B	Attachment 1 of UCCSN-UNR-024 Vol. 10;
		01023693-2-B	Attachment 1 of UCCSN-UNR-024 Vol. 10;
		01023697-2-B	Attachment 1 of UCCSN-UNR-024 Vol. 10;
		01023697-3-B	Attachment 1 of UCCSN-UNR-024 Vol. 10;
		01023697-4-B	Attachment 1 of UCCSN-UNR-024 Vol. 10;
		01023701-2-B	Attachment 1 of UCCSN-UNR-024 Vol. 10;
		01023701-3-B	Attachment 1 of UCCSN-UNR-024 Vol. 10;
		01023701-4-B	Attachment 1 of UCCSN-UNR-024 Vol. 10;
		01023702-1-B	Attachment 1 of UCCSN-UNR-024 Vol. 10;
		01023704-1-B	Attachment 1 of UCCSN-UNR-024 Vol. 10;
		01023704-3-B	Attachment 1 of UCCSN-UNR-024 Vol. 10;
		01023704-4-B	Attachment 1 of UCCSN-UNR-024 Vol. 10;
		01023704-5-B	Attachment 1 of UCCSN-UNR-024 Vol. 10;
		01023704-6-B	Attachment 1 of UCCSN-UNR-024 Vol. 10;
		01023704-7-B	Attachment 1 of UCCSN-UNR-024 Vol. 10;
		01023704-8-B	Attachment 1 of UCCSN-UNR-024 Vol. 10;
		01023704-9-B	Attachment 1 of UCCSN-UNR-024 Vol. 10;
		01023715-1-B	Attachment 1 of UCCSN-UNR-024 Vol. 10;

		01023715-2-B	Attachment 1 of UCCSN-UNR-024 Vol. 10;
		01023715-3-B	Attachment 1 of UCCSN-UNR-024 Vol. 10;
		01023715-4-B	Attachment 1 of UCCSN-UNR-024 Vol. 10;
		01023721-1-B	Attachment 1 of UCCSN-UNR-024 Vol. 10;
		01023721-2-B	Attachment 1 of UCCSN-UNR-024 Vol. 10;
		01023727-1-B	Attachment 1 of UCCSN-UNR-024 Vol. 10;
		01023727-2-B	Attachment 1 of UCCSN-UNR-024 Vol. 10;
		01023734-1-B	Attachment 1 of UCCSN-UNR-024 Vol. 10;
		01023734-2-B	Attachment 1 of UCCSN-UNR-024 Vol. 10;
		01023734-3-B	Attachment 1 of UCCSN-UNR-024 Vol. 10;
		01023734-4-B	Attachment 1 of UCCSN-UNR-024 Vol. 10;
		01023734-5-B	Attachment 1 of UCCSN-UNR-024 Vol. 10;
		01023735-1-B	Attachment 1 of UCCSN-UNR-024 Vol. 10;
		01023735-2-B	Attachment 1 of UCCSN-UNR-024 Vol. 10;
		01023735-3-B	Attachment 1 of UCCSN-UNR-024 Vol. 10;
		01023741-1-B	Attachment 1 of UCCSN-UNR-024 Vol. 10;
		01023741-2-B	Attachment 1 of UCCSN-UNR-024 Vol. 10;
		01023744-1-B	Attachment 1 of UCCSN-UNR-024 Vol. 10;
		01023744-2-B	Attachment 1 of UCCSN-UNR-024 Vol. 10;
		01023746-1-B	Attachment 1 of UCCSN-UNR-024 Vol. 10;
		01023746-2-B	Attachment 1 of UCCSN-UNR-024 Vol. 10;
		01023746-3-B	Attachment 1 of UCCSN-UNR-024 Vol. 10;
		01023747-2-B	Attachment 1 of UCCSN-UNR-024 Vol. 10;
		01023747-4-B	Attachment 1 of UCCSN-UNR-024 Vol. 10;
		01023748-1-B	Attachment 1 of UCCSN-UNR-024 Vol. 10;
		01023748-2-B	Attachment 1 of UCCSN-UNR-024 Vol. 10;
		01023754-1-B	Attachment 1 of UCCSN-UNR-024 Vol. 10;
		01023754-3-B	Attachment 1 of UCCSN-UNR-024 Vol. 10;
		01023755-1-B	Attachment 1 of UCCSN-UNR-024 Vol. 10;
		01023755-2-B	Attachment 1 of UCCSN-UNR-024 Vol. 10;
		01023755-3-B	Attachment 1 of UCCSN-UNR-024 Vol. 10;

		01023756-1-B 01023756-2-B 01023757-1-B 01023757-2-B 01025222-B 01025224-2-B 01025224-3-B 01025226-2-B 01025226-3-B 01025226-4-B 01025226-5-B 01025227-3-B 01025227-4-B 01025227-5-B 01025228-1-B 01025228-2-B 01025228-3-B 01025229-1-B 01025229-2-B 01025229-3-B 01025229-4-B 01025232-2-B 01025232-3-B 01025232-4-B 01025261-3-B	Attachment 1 of UCCSN-UNR-024 Vol. 10; Attachment 1 of UCCSN-UNR-024 Vol. 10;
Table 4.2	018LM.002	The data file: Summary of Brazilian Tests.xls. The following 158 tests are included in the file. 01014733-1-B 01014764-1-B	UCCSN-UNR-024 Vol. 13, pp. 15-19

		01014764-3-B 01023357-2-B 01023359-2-B 01023359-3-B 01023363-4-B 01023363-5-B 01023363-6-B 01023367-3-B 01023367-4-B 01023367-5-B 01023370-2-B 01023370-3-B 01023372-3-B 01023566-2-B 01023567-2-B 01023567-3-B 01023567-4-B 01023570-2-B 01023570-3-B 01023570-4-B 01023571-1-B 01023571-2-B 01023571-3-B 01023571-4-B 01023574-1-B 01023574-2-B 01023574-3-B 01023574-4-B 01023574-5-B 01023574-6-B 01023574-7-B	

		01023576-1-B 01023579-2-B 01023580-1-B 01023581-1-B 01023581-3-B 01023581-4-B 01023582-2-B 01023585-1-B 01023585-2-B 01023586-1-B 01023586-2-B 01023657-6-B 01023657-7-B 01023657-8-B 01023658-1-B 01023658-2-B 01023658-3-B 01023658-4-B 01023658-5-B 01023658-6-B 01023661-1-B 01023661-2-B 01023661-3-B 01023666-1-B 01023666-2-B 01023666-3-B 01023666-4-B 01023668-1-B 01023668-2-B 01023668-4-B 01023668-5-B	

		01023668-6-B 01023668-7-B 01023668-8-B 01023685-1-B 01023685-2-B 01023685-3-B 01023685-4-B 01023685-5-B 01023685-6-B 01023685-7-B 01023685-8-B 01023689-3-B 01023689-4-B 01023689-5-B 01023689-6-B 01023689-7-B 01023690-2-B 01023690-3-B 01023690-4-B 01023690-5-B 01023693-1-B 01023693-2-B 01023697-2-B 01023697-3-B 01023697-4-B 01023701-2-B 01023701-3-B 01023701-4-B 01023702-1-B 01023704-1-B 01023704-3-B	

		01023704-4-B 01023704-5-B 01023704-6-B 01023704-7-B 01023704-8-B 01023704-9-B 01023715-1-B 01023715-2-B 01023715-3-B 01023715-4-B 01023721-1-B 01023721-2-B 01023727-1-B 01023727-2-B 01023734-1-B 01023734-2-B 01023734-3-B 01023734-4-B 01023734-5-B 01023735-1-B 01023735-2-B 01023735-3-B 01023741-1-B 01023741-2-B 01023744-1-B 01023744-2-B 01023746-1-B 01023746-2-B 01023746-3-B 01023747-2-B 01023747-4-B	

		01023748-1-B 01023748-2-B 01023754-1-B 01023754-3-B 01023755-1-B 01023755-2-B 01023755-3-B 01023756-1-B 01023756-2-B 01023757-1-B 01023757-2-B 01025222-B 01025224-2-B 01025224-3-B 01025226-2-B 01025226-3-B 01025226-4-B 01025226-5-B 01025227-3-B 01025227-4-B 01025227-5-B 01025228-1-B 01025228-2-B 01025228-3-B 01025229-1-B 01025229-2-B 01025229-3-B 01025229-4-B 01025232-2-B 01025232-3-B 01025232-4-B	

		01025261-3-B	
Table 5.1	018LM.001	Summary of 01014755-U.doc Summary of 01014979-U.doc Summary of 01014985-U.doc Summary of 01014994-U.doc Summary of 01015001-U.doc Summary of 01015004-U.doc Summary of 01015455-1-U.doc Summary of 01015456-U.doc Summary of 01014723-U.doc Summary of 01014759-U.doc Summary of 01014760-U.doc Summary of 01014765-U.doc Summary of 01014779-1-U.doc Summary of 01014780-U.doc Summary of 01014947-1-U.doc Summary of 01014977-U.doc Summary of 01014986-U.doc Summary of 01015003-U.doc Summary of 01015453-U.doc	Attachment 1 of UCCSN-UNR-024 Vol. 5; Attachment 1 of UCCSN-UNR-024 Vol. 5; Attachment 1 of UCCSN-UNR-024 Vol. 5; Attachment 1 of UCCSN-UNR-024 Vol. 5; Attachment 1 of UCCSN-UNR-024 Vol. 5; Attachment 1 of UCCSN-UNR-024 Vol. 5; Attachment 1 of UCCSN-UNR-024 Vol. 5; Attachment 1 of UCCSN-UNR-024 Vol. 5; Attachment 1 of UCCSN-UNR-024 Vol. 5; Attachment 1 of UCCSN-UNR-024 Vol. 5; Attachment 1 of UCCSN-UNR-024 Vol. 5; Attachment 1 of UCCSN-UNR-024 Vol. 5; Attachment 1 of UCCSN-UNR-024 Vol. 5; Attachment 1 of UCCSN-UNR-024 Vol. 5; Attachment 1 of UCCSN-UNR-024 Vol. 5; Attachment 1 of UCCSN-UNR-024 Vol. 5; Attachment 1 of UCCSN-UNR-024 Vol. 5; Attachment 1 of UCCSN-UNR-024 Vol. 5; Attachment 1 of UCCSN-UNR-024 Vol. 5
Fig. 5.1	018LM.001	01014979-U_270deg.jpg; 01015003-U_180deg.jpg	A summary of the test is in UCCSN-UNR-024 Vol. 13, p. 48; The photo is in TDA only. A summary of the test is in UCCSN-UNR-024 Vol. 13, p. 75; The photo is in TDA only.
Table 5.2	018LM.001	Summary of 01014755-U.doc; Summary of 01014979-U.doc; Summary of 01014985-U.doc;	UCCSN-UNR-024 Vol. 13, p. 47; UCCSN-UNR-024 Vol. 13, p. 48; UCCSN-UNR-024 Vol. 13, p. 49;

		Summary of 01014994-U.doc; Summary of 01015001-U.doc; Summary of 01015004-U.doc; Summary of 01015455-1-U.doc; Summary of 01015456-U.doc; Summary of 01014723-U.doc; Summary of 01014759-U.doc; Summary of 01014760-U.doc; Summary of 01014765-U.doc; Summary of 01014779-1-U.doc; Summary of 01014780-U.doc; Summary of 01014947-1-U.doc; Summary of 01014977-U.doc; Summary of 01014986-U.doc; Summary of 01015003-U.doc; Summary of 01015453-U.doc	UCCSN-UNR-024 Vol. 13, p. 50; UCCSN-UNR-024 Vol. 13, p. 51; UCCSN-UNR-024 Vol. 13, p. 52; UCCSN-UNR-024 Vol. 13, p. 53; UCCSN-UNR-024 Vol. 13, p. 54; UCCSN-UNR-024 Vol. 13, p. 65; UCCSN-UNR-024 Vol. 13, p. 71; UCCSN-UNR-024 Vol. 13, p. 73; UCCSN-UNR-024 Vol. 13, p. 66; UCCSN-UNR-024 Vol. 13, p. 74; UCCSN-UNR-024 Vol. 13, p. 72; UCCSN-UNR-024 Vol. 13, p. 67; UCCSN-UNR-024 Vol. 13, p. 68; UCCSN-UNR-024 Vol. 13, p. 69; UCCSN-UNR-024 Vol. 13, p. 75; UCCSN-UNR-024 Vol. 13, p. 70
Fig. 5.2		This is not QA data.	
Figs. 5.3-5.6	018LM.001	01015453-U (MTS).xls	A summary of the test is in UCCSN-UNR-024 Vol. 13, p. 70.
Table 5.3	018LM.001	Summary of 01014764-2-CU(U) .doc; Summary of 01014950-U.doc; Summary of 01015013-1-U.doc; Summary of 01023357-1-U.doc; Summary of 01023359-1-U.doc; Summary of 01023363-2-U.doc; Summary of 01023372-1-U.doc; Summary of 01023567-CU(U) .doc; Summary of 01025234-2-U.doc	Attachment 1 of UCCSN-UNR-024 Vol. 5; Attachment 1 of UCCSN-UNR-024 Vol. 5; Attachment 1 of UCCSN-UNR-024 Vol. 5; Attachment 4 of UCCSN-UNR-024 Vol. 5; Attachment 4 of UCCSN-UNR-024 Vol. 5; Attachment 4 of UCCSN-UNR-024 Vol. 5; Attachment 4 of UCCSN-UNR-024 Vol. 5; Attachment 1 of UCCSN-UNR-024 Vol. 10; Attachment 1 of UCCSN-UNR-024 Vol. 10
Table 5.4	018LM.001	Summary of 01014764-2-CU(U) .doc; Summary of 01014950-U.doc; Summary of 01015013-1-U.doc;	UCCSN-UNR-024 Vol. 5, pp. 90-91; UCCSN-UNR-024 Vol. 5, p. 78-79; UCCSN-UNR-024 Vol. 5, p. 46-48;

		Summary of 01023357-1-U.doc; Summary of 01023359-1-U.doc; Summary of 01023363-2-U.doc; Summary of 01023372-1-U.doc; Summary of 01023567-CU(U) .doc; Summary of 01025234-2-U.doc	UCCSN-UNR-024 Vol. 5, p. 86; UCCSN-UNR-024 Vol. 5, p. 80; UCCSN-UNR-024 Vol. 5, p. 85; UCCSN-UNR-024 Vol. 5, p. 82; UCCSN-UNR-024 Vol. 10, pp. 25-26; UCCSN-UNR-024 Vol. 10, p. 68

Note:

018LM.001-Uniaxial Compression Tests results
018LM.002-Brazilian Tensile Strength Rock Tests Analysis results
018LM.003-Results from Creep Tests on rock specimens
SNs:

UCCSN-UNR-024 Vol. 5
UCCSN-UNR-024 Vol. 10
UCCSN-UNR-024 Vol. 13